Trends in Analytical Chemistry 144 (2021) 116425

Contents lists available at ScienceDirect

Trends in Analytical Chemistry

journal homepage: www.elsevier.com/locate/trac

Biomimetic solid-state nanochannels for chemical and biological sensing applications

Gregorio Laucirica [a], Yamili Toum Terrones [a], Vanina Cayón [a], María Lorena Cortez [a], Maria Eugenia Toimil-Molares [b], Christina Trautmann [b, c], Waldemar Marmisollé [a], Omar Azzaroni [a, *]

[a] Instituto de Investigaciones Fisicoquímicas Teóricas y Aplicadas (INIFTA), Departamento de Química, Facultad de Ciencias Exactas, Universidad Nacional de La Plata, CONICET – CC 16 Suc. 4, 1900, La Plata, Argentina
[b] GSI Helmholtzzentrum für Schwerionenforschung, 64291, Darmstadt, Germany
[c] Technische Universität Darmstadt, Materialwissenschaft, 64287, Darmstadt, Germany

ARTICLE INFO

Article history:
Available online 2 September 2021

Keywords:
Biosensing
Nanofluidics
Nanochannels
Solid-state nanopores
Molecular recognition

ABSTRACT

Biomimetic solid-state nanochannels enable new modalities for biosensing. In the last decade, these nanofluidic architectures have been widely studied due to their rapid and sensitive detection capabilities. Developing nanofluidic sensors with great ability to sense ions, small biomolecules, and biological macromolecules requires the combination of versatile surface modification strategies with reliable nanofabrication techniques. Solid-state nanochannels display unique ion transport properties and appealing effects arise when their inner surfaces are charged and the confinement length scale is comparable to the range of the electrostatic interactions in solution. In this context, the integration of molecular recognition elements into the nanochannels yields novel nanofluidic elements with tailored sensoric functions. This review describes recent advances in solid-state nanochannel-based (bio)chemical sensors. The topics covered in this work include sensing principles, nanofabrication techniques and strategies adopted for detecting specific targets, such as ions, small molecules, proteins or nucleic acids, among others. The review highlights several exceptionally promising research directions and discusses how the interplay between the interface chemistry, governed by the bio-receptors, and the remarkable ion transport properties of nanochannels plays a critical role in the analytical performance of the developed devices. In the end, we also offer our vision of the future prospects of this field of research.

1. Introduction

Living systems have always been an endless source of inspiration for scientists both in basic and applied research. The link between technological advances and learning from nature has resulted in the design and development of different tools that could meet a wide variety of needs [1]. In this regard, inspired by the great attributes of biological ion channels, the development of fully-abiotic solid-state nanochannels –SSNs- (length much larger than diameter) and nanopores (length and diameter with similar dimensions) has been at the forefront of materials science in recent years [2]. Research in this field is focused on the development of nanostructures that show features of biological ion channels such as selectivity, stimulus responsiveness, and rectification. But in contrast to biological systems, synthetic nanostructures are based on abiotic materials which provide higher robustness, chemical versatility, and mechanical resistance [2–5]. Platforms based on SSNs have been designed to tackle a wide variety of aims related to sensing, energy conversion, filtration, nanoelectronics, etc [6–11]. The present review is focused on recent advances in the development of SSNs for sensing and biosensing applications.

To date, SSNs are made of different materials such as silica, anodic aluminum oxide (AAO), polymers (e.g. polyimide –PI-, polyethylene terephthalate -PET- and polycarbonate –PC-), among others [12,13]. In some cases, fabrication protocols result in channels with surface groups that are able to modulate the surface charge depending on the external conditions. For example, ion-track etching is a well-established technique for the development of SSNs in polymer membranes [14]. Carboxylate groups that arise

* Corresponding author.
E-mail address: azzaroni@inifta.unlp.edu.ar (O. Azzaroni).

https://doi.org/10.1016/j.trac.2021.116425
0165-9936/

from the hydrolysis of polymers during track etching confer a negative surface charge to the channel at pH > 3.5. As discussed in more detail below, these facts have two direct implications: (i) the combination of nanoscale dimension and the charged surface sensitively impact the response of the transmembrane ionic current and (ii) the presence of carboxylate groups provides different inexpensive options for (bio)functionalizing the channel surface.

The precise and adjustable ionic transport of biological ion channels emerges from the possibility of tuning the ratio between size and charge via conformational changes that are triggered by different stimuli [15]. In contrast to biological systems, the fabrication of SSNs with tunable ion transport properties is mainly achieved by decorating the channel walls with stimuli-responsive building blocks [16]. The integration of selective nanoarchitectures makes it possible to design platforms that are responsive to stimuli such as pH, temperature, light, voltage, etc [17–23]. Moreover, a wide variety of sensors and biosensors have been designed by inserting into the nanochannel a specific recognition element for the target analyte [24,25]. Interaction between the target analyte and the recognition element triggers a change of the channel surface properties (e.g. surface charge density, effective channel diameter, or hydrophobicity) that is directly identified by a change of the recorded response [4,16]. The control of the internal channel architecture, i.e., both its geometrical parameters as well as the (bio)chemical features of the surface, is one of the main opportunities but also a great challenge for the creation of new sensing platforms based on SSNs.

Sensing with SSNs can be performed by using different strategies [4,10,24,26,27], which can be divided into two main groups: resistive-pulse (or stochastic) sensing and steady-state current methods. The first approach is a powerful technique that has gained relevance due to its proficiency in single-molecule sensing. This method emerges from its predecessor the Coulter-counting technique [28] and usually involves the registration of ionic current (or bias voltage) as a function of time. When an analyte with a comparable size to the channel aperture is translocated across the channel, it produces a partial blockage that generates a pulse (event) in the transient signal. The magnitude, duration, and shape of the event can be correlated to the analyte nature, whereas the event rate can be related to the analyte concentration [29,30]. This technique has allowed sensing of molecules such as proteins, DNA, RNA, enzymes, and polymers, among others. Up to now, several review articles based on the state-of-art of single-molecule sensing with SSNs and biological ion channels via resistive-pulse technique have been published [29,31–35].

In contrast, sensing with SSNs by steady-state measurements usually requires the recording of the ion current (iontronic output) when a transmembrane voltage is scanned (*I*–*V* curve) in the presence and absence of a particular analyte (Fig. 1) [36]. The presence of a target molecule at a certain concentration triggers a variation in the physicochemical properties of the channel which can be evidenced by changes in the *I*–*V* characteristic curve [2,4]. The parameter extracted from the iontronic signal (e.g. the conductance G- and/or the rectification ratio) is correlated with the analyte concentration. While this method is not useful for single-molecule detection in real-time, it has gained interest in the sensor field due to its ability to transduce the presence of target analytes into reproducible iontronic signals. Contrary to resistive-pulse sensing, the steady-state approach requires simple data treatment and instrumentation. Furthermore, this technique is useful for the quantification of small molecules since it is not a prerequisite to use channels with diameters in the order of the target analyte size. Therefore, the same nanofabrication methods can be applied to produce channels that enable the efficient sensing of molecules which are 1–2 orders of magnitude smaller in size.

In this review, we address recent advances in the development of sensing and biosensing platforms based on solid-state nanochannels that operate in steady-state conditions (Fig. 1). In the first section, fundamental concepts on the transport in SSN and the transducing mechanisms are discussed. In the second section, the main nanofabrication methods for the construction of nanofluidic devices in polymers, AAO, and glass are addressed. In the third and four sections, the most common methods for the nanofabrication, functionalization, and integration of recognition elements onto the surface of the different nanofluidic devices are summarized. Then we present some examples of different sensing devices reported in the last years which are divided into four sections according to the nature of the target moiety: ions (Section 5); gases (Section 6); nucleic acids, proteins, cells, and virus (Section 7); and finally a group composed of drugs, amino-acids, sugars, neurotransmitters and pollutants (Section 8). Then, we give a summary of the different strategies employed for the construction of (bio)sensing platforms. We discuss both the advantages and drawbacks of the different recognition elements' integration methods as well as the strengths and weaknesses of the different families of recognition elements. Also, the future challenges in the design and development of (bio) sensing platforms based on SSNs with technological applications are discussed. Finally, in the last section, we present a summary of the state-of-the-art of this topic and some perspectives on the evolution of the SSNs-based (bio)sensors field. We hope that this article will be of help to scientists that are eager to explore new horizons in the nanochannel research field and to discover new principles and applications in biosensing.

2. Ion transport in SSN - basic concepts

Solid-state nanochannels allow the precise control of transport processes through their structure and as such are suitable candidates for the development of sensing and biosensing platforms [9,24,36]. In a typical steady-state experiment, a membrane containing nanochannels (single-channel or multi-channel membrane) is placed between the two halves of a conductivity cell filled with an electrolyte (Fig. 1, -iontronic output section-). The electrodes inserted in each half cell are connected to a sourcemeter (or potentiostat) in order to apply a transmembrane voltage. By recording current-voltage curves (*I*–*V* curves), the ion transport across the channel is monitored [20]. In contrast to electronic devices, the signal carriers are based on ions, hence the response is commonly referred to as *iontronic output* [37,38].

While it is not the most common approach, the ion transport properties across the nanofluidic devices can be also studied by electrochemical impedance spectroscopy (EIS) [39,40]. In this method, a three-electrode set-up is arranged by placing the working electrode (e.g. Pt or Au) in one of the half cells and the reference (Ag/AgCl) and counter-electrode (Pt) in the other half cell [41,42]. The impedance is measured at different frequencies (e.g. from 1 Hz to 1 MHz) and then, the experimental results are interpreted and fitted by modeling the behavior to an equivalent circuit that enables the estimation of the membrane resistance, among other parameters [41,42].

The steady-state approach has gained increasing interest owing to its experimental simplicity. However, the design of SSNs-based devices capable to specifically respond to target molecules and developing reproducible ionic signals remains a major challenge. For the fabrication of nanofluidic sensing platforms, the focus is typically on the integration of recognition elements on the channel walls that, in presence of the analyte, trigger changes in the physicochemical properties of the nanochannel and concomitantly, induce a variation of the ion transport (Fig. 1). In order to convert physicochemical changes in the channel into iontronic signals, the

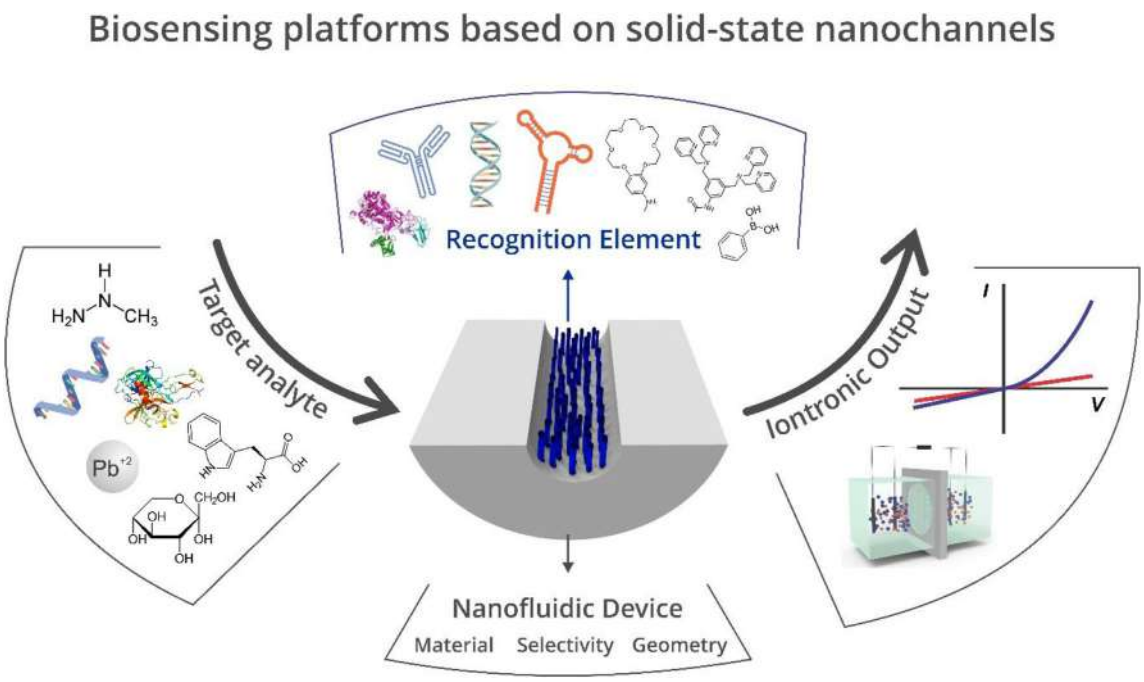

Fig. 1. Scheme summarizing the crucial variables that take part in the design of biomimetic smart nanochannels for biosensing purposes.

analyte must either change the surface charge (2.1) or the effective size of the channel (steric effects) (2.2). It is worth mentioning that wettability changes in the channel commonly cause variations in the iontronic signal, but, this mechanism is rather unusual in sensing applications [4].

Behind the aforementioned sensing strategies, nanoconfinement effects play crucial roles that determine the importance of SSNs-based devices for sensing purposes. Thus, in Section 2.3 we will address the significance of these effects and how they serve to achieve sensing with SSNs allowing overcoming difficulties that arise in traditional bulk sensing strategies.

2.1. Response modulated by changes in surface charge

Exposing a charged surface to an electrolyte leads to a redistribution of ionic species with the purpose of balancing the surface charge [43,44]. In particular, counter-ions are attracted to the vicinity of the charged surface due to electrostatic attraction, whereas co-ions are repelled. These facts give rise to the so-called electrical double layer (EDL) whose characteristic length is usually described by means of the Debye length (λ_D). Commonly, this parameter is considered to be the effective distance at which the effects of the charged surface operate, and, of course, this depends on the nature and concentration of the electrolyte. The Debye length acquires values of a few nanometers in usual electrolyte solutions ($\lambda_D \sim 0.96$ nm for 0.1 M KCl and $\lambda_D \sim 3$ nm for 0.01 M KCl). Thus, λ_D has huge implications on the ion transport of nanofluidic devices when the diameter of a charged channel is comparable to λ_D. At this condition, the concentration inside the channel is polarized, i.e. counter-ions are enriched whereas co-ions are depleted, in a phenomenon called *ion concentration polarization* (ICP) [45,46]. Concomitantly, the ion transport is surface-charge-governed and the iontronic output offers information about the surface charge magnitude. For a cylindrical channel with a certain diameter, the *I*–*V* curve is characterized by an ohmic behavior, i.e., showing a linear relationship between the current and voltage, in which the magnitude of the surface charge determines the channel conductance –*G*- (i.e. slope of *I*–*V* curve) (Fig. 2(A)) [2,12]. Hence, if the interaction between the recognition element and the analyte promotes concentration-dependent changes on the surface charge density of the channel, the exposure to the analyte leads to a variation of the channel conductance (or resistance) (Fig. 2(C)) [47].

It is widely accepted that the disruption of electrical potential symmetry leads to ion current rectification, i.e. a non-ohmic (non-linear *I*–*V* curves) behavior in which the ion flux is favored at one polarity voltage compared with the opposite polarity (diode-like behavior) (Fig. 2(B)) [48–53]. This broken symmetry can be obtained by an asymmetric channel shape (e.g. conical) or due to asymmetrically functionalized channels [48,54]. In asymmetric-shaped channels, the transport properties are strongly dependent on geometry parameters, such as the tip and base diameter, the shape, and the nanochannel length [49,55,56]. Furthermore, in contrast to symmetrical (cylindrical) channels, the response is mainly dictated by the interaction of mobile ions and surface-charged groups on the narrow tip region [57,58]. Considering this, it is usually asserted that if the size of the charged channel (or the tip in asymmetric channels) is comparable to λ_D, the surface charges promote counter-ion accumulation, and concomitantly, the response is strongly influenced by the surface charge density magnitude [59,60]. However, it is worth mentioning that it is possible to obtain rectifying behavior in highly charged channels with sizes much larger than λ_D.

As the conductance of asymmetrical channels depends on voltage polarity, usually, the response variations are evidenced via the rectification efficiency or rectification factor (f_{rec}) which is defined as the ratio of current at the high conductance branch and the low conductance branch at a fixed voltage, for example, |I(1 V)/I(-1 V)| in Fig. 2(B). Therefore, changes in the surface charge density can be evidenced through changes in f_{rec} (Fig. 2(C)).

Furthermore, in asymmetrical channels, the *I*–*V* curve is not only dependent on the surface charge magnitude but also its sign [23,59]. As the nature of the surface charges determines the direction of the rectified current, the rectification is characterized both by its magnitude given by f_{rec} and its direction. Thus, two types

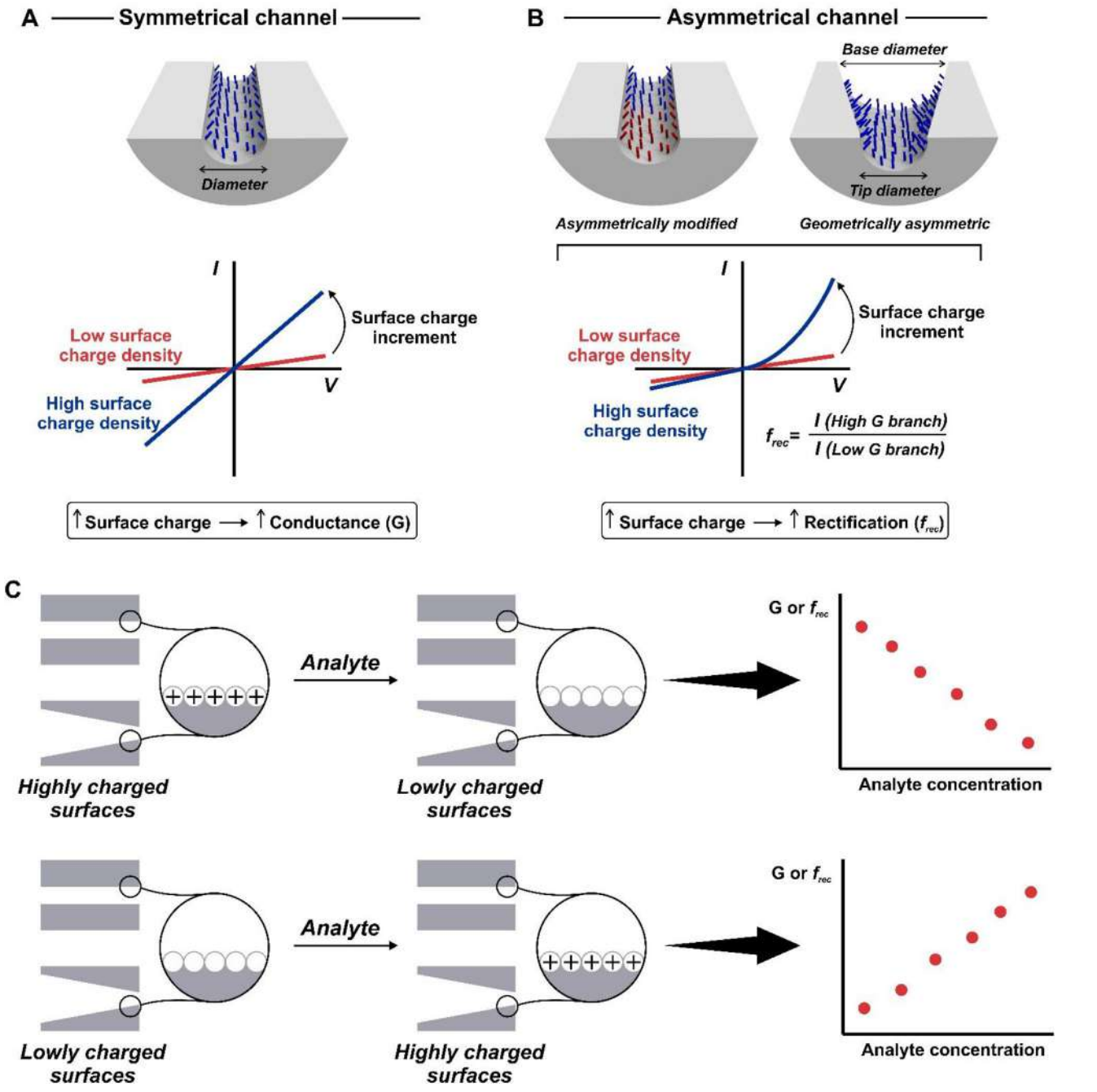

Fig. 2. Simplified scheme describing **(A)** symmetrical and **(B)** asymmetrical channels. The figure also indicates the expected variations in the iontronic output: increasing the surface charge promotes an increment in the channel conductance for symmetrical channels (left) and an increment in the rectification for asymmetrical channels (right). f_{rec} and *G* refer to rectification factor and conductance, respectively. **(C)** Simplified scheme describing the relationship between the changes in the channel surface charge due to the exposition to the analyte and the final results in terms of conductance −G- or rectification factor −f_{rec}-.

of rectification regimes are observed: cation-driven rectification (or cation-selective rectification) for negatively charged channels and anion-driven rectification (or anion-selective rectification) for positively charged channels (Fig. 3) [21]. If the interaction between the recognition element and the analyte in asymmetrical channels promotes concentration-dependent changes on the surface charge density they can be identified through the variations of rectification magnitude (f_{rec}) and direction [61–63].

A detailed quantitative description of the ion transport across nanochannels is possible through numerical simulation via Poisson-Nernst-Planck (PNP) formalism [12,57,64,65]. As the name suggests, this formalism combines the Poisson equation that describes the relationship between the electrical potential ($\nabla\phi$) and the charge density with the Nernst-Planck equation that describes the ion fluxes (J_i) across the nanochannel. The former can be expressed as follows [57].

$$\nabla^2\phi = \frac{F^2}{\varepsilon RT}(C_- - C_+) \quad (1)$$

where ε is the dielectric permittivity, R is the ideal gas constant, T is the temperature, F is the Faraday constant, and C_- and C_+ correspond to the anion and cation concentrations, respectively.

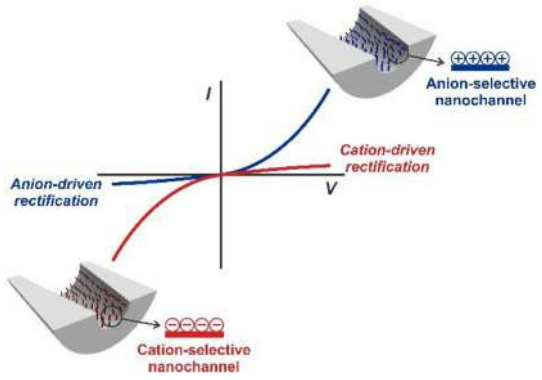

Fig. 3. Directionality of ion current rectification for positively charged channels (anion-selective) resulting in anion-driven rectification (blue) and negatively charged channels (cation-selective) resulting in cation-driven rectification (red).

For its part, the Nernst-Planck equation describes the ion fluxes across the channel due to the contribution of both concentration-driven flow (Fick's first law −first term-) as well as the ion migration under an electrical field (second term) [57].

$$J_i = -D_i(\nabla C_i + C_i z_i \nabla \phi) \quad (2)$$

where D_i, C_i, and z_i are the diffusivity, concentration, and valence number of ion i, respectively. Finally, considering steady-state conditions [57].

$$\nabla \cdot J_i = 0 \quad (3)$$

This formalism allows the calculation of ion concentration and electrical potential profile along the channel. While numerical methods have been mostly used for the study of basic concepts of ion transport, their use can also play a central role in the design, development, and optimization of SSNs-based sensing platforms [49,57,66]. In particular, numerical results can be a key for understanding both the sensing mechanism as well as how the variation of different parameters related to the electrolyte, channel geometry, surface charge, or presence of recognition elements, can affect the output signal and, therefore, the sensing capability [67–69]. Further details about the different models for describing the ion transport in solid-state nanochannels can be found in previous review articles [12,64].

2.2. Response modulated by changes on effective channel size

Considering that the iontronic signal is determined by the ion transport across the channel, it is expected that, besides the dependence on surface charge density, the response is influenced by the effective channel size [45,70,71]. This fact leads to the second most used strategy for the development of sensing and biosensing platforms (Fig. 4). The iontronic current directly decreases if the effective channel size is reduced because target molecules partially or completely block the channel (Fig. 4(A)). A similar effect occurs when an analyte triggers a spatial reorganization of molecular systems grafted onto the channel wall [47,72]. In some cases, the analyte can promote the release of recognition elements yielding an increment on the effective channel size and concomitantly, an increment (decrease) on the channel conductance (resistance) (Fig. 4(B)) [73].

Sometimes the channel size decrease (or increase) promoted by the analyte is concentration-dependent and quantitative analysis becomes possible by recording conductance (or resistance) vs analyte concentration curves (Fig. 4(C)).

2.3. Nanoconfinement effects

Beyond the specific sensing mechanism, most of the SSNs-based sensing platforms that will be addressed in this review share a fundamental approach. As we previously mentioned, the attachment of recognition elements onto the channel walls provides the SSNs responsiveness to target analytes, i.e. the interaction with the target analyte generates some change either in the chemical or physical variables of the surface (chemical input), enabling the transduction into a readable output signal (iontronic output). Within this framework, it is important to remark that the nanofluidic device does not play a secondary role. Conversely, SSNs constitute the fundamental machinery that makes possible the conversion of the chemical input into an iontronic signal [4]. On the other hand, the nanoscale generates marked effects in chemical and physical interactions, the so-called “nanoconfinement effects” -derived from nanoconfined spaces and interfaces with sizes approaching those of target molecules- that play a central role both during the immobilization of recognition elements onto the channel surface as well as in the interaction of these molecular systems with the analyte [74].

For instance, the functionalization of SSNs with polyelectrolytes by electrostatic self-assembly has shown dramatic changes with respect to the behavior exhibited in flat surfaces (see Section 4.3.5 for further details) [74]. Moreover, the nanoconfinement promotes new forms of polymer organization that strongly affect the acid-base equilibria and therefore, the ion transport properties [65,75–79]. As an example, Tagliazucchi et al. showed by using molecular theory that the apparent pKa for the poly(4-vinyl pyridine) brushes inside of a cylindrical channel (diameter = 15 nm) decreases two unities compared with the bulk value [75]. This displacement of the equilibrium towards the uncharged state was ascribed to the charge regulation mechanism which aims to diminish the local electrostatic repulsion. Similarly, profound nanoconfinement effects have been observed in many types of colloidal nanoparticles (Au and SiO_2 nanoparticles (NPs) for example), with strong implications on NPs based sensors [80–82]. Analogously, the pKa of polyelectrolytes in functionalized silica mesopores was also affected by nanoscale confinement [76].

Last but not least, the chemical reactivity and the interaction between different compounds also undergo profound changes due to the nanoconfinement [83,84]. As an example, the interaction between divalent anions and amino groups inside of a polymeric nanochannel evidenced an increase of 1 order of magnitude in the binding constants compared with the value displayed in the microscale [82,85]. In the case of biomolecules such as enzymes, changes in the activity and kinetic constants due to confinement were also reported [86–88]. In particular, glucose oxidase (GOx) revealed a diminution in its activity as the channel size diminished which was attributed to the increment of steric hindrance issues due to confinement [87]. However, even in channels with 50 nm of diameter, GOx activity was larger than in the bulk solution. In contrast, the kinetic reaction constant increased for narrower channels which was explained due to the shorter diffusion time required for the substrate to reach the enzyme in small channels. As another example, DNA hybridization reaction is also highly influenced by nanoscale (see Section 7.1.2) [89–91]. In this case, the nanoconfined space given by the nanochannel promotes a diminution in the dissociation constant (i.e. DNA hy-

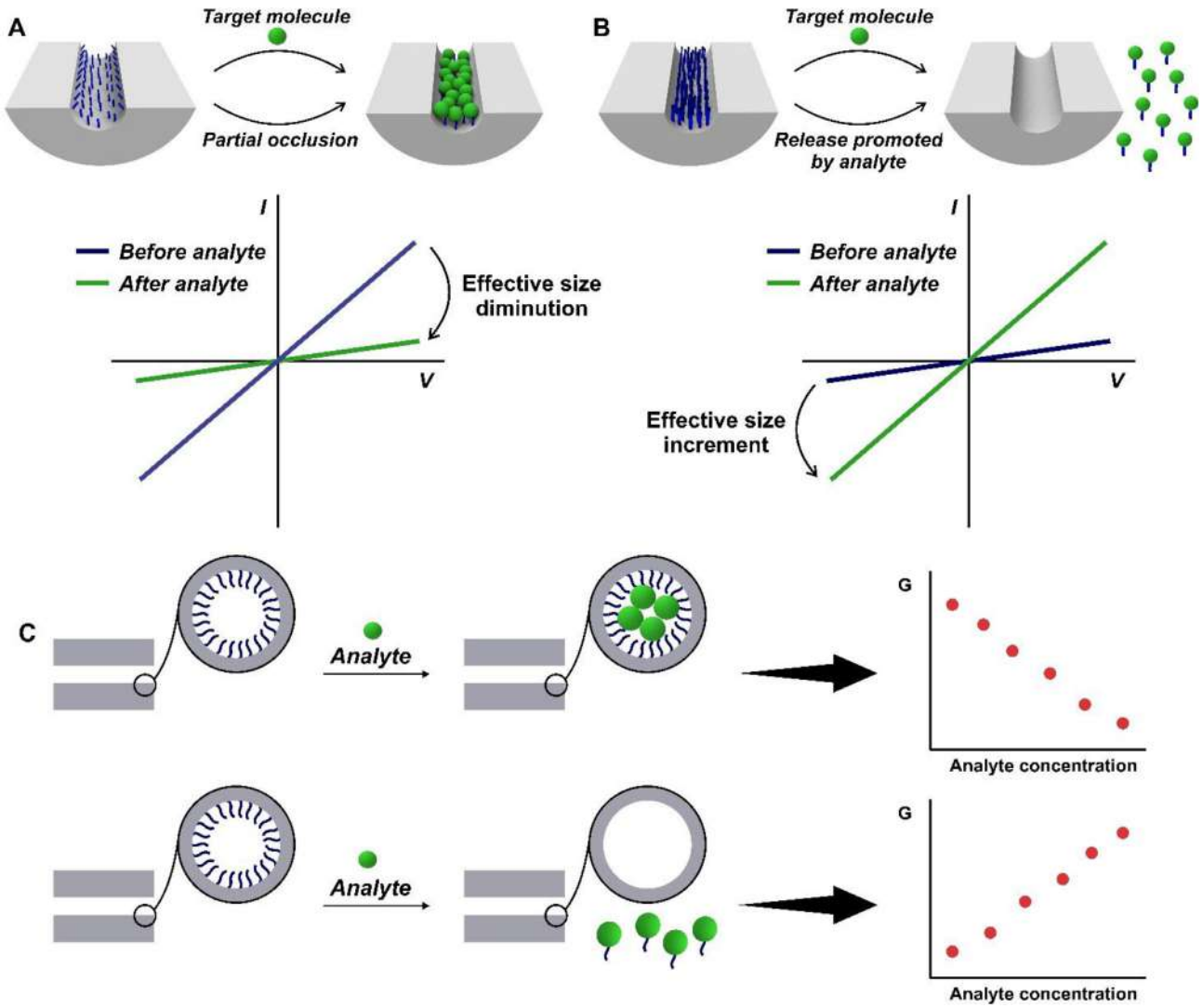

Fig. 4. Illustration of major mechanisms related to steric effects. **(A)** The analyte interacts with the recognition element generating partial channel blockage and therefore, decreasing the effective channel size. **(B)** The analyte interacts with the recognition element and releases it from the channel, thus incrementing the effective channel size. **(C)** Simplified scheme describing the relationship between the changes in the channel effective size due to the exposition to the analyte and the final results in terms of conductance −G-.

bridization is favored) compared with the values obtained in microchannels and bulk solution.

3. Nanofabrication techniques

3.1. Ion-track-etching technology

The ion-track-etching technique allows the creation of nanochannels in a wide variety of materials such as polyethylene terephthalate (PET), polycarbonate (PC), polyimide (PI), silicon dioxide (SiO_2), etc [92–96]. For this, in a first step, a membrane with several micrometer thicknesses (~10 μM) is irradiated with swift heavy ions (e.g. Au, U, Pb, etc) with energies in the range of MeV-GeV [14,94,97,98]. Each ion induces localized electronic excitation and ionization processes along its trajectory. In polymers, chemical bonds are destroyed and small volatile fragments (e.g., H_2, CO, CO_2, hydrocarbons) easily outgas [99,100]. The final consequence of this process is the formation of a damaged region in the material along the ion projectile path called "ion track" that presents different physical and chemical properties regarding the rest of the membrane (Fig. 5(A)-i) [98,101–103].

In the chemical etching procedure, the second step of the ion-track-etching, each ion track is selectively dissolved to form a nanometric channel [94]. Therefore, it is possible to accurately modulate the number of channels per area unity (pore density) by adjusting the fluence of ions (ions per unit area) during irradiation (Fig. 5(A)-ii). This technique has demonstrated the capability to create polymer membranes with pore densities from 1 to values greater than 10^{10} channels per cm^2 [66]. Irradiation with one single ion requires monitoring of individual ions hitting the sample, as available at the GSI single ion irradiation facility [104].

The etching procedure is crucial since it determines the size and geometry of the final channel (Fig. 5(A)-iii) [98,105]. The possibility to precisely tailor the channel geometry is very important from a technological perspective since it entails the possibility to influence the iontronic response. In the case of

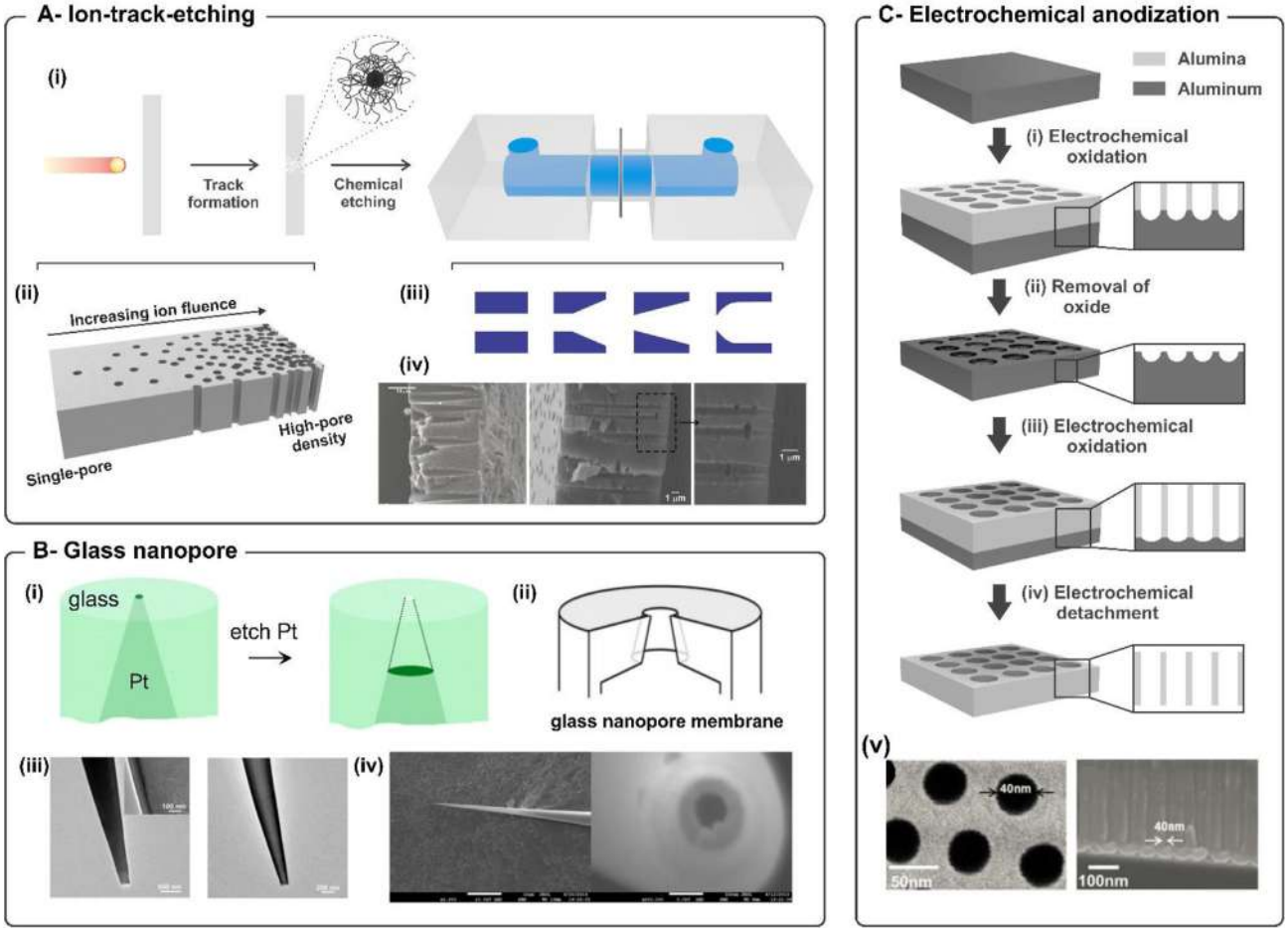

Fig. 5. **(A)** (i) Schematic illustration of ion-track-etching procedure and (ii) different fluences regimes to obtain membranes with different pore-densities. (iii) Scheme of some of the channel geometries obtained by this nanofabrication method. (iv) SEM images of membrane cross-sections containing conical nanochannels —left- and bullet-shaped channels —center and right-. Reproduced with permission [137]. Copyright © 2018 WILEY-VCH Verlag GmbH & Co. KGaA, Weinheim. Reproduced with permission [138]. Copyright © 2019, The Royal Society of Chemistry. **(B)** (i) Scheme depicting the fabrication process of the glass nanopore electrodes and (ii) the final glass nanopore. Reproduced with permissions [115,117]. Copyright 2004 and Copyright 2007, American Chemical Society. (iii) TEM images of the BSA-Au NC film-modified glass nanopore tip (left) and the unmodified (Au-free) glass nanopore tip (right). Reproduced with permission [119]. Copyright 2017, American Chemical Society. (iv) SEM images of the single glass nanopore side view (left) and end-on view (right). Reproduced with permission [120]. Copyright 2020, Elsevier. **(C)** (i-iv) Steps involved in the nanofabrication of AAO nanochannel arrays by electrochemical anodization. Inspired in Ref. [127]. Copyright 2004, American Chemical Society. (v) SEM images of AAO membrane (-left- top; -right- cross-section). Reproduced with permission [129]. Copyright 2018, American Chemical Society.

materials like PET and PC, the etching procedure usually involves the immersion of the membrane in NaOH solutions with concentrations in the range of 2 M–9 M. In order to create asymmetrical channels like conical or bullet-shaped channels, the etching is usually performed in asymmetrical conditions, i.e. one side of the membrane is exposed to highly concentrated NaOH solutions (6 M – 9 M NaOH), whereas the remaining side is soaked with an acidic stopping solution —conical geometry- or with NaOH solution with the addition of surfactant —bullet geometry- (Fig. 5(A)-iv) [48,106–109]. In other cases, the asymmetry can be directly delivered by previously exposing only one side of the membrane to UV light [110]. In the case of PI membranes, NaOCl solution with a certain content of active Cl (usually ~13%) is the most widely used as etchant and, the asymmetric etching is carried out using a reducing agent as the stopping solution [111–113]. In all cases, the etching process can be analyzed in real-time by recording the ionic current at a certain transmembrane voltage value [114]. Moreover, these procedures can be performed with different combinations of temperature, time, applied voltage, UV light exposure time, etchant identity, and additive concentrations that determine the final geometrical features.

3.2. Glass nanopores

Two central approaches to fabricate nanofluidic devices that do not include drilling with ion or electron sources are the fabrication of nanopipettes and glass nanopores [12]. In 2004, White and co-workers reported for the first time the fabrication and electrochemical characterization of truncated cone-shaped nanopore electrodes called “glass nanopores” from that moment on [115]. The relatively straightforward fabrication of glass nanopores with pore orifice radii less than 100 nm includes the steps (Fig. 5(B)-i): (1) sealing an atomically sharp Pt wire in a glass capillary, (2) polishing the capillary until a nanometric Pt disk is exposed and, (3) electrochemical etching of the exposed Pt to obtain the conical-shaped nanopore in glass (Fig. 5(B)-ii) [116–118]. These glass nanopore electrodes are opened to solution through a single orifice and present some advantages compared to free-standing membranes (i.e. track-etched polymeric membranes) such as the mechanical robustness of the solid electrode and the presence of the transduction element (Pt wire) inside the nanopore, which allows to finely studying the transport of molecules in nanoconfined structures [115]. Even though glass nanopores have been a pioneered

contribution for the development of ultra-microelectrodes for analytical purposes, they operate with low currents (pA) and low ratios signal to noise, which makes them more difficult to use compared to other commercially available electrodes.

Otherwise, naked glass nanopores fabricated by a CO_2-laser-based micropipette puller from borosilicate capillary glasses have attracted attention as they offer significant advantages of low cost, ease to synthesize, excellent mechanical and chemical stability, and adjustable orifice diameters [119]. However, in order to use these glass nanopores as sensors, a suitable and controllable functionalization of the working region must be achieved but, until now, finely-tuned surface functionalization strategies are scarce. Here we reviewed the mineralization strategy presented by Cao et al., in which a glass nanopore is decorated with structurally well-defined gold nanocluster films based on the capability of a common commercially available BSA protein (Fig. 5(B)-iii) [119]. Recently, a similar fabrication strategy that included the synthesis of an aptamer-based biosensor in a borosilicate glass-conical shaped nanopore was reported (Fig. 5(B)-iv) [120]. The successful functionalization of the glass surface was assessed by incubation with aminopropyltriethoxysilane, a standard procedure for modifying glass surfaces.

3.3. Electrochemical anodization method

The creation of highly ordered channels with nanometric dimensions in materials such as aluminum oxide (alumina) and titanium dioxide (titania) has been possible by employing a low-cost method based on electrochemical oxidations (anodization) [121–126]. For instance, in the case of aluminum membranes, the application of a certain external voltage on the Al surface produces an insulating oxide barrier in the film. When this oxidation process is performed in acidic conditions, the oxide structure is slowly dissolved giving rise to the formation of a porous structure. Considering this, one widely used approach for the creation of AAO-based membranes involves a two-step electrochemical anodization process. In the first step, the acidic anodization of a clean aluminum foil forms an alumina membrane (Fig. 5(C)-i). The oxide layer is subsequently removed by exposing it to phosphochromic acid solution which gives rise to a textured pattern of concave Al substrate that provides the initial sites to create the alumina pores in a second anodization stage (Fig. 5(C)-ii) [127,128]. Thus, in a second step, the Al textured substrate is again exposed to acidic anodization yielding the creation of an alumina layer with highly ordered pores (Fig. 5(C)-iii). Finally, the AAO membrane is obtained by separating the alumina layer from the Al barrier layer with the application of a voltage pulse or by chemical etching (Fig. 5(C)-iv) [127,129]. Recent works have demonstrated the existence of sub-nanometer pores (so-called ion-channels) in the barrier layer enabling the use of the AAO porous membrane even without detaching the barrier layer (nanochannel and ion-channel hybrid structure based on AAO) [130,131]. Using this one and other similar protocols, it is possible to obtain AAO membranes containing nanochannels with diameters ranging from 4 to 200 nm, pore density up to 10^{11} pores/cm^2, and membrane thicknesses between 0.1 μm and 300 μm (Fig. 5(C)-v). These magnitudes can be modulated by tuning the temperature, electrolyte concentration, applied voltage, etc [124]. It is worth mentioning that AAO commercial membranes with different pore sizes are widely commercialized by different technological companies [132].

The electrochemical anodization method can be also used for the creation of nanofluidic devices with sensing purposes in other materials such as TiO_2 [47,126]. Titania represents an interesting alternative for the development of functional nanoarchitectures due to its high chemical stability and its relatively low health risk [133]. The synthesis of TiO_2 nanochannels by electrochemical anodization usually involves the oxidation of highly pure Ti foils in fluorine-containing ethylene glycol and the subsequent detachment of the formed TiO_2 membrane from the metallic Ti substrate [134]. Similar to AAO nanofabrication, in TiO_2-nanochannels fabrication by electrochemical anodization, channel diameter and length can be modulated by tuning different experimental parameters such as applied voltage and time [134–136].

4. Functionalization of solid-state nanochannels and nanoconfinement implications

The strategies employed for the attachment of the recognition element on the SSN surface acquire a central role in the creation of SSNs-based (bio)sensors [139]. While the specific conditions of each functionalization method depend on the nature of the surface and the molecular system to be anchored, there are certain general aspects to be considered. In this section, we give the reader a brief overview of the most common protocols for the integration of recognition elements into nanofluidic devices.

4.1. Gold deposition

The strong interaction between thiol groups (-SH) and noble metals provides a straightforward route for the integration of recognition elements onto gold-coated surfaces [13]. When the material surface is not composed of a native gold layer, as is the case for all of the nanofluidic devices addressed in this review, a gold layer can be created after the nanofabrication by two classical methods: (1) gold electroless and (2) sputtering (Fig. 6(A)).

In the electroless method, gold is deposited onto the surface from a solution containing a gold source (e.g. sodium disulfitoaurate(I) -$Na_3Au(SO_3)_2$-) and a reducing agent (e.g. formaldehyde –HCHO-), which produce a metal film deposition as a consequence of a spontaneous redox reaction, such as the following [13,140,141]:

$$Au(SO_3)_2^{3-} + HCHO + 3\ OH^- \rightarrow 2\ Au + 4SO_3^{2-} + HCOO^- + 2\ H_2O$$

In aqueous solutions, the reaction rate is very low, and therefore, it is assumed that Au(I) is practically not reduced in that conditions. In order to accelerate the reaction, Ag nanoparticles are used as catalysts, providing an alternate path for the reduction of Au(I) to form Au nanoparticles (Au^o) that act as nuclei for the final Au^o film growth [13,140,141].

In this method, the layer thickness can be adjusted by controlling the immersion time of the SSN membrane covered by Ag^o nanoparticles into the solution containing the gold source and the reducing agent [13]. However, due to the lack of control in the morphological growth of gold by employing this protocol, some authors have proposed slight variations such as pH control and the addition of protecting agents as 4-(dimethylamino)pyridine [142]. In this way, even thin films of 10–15 nm thickness can be obtained.

In contrast to the electroless method, the Au-sputtering strategy gives rise to asymmetrically modified membranes, i.e. the gold layer is deposited only onto one side of the membrane [20,50,92,93]. Furthermore, the formed layer is endowed with excellent electrical properties, which enable the subsequent integration of the desired building blocks via electrochemical techniques such as electropolymerization [137].

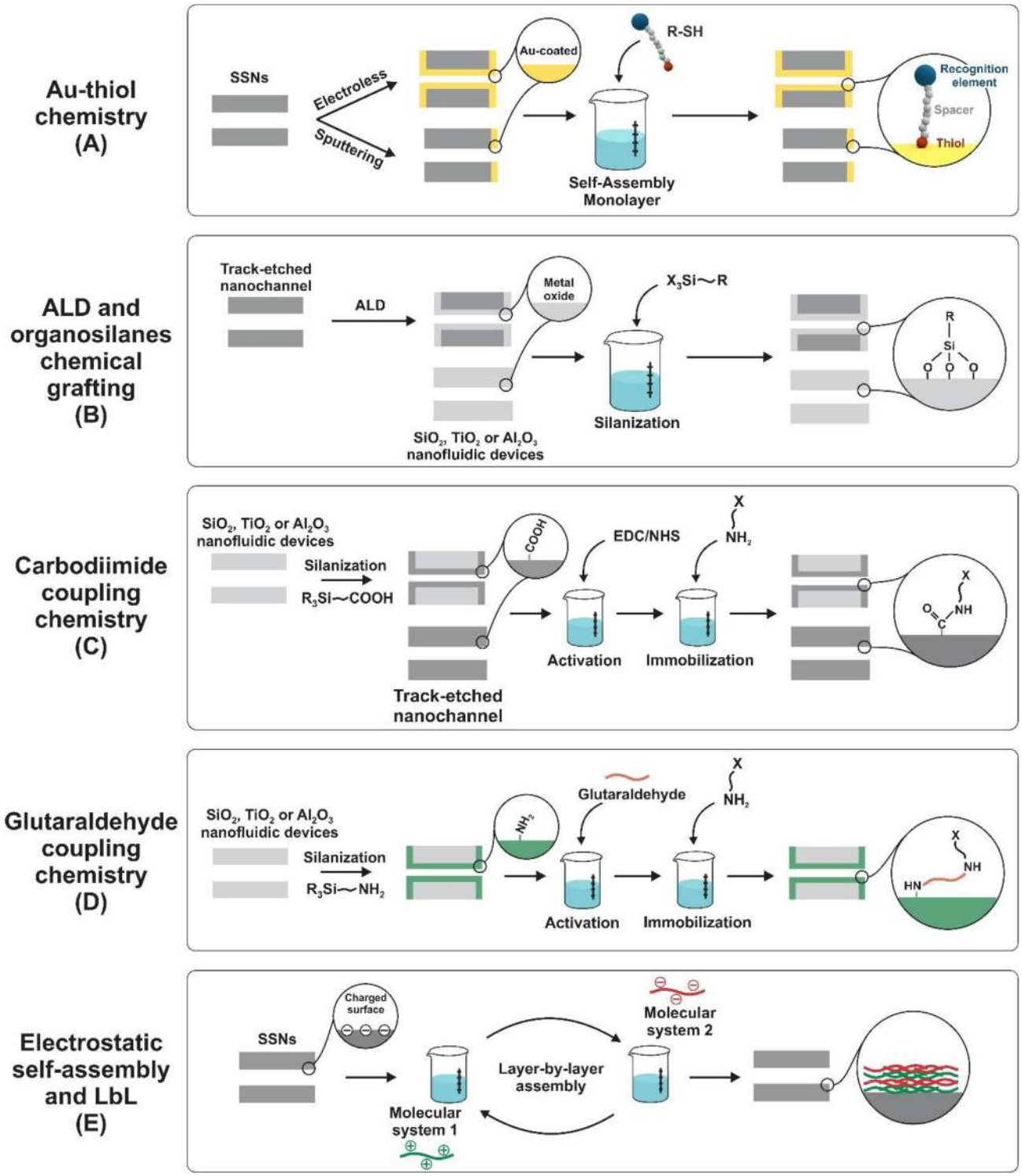

Fig. 6. Schematic illustration summarizing different functionalization strategies: **(A)** self-assembled monolayers (SAM) via thiol-Au chemistry; **(B)** ALD and chemical grafting of organosilanes −silanization-; **(C)** carbodiimide coupling chemistry; **(D)** glutaraldehyde coupling chemistry and (E) electrostatic self-assembly and LbL.

4.2. Atomic layer deposition (ALD)

Inorganic oxide surfaces such as SiO_2, TiO_2, and Al_2O_3, provide robust and simple alternatives for the immobilization of recognition elements via chemical grafting or silanization reactions. If the SSNs do not contain SiO_2, TiO_2, or Al_2O_3 after the nanofabrication, as is the case of track-etched SSNs, atomic layer deposition (ALD) emerges as an affordable way to introduce them (Fig. 6(B)) [143−145]. ALD is a functionalization technique based on the sequential and self-limiting gas-solid surface reactions of two reactants in the gas phase [146]. The self-limiting nature ensures the deposition of SiO_2, TiO_2, and Al_2O_3 with not only an ultraprecise control of the layer thickness but also the control of the material composition at the atomic level [143,144,146,147]. Experimentally,

the film growth via ALD is performed in a cyclic way with, typically, four steps per cycle: (a) substrate exposure to the first precursor, (b) purge of the reaction chamber, (c) substrate exposure to the second precursor and (d) purge of the reaction chamber. By modulating the number of cycles, it is possible to fine-tune the film thickness at the monolayer level [146]. This protocol has been successfully employed to deposit SiO_2, TiO_2, and Al_2O_3 on different nanofluidic devices such as track-etched (PC, PET, and PI) and AAO membranes [144,145,148–150]. This technique not only provides possibility fertile layer for its further derivatization with different inorganic compounds (e.g. see silanization method in Section 4.3.2) but also allows the accurate control in the layer thickness to precisely adjust the channel size even after the nanofabrication process (top-down approach) [144]. Also, in the case of track-etched channels, the ALD-coating shows higher stability compared with the uncoated membrane which is a very interesting feature facing up the development of platforms with long-term stability [143]. In contrast, the long time required to grow thicker films and the necessity of specialized instrumental facilities can be considered as the main drawbacks [151].

4.3. Integration of recognition elements

4.3.1. Self-assembled monolayer (SAMs) – Au-thiol chemistry

After the Au-deposition (Section 4.1), there are different chemical routes for the immobilization of the recognition elements. One of the most popular methods is the creation of self-assembled monolayers (SAMs) via thiol-Au interaction (Fig. 6(A)) [152–155]. SAMs onto the gold layer can be obtained by immersing the membrane into a solution of a molecule that contains the desired functionality and a thiol group. As an advantage, there is a wide diversity of commercial biomolecules linked by a spacer (a long aliphatic or nucleotide chain) to a terminal thiol group in order to prevent steric hindrance issues (Fig. 6(A)) [152]. This method, mainly characterized by its simplicity and stability provided by thiol-Au interactions, has been used for the attachment of several synthetic and biological molecules into SSNs, such as polymers [156], aliphatic chains [157,158], amino acids [159], DNA [160] and antibodies [161]. In particular, self-assembled monolayers displaying reactive terminal groups have been extensively used to modify surfaces with polymer brushes via surface-initiated polymerization techniques [162–166].

4.3.2. Silanization

The grafting reaction so-called “silanization” has been one of the most common methods for the functionalization of silica surfaces but the findings have been successfully extended to other metal oxides such as ZnO, TiO_2, and Al_2O_3 [12,167]. Organosilanes are a family of compounds with the general formula R_3SiX, R_2SiX_2, or $RSiX_3$, where X is a hydrolyzable group and R is the desired organic group (Fig. 6(B)) [13]. More specifically, the reaction involves the nucleophilic attack of a surface silanol group to the silicon atom of the silane [167]. Experimentally, this protocol usually entails the immersion of a previously cleaned surface into an organic or aqueous solution of the silane [168]. From a synthetic point of view, silanization offers a simple way to obtain organic functionalization in different nanofluidic devices with the high stability provided by the covalent bond. Furthermore, there is a vast library of commercially available silanes, which makes the approach more accessible. Considering the native surface after the nanofabrication, silanization is the most employed method in glass nanopores and membranes created by electrochemical anodization [169].

4.3.3. Carbodiimide chemistry

Carbodiimide chemistry is a common method to covalently couple carboxylic groups with primary amines to create stable amide bonds (Fig. 6(C)). Usually, this method involves a two-step reaction by using N-(3-dimethylaminopropyl)-N′-ethylcarbodiimide (EDC) together with N-hydroxysuccinimide (NHS) or N-hydroxysulphosuccinimide (NHSS) (although pentafluorophenol –PFP- can be used instead of NHS) [12] [13,152,170,171]. While the NHS (or analogues) is not required to perform the cross-linking, its inclusion in the protocol increases the EDC-mediated coupling efficiency [152,167,170]. EDC activates the carboxyl groups onto the surface yielding an unstable amine-reactive intermediate (O-acylisourea). In order to partially stabilize it, NHS (or analogues) reacts with the amine-reactive intermediate to form a semi-stable active ester. This ester group can react with amino groups available in the recognition element to form a stable amide bond and, therefore, to allow its anchoring onto the surface. Experimentally, the protocol is usually carried out by immersing the COOH-containing membrane into an aqueous solution of EDC and NHSS (e.g. 10 mM EDC + 20 mM NHSS) for 20–60 min [13,67]. Then, the membrane is washed and subsequently soaked into a solution that contains the molecular system with the primary amine groups.

Considering the chemical nature of the surface after the nanofabrication, this method is widely used for the functionalization of carboxylate groups in track-etched membranes [71,95,172,173]. In the case of other types of nanofluidic devices such as glass nanopores, -COOH groups can be previously integrated onto the surface (e.g. via silanization reaction) for the subsequent modification with the recognition element via carbodiimide coupling chemistry (Fig. 6(C)) [174]. Moreover, as biomolecules such as proteins, enzymes, and antibodies, usually contain several amino groups in their structures, this method is also widely used for biofunctionalization [152]. For its part, predesigned recognition elements can be synthesized or directly purchased with primary amino groups (e.g. macrocyclic molecules or aptamers) which position this protocol as a straightforward method for the decoration of a wide variety of surfaces. In contrast, there is a lack of control associated with this modification technique which can result in the immobilization of recognition elements in inappropriate or non-functional orientations [170,175,176]. Finally, it is imperative to make an adequate choice of the buffer to be employed to prevent its reaction with the intermediates as well as the optimization of several experimental parameters such as agent concentrations, pH, and reaction time [170,176].

4.3.4. Glutaraldehyde coupling

Glutaraldehyde (OHC-$(CH_2)_3$-CHO) route is a widely employed strategy to covalently immobilize biomolecules containing $-NH_2$ terminal groups into amino-terminated surfaces (Fig. 6(D)) [167,177]. Commercial solutions contain glutaraldehyde in different forms including oligomers that form α,β-unsaturated aldehydes after dehydration [178]. While the exact reaction mechanism remains unclear, the most accepted one involves the Michael addition of $-NH_2$ to α,β-double bonds yielding a stable secondary amine [178]. Experimentally, this method includes the previous activation of the amino-terminated groups of the surface with an aqueous glutaraldehyde solution and the final immersion into the solution that contains the biomolecule to be attached [179]. Added to its simplicity, the improvement in the stability and catalytic features are some of the main advantages of glutaraldehyde coupling [167]. Also, in contrast to carbodiimide coupling chemistry, this protocol introduces a long spacer between the surface and the protein that minimizes steric hindrance issues [167].

Considering that, in general, nanofluidic devices addressed in this review do not contain native $-NH_2$ terminal groups, it is required the previous functionalization of the surface with amino-terminated groups. In the case of SiO_2, Al_2O_3, and TiO_2, this can be easily achieved via surface silanization with (3-aminopropyl)-triethoxysilane (APTES) which position it as a widely employed strategy (Fig. 6(D)) [179–182].

4.3.5. Electrostatic self-assembly

Electrostatic self-assembly of polyelectrolytes and biomolecules constitutes another very simple and versatile method for the functionalization of surfaces (Fig. 6(E)) [183–185]. This method usually entails the immersion of the charged surface into a solution with a polyelectrolyte or biomolecule to be attached to the surface [12,13]. The main requirement for the functionalization is that the macromolecule to be attached contains opposite charged groups to those in the surface [186–188]. Thus, when the surface is in presence of the charged polyelectrolytes or biomolecules, they are adsorbed due to electrostatic attractions [189,190]. The electrostatic self-assembly can be performed by taking advantage of the native charge of the nanofluidic device after the nanofabrication (e.g. negatives charges on glass nanopores, nanopipettes, and track-etched nanochannels) or after the surface modification via silanization with APTES (e.g. in the case of AAO membranes) [77,85,138,191,192]. Also, the application of an external electric field during the modification can accelerate the immobilization process [193]. It is worth mentioning that, considering the size of polyelectrolytes, nanoconfinement effects play a central role during the derivatization of nanocurved structures via electrostatic self-assembly. For this reason, different variables such as pH, ionic strength, channel size, and polyelectrolyte molecular weight have to be carefully optimized in order to obtain a homogeneous film [194,195].

Interestingly, the adsorption of a polyelectrolyte inverts the surface charge which allows the subsequent modification with a different molecular system (e.g. another polyelectrolyte or biomolecule) with an opposite charge to that of the polyelectrolyte (Fig. 6(E)) [61]. This protocol called layer-by-layer (LbL) self-assembly was firstly introduced by Decher in flat surfaces and also constitutes a popular strategy for the functionalization of nanochannels [77,193,196–198]. In a similar way to electrostatic self-assembly, the LbL approach is also drastically affected by nanoconfinement effects [77,191,199,200]. For instance, some authors have found that the growth of an LbL film is limited by the channel size [191,199,201]. When the film thickness reaches values comparable to the channel size, the LbL assembly is saturated due to the impediment of polyelectrolytes to further infiltrate into the channel [199,200]. This effect is accompanied by the gradual loss of overcompensation of the charge after each step [77].

Finally, while these methods based on non-covalent interactions are very simple and versatile, the stability of the final film may be worse than that provided by covalent bonds.

5. Ion sensing platforms based on biomimetic nanochannels

Ions in living organisms play an important role in maintaining normal physiological conditions and regulating several biological processes including muscle function and nerve impulse [15]. Also, in some cases, disturbances in the ion concentration in the human body can cause serious health disorders [202–204]. For these reasons, the quantification of ion concentration in different samples such as human fluids, effluents, water, and food, has gained significant interest [205–207]. However, the low ion concentrations and the complexity of biological fluids turn ion monitoring and quantification into a great challenge. In this context, the design of ion-selective (bio)sensors based on solid-state nanochannels has emerged as a suitable and low-cost alternative to tackle this aim.

As mentioned above, sensing with nanochannels by steady-state measurement requires the analyte to promote changes in the physicochemical properties of the nanochannel such as surface charge or effective diameter. The main challenge of this approach is the selection of an ion recognition element that can be used to decorate the nanochannel surface and at the same time provide high sensitivity, selectivity, stability, and reproducibility. The following section focuses on various strategies that have recently been reported for the development of ion sensing platforms based on SSNs.

5.1. Ion detection via host-guest supramolecular interactions

In order to create sensing nanochannels based on the capture of target ions, the inner channel surface has to be functionalized with a suitable recognition element (key-lock principle). In this regard, crown ethers, calixarenes, and pillarenes are attractive options due to their high selectivity, chemical stability, and easy integration onto the nanochannel's surface [208]. The ion selectivity of these supramolecular host compounds relies on a complex relationship between the cavity and the size of the ion to be captured [209,210]. In the nanofluidic field, seminal works by different groups have demonstrated that crown ethers in combination with track-etched nanochannels can be used to establish robust and selective ion-responsive nanodevices. Pérez-Mitta et al. described the construction of a K^+-responsive system based on the modification of a bullet-shaped PET nanochannel with 4′-aminobenzo-18-crown-6 (or 18-crown-6 units) [67]. The attachment of the crown ether onto the nanochannel surface was accomplished by the well-known N-(3-dimethylaminopropyl)-N′-ethylcarbodiimide (EDC)/N-hydroxysulfosuccinimide (NHSS) coupling reaction. Supported by Poisson-Nernst-Planck (PNP) simulations and evidenced through the iontronic response, the system displayed a programmable surface charge density by modulating the K^+ concentration. Furthermore, the 18-crown-6 units-modified channels showed good selectivity towards potassium ions in comparison with other alkaline metals. Lei Jiang and coworkers developed a similar design to create a K^+-responsive nanochannel by functionalizing conical-shaped channels with 18-crown-6 units. By replacing the 18-crown-6 units with 15-crown-5 units, they developed a Na^+ selective and highly sensitive system [211]. They demonstrated that by changing the cavity size of the crown compound, a wide variety of target ions can be captured [69,212–215]. These results illustrate the great potential of crown ether-modified nanochannels for sensing nanofluidic devices. Since then, several other host-guest supramolecular combinations were exploited as ion-responsive systems; some of them are described below.

K^+-responsive channel. Wu et al. reported a K^+-responsive system based on the crosslinking of 4′-aminobenzo-18-crown-6 into a funnel-shaped PET single nanochannel (Fig. 7) [216]. They showed that the previous exposition of the modified channel to a K^+ solution promotes the potassium immobilization into the cavity which alters both the surface charge density and wettability of the channel. Concomitantly, the iontronic output is modified even when the measurement is carried out in the absence of K^+ ions (Fig. 7(B)). Then, the application of transmembrane voltage around 4 V stimulates the release of adsorbed potassium and the system recovers the initial condition (Fig. 7(C)). Besides the capability to bind potassium cations in a highly sensitive way (even at 10^{-15} M), this system showed good reversibility as well as a voltage-gated response. This makes it an interesting candidate for potential applications in fields such as sensing and drug release.

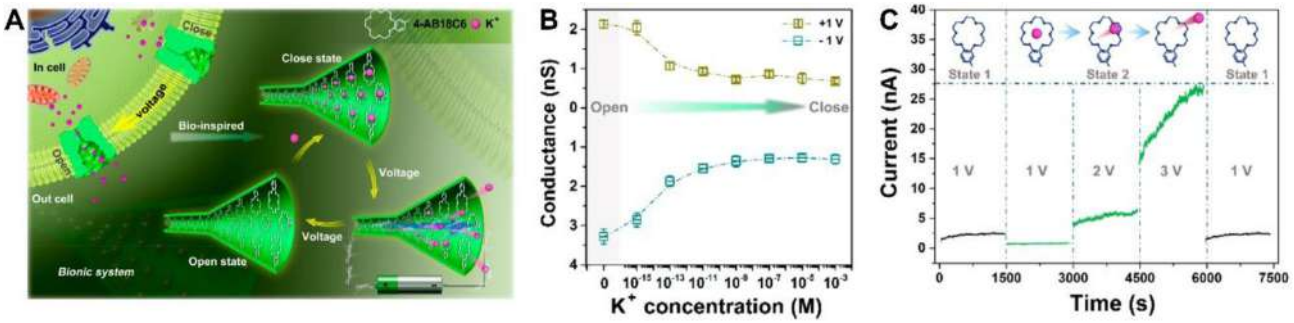

Fig. 7. **(A)** Scheme of ion channels in a biological cell (left) and a bioinspired synthetic membrane (right) with an illustration of the K^+-responsiveness of the crown ether-modified channel. **(B)** Conductance of single nanochannel at +1 and −1 V as a function of the concentration of the KCl electrolyte. **(C)** Ion currents at the different transmembrane voltages as a function of time. The cartoon illustrates the dependence of capture and release of K^+ with transmembrane voltage. Reproduced with permission from Ref. [216]. Copyright © 2017, American Chemical Society.

Ali et al. presented the development of a K^+-responsive channel by the covalent attachment of a predesigned amine-terminated bispodand (acyclic polyether) moiety (pseudo-crown ether group) into a conical PET nanochannel [217]. While this recognition element differs from the preformed crown ether, the final structure generates a similar ion-specific cavity that allows a supramolecular host-guest interaction in the nanochannel. The system exhibited a selective and stable response towards K^+ ions in the concentration range from 10 μM to 100 mM. Furthermore, they showed that the presence of K^+ during the synthesis of the pseudo-crown ether group is crucial for the building up of the K^+ recognition cavity. Similar strategies were employed for the development of Li^+, Cs^+, and Pb^{2+} selective sensing platforms [69,212–215].

Hg^{2+}-responsive channel. Zhang et al. developed a Hg^{2+}-tunable ion gating mechanism in a conical PET nanochannel decorated with mercaptoacetic acidpillar [5]arene (MAP5) [218]. For this aim, they first crosslinked 1,6-hexanediamine (HDA) to the channel surface by carbodiimide coupling chemistry. The HDA-modified channel exhibited a positive surface charge with current rectifying behavior ascribed to the presence of amine groups of HDA. Then, the predesigned MAP5 was anchored on the HAD-modified surface by exploiting the molecular recognition interactions between the amine groups and MAP5. The attachment of MAP5 led to an inversion in the diode-like behavior owing to the negative charge of the pillarene. The exposition of the MAP5/HDA-modified channel to 10 μM Hg^{2+} promoted the formation of Hg^{2+}-MAP5 complexes yielding a subsequent release of MAP5 from the channel. This fact was attributed to the preference of MAP5 towards Hg^{2+} ions instead of the alkylamine groups. Concomitantly, the response in the presence of Hg^{2+} displayed a remarkable decrease in the ionic current (ion gating) attributable to the partial loss of negative surface charges. Finally, this system showed both high selectivity to Hg^{2+} ions and a reversible behavior by alternating the exposition to MAP5 and Hg^{2+} solutions.

Pyrophosphate (PPi)-responsive channel. Zhu et al. developed a PPi-modulated nanofluidic device by introducing an isoniazid functionalized calix [4]arene (C4NP) into a conical nanochannel in polyimide [219]. Firstly, the channel surface was modified with azide-propylamine via EDC/NHS reaction, and afterward, the predesigned recognition element C4NP was attached to the surface through copper-catalyzed azide-alkyne click chemistry. The successful modification of each step was evidenced by recording the *I*–*V* curves. In this regard, the attachment of C4NP onto the surface led to a loss of negative surface charge and, concomitantly, a decrease in the ionic current. However, the exposition of modified-channel to PPi in the range of concentration from 10 nM to 1 mM caused a remarkable increment in the rectification which was ascribed to the increment of the negative surface charge due to the formation of C4NP-PPi complexes. Moreover, by exploiting the supramolecular host-guest interaction between C4NP and PPi, the system exhibited a highly selective response toward PPi in the presence of other analytes such as $H_2PO_4^-$, ATP, and ADP.

5.2. Ion detection by biofunctionalized nanochannels

As mentioned, the appropriate selection of ion recognition elements is crucial to develop a sensor with the desired selectivity, sensibility, and robustness. In this context, surface functionalization with biological compounds such as DNA, RNA, enzymes, proteins, aptamers, antibodies, among others, has attracted attention because they provide: (1) a specific recognition of target analytes, (2) high efficiency for specific coupled reactions, as it is the case of enzymes, and (3) the possibility of promoting a signal amplification by combining biomolecular systems and nanotechnology [25]. The synergistic combination of the capability of biological macromolecules to bind/react with specific analytes and the inherent properties of signal amplification of solid-state nanochannels can be a key in the development of biosensors transferable to technological devices [220].

Given this scenario, the following subsections describe some of the most relevant advances in the development of ion sensors based on biofunctionalized nanochannels [47,180,221–224].

Cu^{2+}-responsive channel. Chen et al. combined a specific Cu^{2+}-induced self-cleaving DNAzyme with a conical PET multi-nanochannel membrane in order to build a nanofluidic device with Cu^{2+}-modulated ion transport properties [221]. This system was constructed by grafting to the nanochannel surface a short DNA sequence (DNA(2)) which is partially complementary to DNAzyme (DNA(1)) and, therefore, partially hybridizes DNA(1) to form a double-stranded DNA (dsDNA). The selected DNAzyme is endowed with a Cu^{2+} activated self-cleaving site. Besides allowing to attach the DNA(1) to the nanochannel wall, DNA(2) prevents DNA(1) from spontaneous cleavage and excessive folding. The modified channel showed a diode-like behavior characterized by a negative surface charge which was ascribed to the high negative charge provided by dsDNA. However, the exposition to Cu^{2+} promoted a break of DNA(1) into three fragments and its subsequent dissolution, which triggered a remarkable decrease in surface charge density. These facts resulted in a decrease in the rectification factor for concentrations of Cu^{2+} between 10 nM and 1 mM. Furthermore, the system displayed a selective response to Cu^{2+} compared with other divalent cations. A similar strategy based on the integration of a DNAzyme onto the channel walls was reported for the development of a Zn^{2+} sensor.

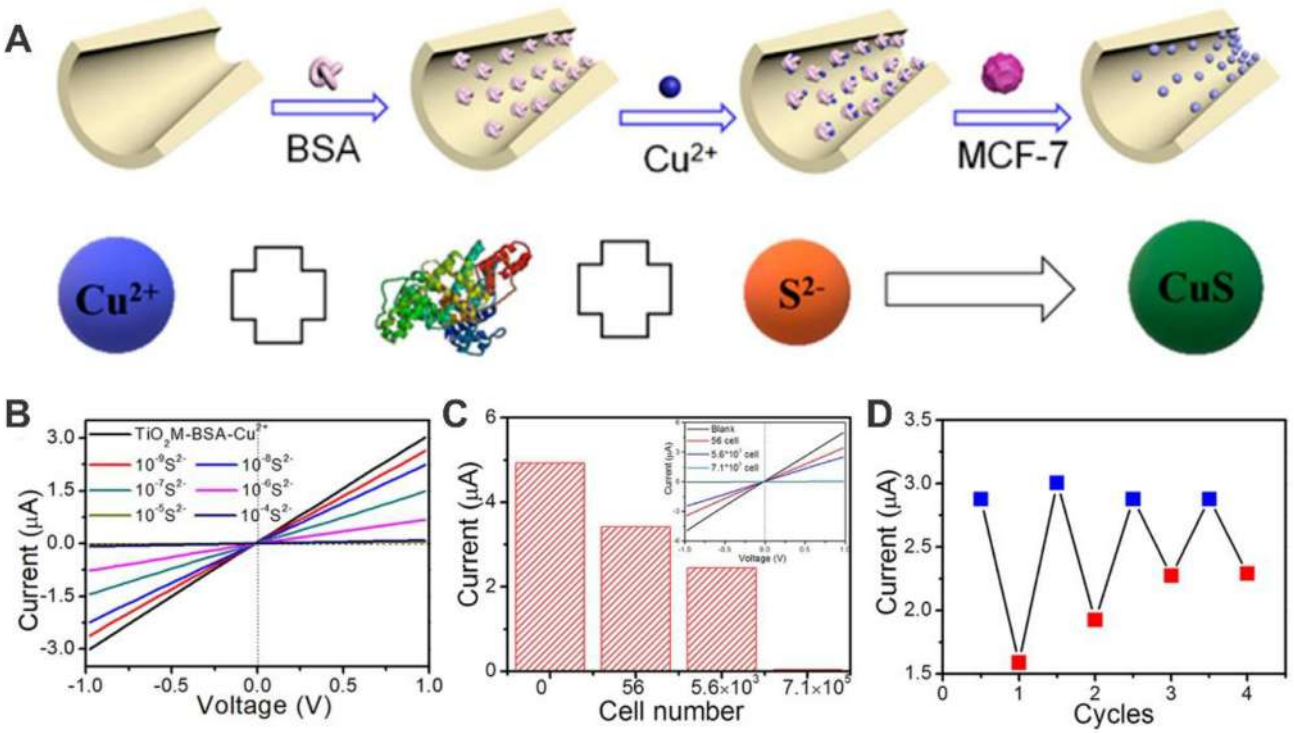

Fig. 8. **(A)** Schematic illustration of each functionalization step of sulfide-responsive nanodevice. **(B)** *I*–*V* curves at different sulfide concentrations. **(C)** Transmembrane current at +1 V for different cell numbers. **(D)** Switchability test of sulfide-responsive nanodevice. Reproduced with permission from Ref. [47]. Copyright © 2019, American Chemical Society.

S^{2-}-responsive channel. Guo et al. reported a sulfide-responsive system based on the generation of CuS precipitates in TiO_2 nanochannel arrays biofunctionalized with bovine serum albumin (BSA) (Fig. 8(A)) [47]. The BSA was stabilized on the channel surface by the bidentate interaction between hydroxyl groups of TiO_2 and carboxyl groups of BSA. The anchored BSA protein allowed the subsequent immobilization of Cu^{2+} ions via electrostatic interaction. In the presence of S^{2-}, the biomineralization of BSA molecules is triggered by the reaction between Cu^{2+} and S^{2-} to form CuS precipitates. CuS nanocrystals generate a partial occlusion of the channel yielding a decrease in the transmembrane current. The system exhibited a selective S^{2-} response in the wide concentration range from 1 nM to 0.1 mM (Fig. 8(B)). Moreover, the re-dissolution of CuS crystal in acidic media allowed sensor reusability. Considering that the accumulation of H_2S is one feature of tumor cells, the authors evaluated the potential application of this sensor in tumor diagnosis [225]. Results showed that the nanofluidic device was useful for the detection of H_2S released by MCF-7 tumor cells (limit of detection was 56 cells) with reusability of four cycles (Fig. 8(C) and (D)).

$O_2{}^{*-}$-responsive channel. Pourmand and coworkers reported the development of a highly selective superoxide radical sensor ($O_2{}^{*-}$) based on the covalent immobilization of the hemeprotein Cytochrome c (Cyt c) on the surface of a quartz nanopipette [226]. In order to attach the Cyt c, the nanopipette was firstly modified with (3-aminopropyl) triethoxysilane (APTES). Then, the amine groups present in APTES were used as binding sites for the Cyt c. The Cyt c-modified nanopipette exhibited a rectifying behavior ascribed to the asymmetry and the negative charges provided by the hemeprotein at physiological pH. In the presence of reactive oxygen species in the range of 0.2 μM–1.6 μM, the Fe^{3+} contained in the Cyt c was reduced to Fe^{2+} increasing the magnitude of the negative surface charge, which led to an enlargement in the rectification factor. Under this configuration, the system proved its capability to sense the changes in $O_2{}^{*-}$ levels in breast epithelial cells after different biochemical manipulations. Importantly, the device maintained 80% of its response capability after a 30-days storage period at 4°C in dark conditions.

5.3. Other molecular mechanisms for ion detection

The following subsection reviews some of the recent works that describe the development of ion-responsive systems based on functionalized nanochannels with artificial ion recognition elements that do not operate by a host-guest specific interaction [227,228]. Due to the diversity of reported strategies, it is appropriate to divide this section according to the interaction type between the ion recognition element and the target ion, as follows: (1) non-covalent binding [129,229] [–] [237], (2) covalent binding [238], and (3) cleavage promoted by the analyte.

5.3.1. Ion detection via non-covalent binding

Cu^{2+}-responsive channel. Zhao et al. presented a Cu^{2+} sensor based on a nanochannel array of AAO functionalized with polyglutamic acid (PGA) by physical adsorption [129]. Due to the asymmetric structure and the negative charge of PGA, the system exhibited a rectifying behavior characterized by high and low conductance branches at −1 and +1 V, respectively. The addition of Cu^{2+} ions in the concentration range from 0.3 fM to 20 mM promoted the formation of Cu^{2+}-PGA complexes that generated a decrease in the negative charge of the surface and, concomitantly, a diminution in the rectification factor. Also, the Cu^{2+}-PGA complex could be dissociated through the exposition of the array to acidic pH which allowed the reusability of the device. The sensor not only enabled a selective detection of Cu^{2+} in aqueous solutions but also displayed a successful Cu^{2+}-response in a complex matrix such as human blood.

UO^{2+}-responsive channel. More recently, an ultra-trace uranyl (UO^{2+}) sensor based on 4-Amino Benzamidoxime (ABX)-modified

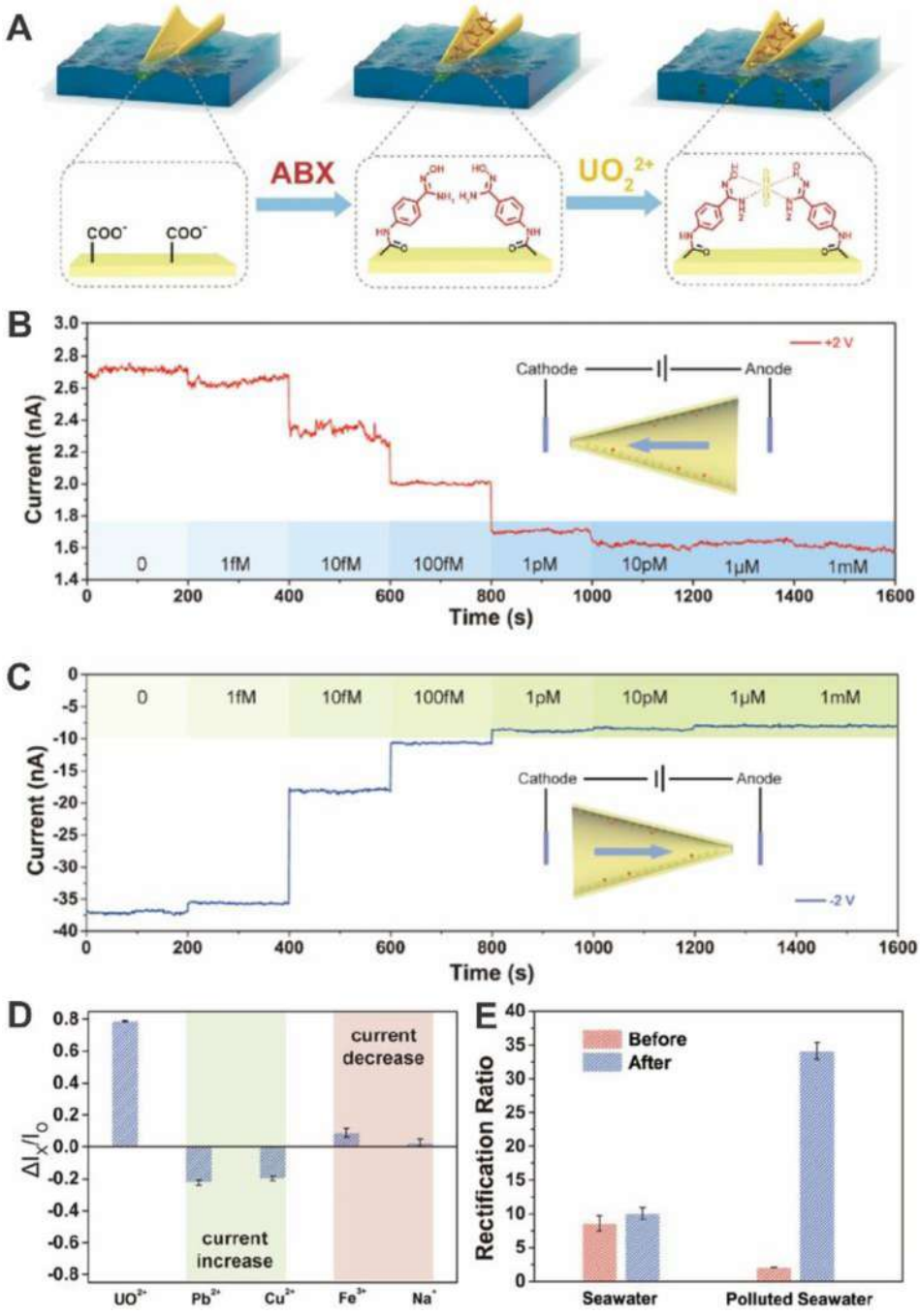

Fig. 9. **(A)** Nanochannel surface functionalization with ABX, and subsequent UO_2^{2+} ion complexation. Chronoamperometry at +2 V **(B)** and −2 V **(C)** for different UO_2^{2+} ion concentrations. **(D)** Relative increase or decrease of ion current in the presence of different cations. **(E)** Rectification ratio before and after exposition to seawater and to UO_2^{2+}-polluted seawater (1 mM). The device was able to detect UO_2^+ in a complex matrix such as polluted seawater. Reproduced with permissions from Ref. [239]. Copyright © 2019 American Chemical Society.

conical PI nanochannel was reported [239]. In a first step, the ABX was crosslinked onto the nanochannel surface by EDC/NHS chemistry leading to a rectifying behavior due to the asymmetric geometry and the negatively charged surface (Fig. 9(A)). The subsequent exposition to UO^{2+} in the range of concentrations from 1 fM to 1 mM at pH = 5 triggered a decrease in the transmembrane current with increasing uranyl concentration (Fig. 9(B) and (C)). Supported by contact angle and zeta-potential measurements, this behavior was ascribed to an increment in the hydrophobicity promoted by UO^{2+} complexation. Furthermore, the exposure to tartaric acid allowed the removal of UO^{2+} adsorbed on the channel surface which made it possible to obtain a reversible current switching. Also, the system revealed a selective behavior towards UO^{2+} regarding other positive ions such as Pb^{2+}, Cu^{2+}, Fe^{3+}, and Na^+ (Fig. 9(D)). Additional experiments showed that this system is able to respond to the target analyte even in a complex matrix such as seawater (Fig. 9(E)). Besides the application of this system in the field of sensor technology, the device demonstrated the ability to

remove UO^{2+} ions from samples contaminated with uranyl, which facilitates the spreading and proliferation of mesenchymal stem cells in UO^{2+} polluted environments, conferring additional importance about its usefulness.

5.3.2. Ion detection via covalent binding

Although this is not the most common strategy, in recent years, some authors have presented ion-responsive platforms in which the interaction between the recognition element and target ion is based on covalent bonding. This strategy leads to stronger and stable bonds but it reduces the possibility of sensor reusability. The following cases correspond to systems using the covalent attachment strategy as recognition and binding mechanism for biosensing.

NO_2^--responsive channel. In 2018 Lei Jiang and coworkers presented a nanochannel with ionic transport modulated by NO_2^- [240]. In the first step, the surface of a single conical PET nanochannel was modified with p-phenylenediamine (p-PD). The p-PD-modified channel displayed a rectifying behavior induced by the asymmetric geometry and the positive charge provided by the amine groups of the p-PD. The subsequent exposition to 10 nM NO_2^- at pH = 3 reverted the rectifying behavior indicating an inversion of surface charge polarity. This effect was explained by the diazotization reaction between the amine group of p-PD and NO_2^- to form neutral hydroxide of phenyldiazonium and the presence of residual carboxylate groups on the surface of PET (Fig. 10(A)). The response showed a dependence on the NO_2^- concentration in the range from 10 pM to 100 nM. Also, the presence of other anions as phosphate, sulfate, and sulfite did not cause

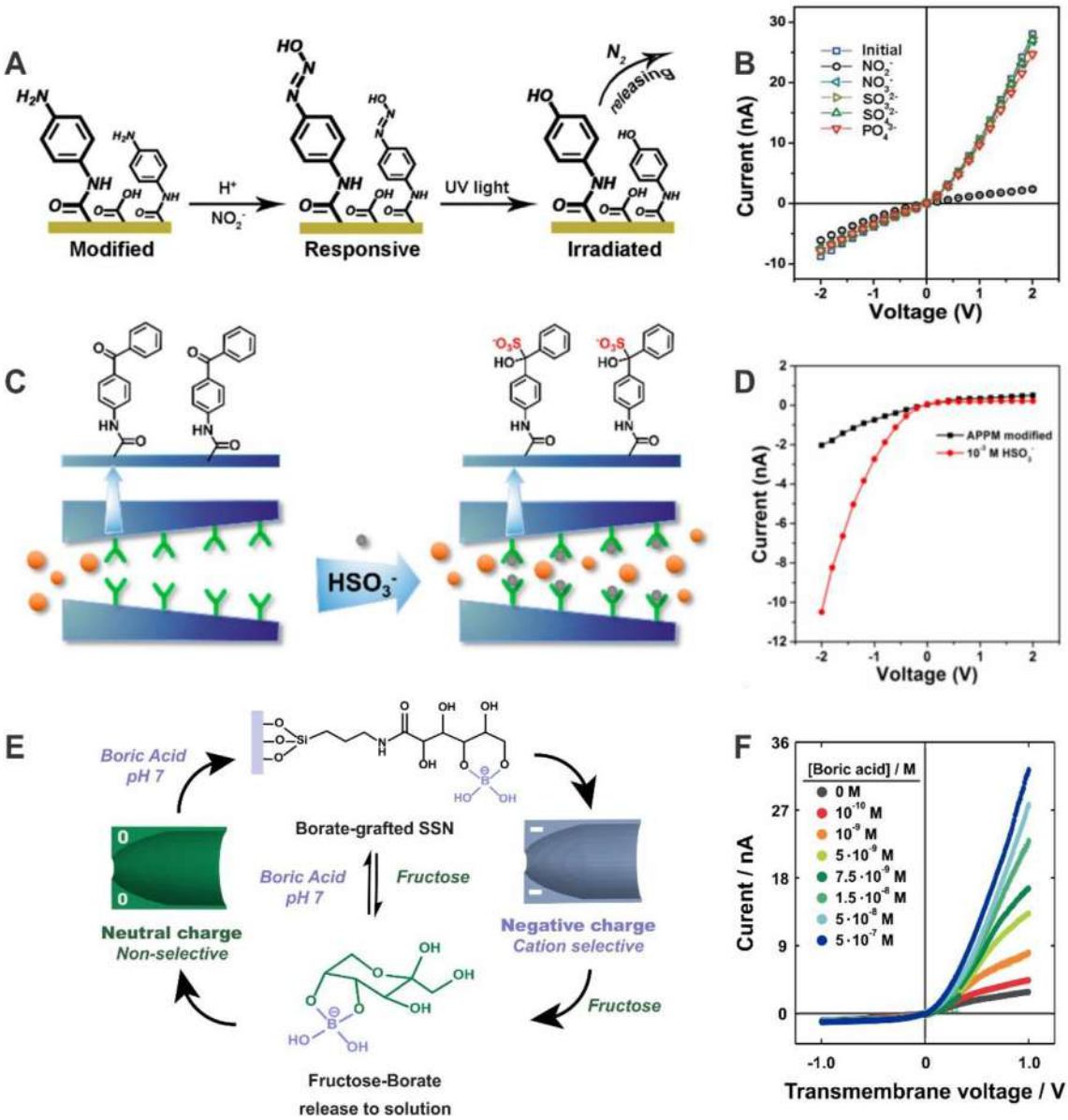

Fig. 10. **(A)** Sensing mechanism for the NO_2-responsive channel. **(B)** *I–V* curves in the presence of different anions. The device displayed a selective response towards NO_2. Reproduced with permissions from Ref. [240]. Copyright © 2018 American Chemical Society. **(C)** Sensing mechanism for HSO_3^- in APPM-modified channel. **(D)** *I–V* curves in the absence and presence (1 mM) of the analyte for APPM-modified channel. Reproduced with permissions from Ref. [241]. Copyright © 2020 American Chemical Society. **(E)** Sensing mechanism for the borate-responsive channel. Subsequent exposition to fructose led to the release of borate anions allowing the reusability of the sensor. **(F)** *I–V* curves for different borate ion concentrations. Reproduced from Refs. [145,239] with permission from the Royal Society of Chemistry.

significant changes in the iontronic response (Fig. 10(B)). Finally, when exposed to UV light the system proved to be useful for the harmless conversion of NO_2^- into N_2.

HSO_3^--responsive channel. Chen et al. developed a platform for sensing and removing bisulfite based on the modification of a single conical PET nanochannel with 4-aminophenyl-phenyl-Methanone (APPM) (Fig. 10(C)) [241]. For this aim, the APPM was immobilized onto the nanochannel surface by a traditional EDC/PFP conjugation reaction. The response of the APPM-modified channel was characterized by a non-ohmic behavior with low transmembrane currents (OFF state) which was attributed to the low charge state and hydrophobicity of APPM. The hydrophobicity argument was supported by contact angle measurements showing increased angles after APPM-functionalization. The exposition of the APPM-modified membrane to HSO_3^- solution generated a remarkable increment in the rectification ratio and the gating ratio (ON state) for bisulfite concentrations going from 1 μM to 1 mM (Fig. 10(D)). Supported by PNP simulations, this fact was ascribed to the increase of the negative surface charge and hydrophilicity because of the covalent binding of HSO_3^- to the ketone group of the APPM-modified surface (Fig. 10(C)). The sensing platform evidenced a selective response. Also, owing to the reversible character of this nucleophilic reaction, the HSO_3^- could be removed by exposing the HSO_3^--APPM-modified channel to an acid solution. By adding reconditioning steps, the device displayed a reversible response. Besides the sensing capability, this system exhibited good performance for removing bisulfite excess in living L02 cells.

Borate-detection nanosensor. Another functionalization method for producing responsive nanochannels is based on the atomic layer deposition (ALD) technique [144]. In recent work, the glycosylation of a SiO_2-coated PET nanochannel for the detection of borate anions was obtained by combining both track-etched and ALD technologies [145]. The etched-nanochannel surface was coated with silica (SiO_2) by ALD and subsequently functionalized with N-(3-triethoxysilylpropyl)-gluconamide (silanization reaction) in order to obtain a glycosylated channel (PET/SiO_2/Glu). In the presence of borate ions, a negative surface charge is induced by sugar-borate complexation, leading to modulations of the ionic transport (Fig. 10(E)). Initially, the PET/SiO_2 nanochannel is negatively charged due to silanol groups on the surface (cation-selective channel). After silanization, the glycosylated (PET/SiO_2/Glu) channel presents a neutral surface (non-selective behavior). Then, the exposition of PET/SiO_2/Glu to a boric acid solution at pH 7 promoted the formation of negatively charged sugar-borate complexes and the nanochannel recovered the initial rectification state (cation-selective) (Fig. 10(F)). The borate-responsiveness was explained by a binding model that describes the interaction between the glycol groups on the nanochannel walls and borate anions, which satisfactorily fitted the dependence of the rectification factors on borate concentration. Finally, the nanodevice exhibited a reversible response towards borate/fructose exposition cycles since the fructose competition with the glycosylated surface allowed the release of the complexed borate anions (Fig. 10(E)). Additionally, the system was highly selective compared with other relevant anions such as phosphate, sulfate, and nitrate.

5.3.3. Ion detection via induced cleavage

Similar to the DNAzymes, it is possible to create a fully abiotic sensing platform based on the cleavage of the recognition element induced by the target ion. Within this framework, Ali et al. developed an F^--responsive channel based on a single PET conical nanochannel modified with protected fluorescein (Fcn) [242]. The hydroxyl groups of amine-terminated fluorescein were first protected by tert-butyldiphenylsilyl (TBDPS) moieties to form Fcn-TBDPS—NH_2 and then covalently attached to the channel surface through the amine group via EDC/PFP chemistry (PET/Fcn-TBDPS). After modification, the channel exhibited a *quasi-ohmic* behavior with a low transmembrane conductance due to the low surface charge density of PET/Fcn-TBDPS. However, the addition of F^- promoted the cleavage of the Fcn-TBDPS surface groups in the Si—O bonds and the subsequent removal of F-TBDPS groups from the channel. This process brings carboxyl and hydroxyl groups onto the surface, which induced an increment in the negative surface charge density and, concomitantly, in the rectification factor. Furthermore, the sensing platform exhibited a selective response to F^- compared with other monovalent and divalent anions such as Cl^-, Br^-, I^- and SO_4^{2-}.

6. Gas sensing platforms based on biomimetic nanochannels

CO_2. Carbon dioxide (CO_2) in the atmosphere is one of the most important sensory cues for many animals and insects [243,244]. Mosquitoes, for example, can locate and navigate their hosts even at night by detecting CO_2 with odorant-gated ion channels in their olfactory sensory neurons (OSNs) [245—248]. Therefore, the design and construction of biomimetic CO_2-driven ionic gates with high performance in sensitivity and selectivity are still highly in demand. In this context, Shang et al. developed an OSNs-mimetic CO_2-driven ionic gate by combining a single conical PI nanochannel with the CO_2-responsive APTE (1-(4-amino-phenyl)-2,2,2-trifluoro-ethanone) molecules via NHSS/EDC chemistry [245]. The APTE modification on the inner walls practically neutralizes the negative surface charge of etched PI and increases the hydrophobicity, yielding a hindrance of the ionic transport, resulting in an OFF state. However, when CO_2 is bubbled in the electrolytic solution, it partially produces carbonate, which coordinates with molecules of APTE, leading to a negative charge in the surface of the nanochannels and restoring the initial diode-like behavior (ON state). Consequently, the channel becomes hydrophilic and cation-selective. These results indicate that CO_2 can efficiently switch the charge state of APTE-modified nanochannel from the OFF state to the ON state. Also, the high selectivity of the ionic gate induced by CO_2 was successfully proved by control experiments with different kinds of gases. Finally, the biomimetic CO_2-driven ionic gate exhibited both switchability and stabilized reversibility by the addition and removal of CO_2.

NO. Accumulating evidence indicates that nitric oxide (NO) is an important signaling agent involved in various biological processes by regulating ion flux across cell membrane channels [249,250]. Recently, Han et al. fabricated an artificial NO-responsive nanofluidic sensor that exhibited high NO specificity and sensitivity through the cyclization reaction of aromatic diamines in the presence of NO [251]. The NO-responsive nanosensor was prepared from the immobilization of 2,3-diaminobenzene acid (ABA) in a single PET conical nanochannel. Initially, the unmodified nanochannel was negatively charged owing to the presence of carboxylate groups on the surface, causing ion current rectification (cation-selective surface). When ethylenediamine (EA) was immobilized on the nanochannels, the surface became positively charged (anion-selective), causing an evident change in the rectifying features. After neutral ABA was conjugated with the $-NH_2$ group of EA by coupling chemistry, the positive charge of the channel walls decreased and, in consequence, the iontronic response displayed a diminution in the ion current rectification. When the modified channel is exposed to NO (produced *in situ* by reaction between HNO_2 and H_2SO_4), the $-NH_2$ groups of ABA react to form benzotriazol derivatives through the cyclization reaction which generates changes in the surface charge density. This fact allowed the study by conductometric measurements as it affected both the ion rectification and gating

properties. Finally, this system exhibited high selectivity, excellent stability, and a fast response rate.

Also, Lei Ge et al. designed a switchable NO-responsive PET-nanochannel platform by exploiting a reversible N-nitrosation reaction of rhodamine 6G (R6G) inside multipore membranes [252]. In order to immobilize R6G on the nanochannels surface by self-assembly, amino-3A-deoxy-(2AS, 3AS)-beta-cyclodextrin (NH_2-β-CD) as an intermediate was grafted into the nanochannels to include R6G because of its hydrophobic cavity and hydrophilic external surface. R6G acts as a ligand and it can readily react with NO through the N-nitrosation reaction. This reaction between the aromatic secondary amine and NO can be regulated by UV light. As a result, the ion transport could realize reversible switching in the presence of NO and UV light. When NO binds to the R6G assembled in the nanochannels, the surface charge increases due to the reduction of proton binding ability of R6G yielding a high ionic current (ON state). After exposition to UV light, the nanochannels release NO and turn into the OFF state with a lower surface charge and a low ionic current. The nanodevice exhibited high sensitivity (detection limit of 35.3 fM) and selectivity towards NO over other gas molecules and biomolecules. More interestingly, the system also showed good performances for *in situ* monitoring of NO released from human umbilical vein endothelial cells.

HCHO. Formaldehyde (HCHO) is a highly volatile aldehyde widely used in wood-based materials employed in construction and furniture production. Considering that this agent promotes undesirable effects on human health such as cancer, damage to the central nervous system and irritation on noise and eyes, the creation of a sensing platform capable to detect and remove HCHO from the environment is highly desirable [253,254]. In 2019, Wu et al. reported the development of a formaldehyde sensor based on a conical multichannel PET membrane modified with ethylenediamine (EDA) [255]. The recognition element EDA was attached to the channel surface by EDC/NHSS coupling reaction giving rise to an amino-terminated surface. In presence of HCHO, a nucleophilic addition reaction is produced between the HCHO and the surface amino groups yielding an imino-terminated surface. This change in the chemical nature of the surface promotes a decrease in the hydrophilicity of the channel surface, and consequently, a diminution in the ion current. By exploiting this nucleophilic addition reaction, the device was able to selectively detect HCHO in the concentration range of $10^{-9} - 10^{-6}$ mg/ml. Furthermore, immunofluorescence analysis of meschenchymal stem cells grown in HCHO media indicated that this platform can significantly remove the analyte from the environment.

7. Sensing of nucleic acids, proteins, and cells via integration of biomolecular architectures into nanochannels

7.1. Nucleic acids sensing

The integration of DNA into solid-state nanochannels to build artificial ion channels was first reported by Martin and co-workers early in 2004 [160]. In this seminal work, Harrell et al. presented the construction of single conically-shaped PC-based nanochannels coated with a thin layer of gold in order to adjust the tip diameter and offer an appropriate surface for functionalization. Single-stranded DNA molecules of different lengths were covalently attached to the gold surface. In contrast to DNA-free devices, the DNA-containing nanochannels rectified the ion current displaying an ON-state at negative transmembrane potentials and an OFF state at positive potentials. The authors proposed that the current rectification in presence of a DNA-surface required the electrophoretic insertion of the DNA chains into (OFF state) and out of (ON state) the channel depending on the polarization of the transmembrane potential, yielding a marked diode-like behavior. As a result of their investigations, the authors demonstrated that the extent of rectification could be regulated precisely by either a simple biochemical method (varying the DNA chain length) or a simple physical method (varying the nanochannel mouth diameter).

Since then, many efforts have been devoted to the integration of DNA architectures into solid-state nanochannels in order to achieve the detection of not only nucleic acid molecules but also ions and small molecules, as pointed out in previous sections. This section is focused on the state of the art of nucleic acid-sensing with solid-state nanochannels. All devices reviewed in this section rely on the hybridization strategy as the recognition and binding mechanism. Hybridization is the process by which a synthetic DNA probe or primer binds via Watson–Crick base pairing to a biological DNA target sequence [256]. Nowadays this process is the basis of many DNA analysis and diagnostic techniques because of its simplicity and robustness. However, in many cases, it has to be combined with amplification techniques in order to increase sensitivity [256]. In 2005, Vlassiouk et al. reported for the first time the use of hybridization as a strategy to detect target DNA with AAO membranes [257]. Since then, many examples of nucleic acid sensors based on a hybridization mechanism in different types of nanochannels have been reported, some of which are presented here.

7.1.1. Single-stranded DNA/RNA sensing

Sun et al. developed nanofluidic channels for label-free, ultrasensitive, and highly sequence-specific detection of DNA (Fig. 11) [258]. In this case, the DNA probe oligonucleotides were immobilized by self-assembly on PEI-modified conical track-etched PET nanochannels. Then, BSA was adsorbed in order to avoid further non-specific interactions with other negatively charged analytes (Fig. 11(A) and (B)). After that, DNA detection was assessed by monitoring the rectification efficiency of the diode-like iontronic behavior upon hybridization. The as-prepared nanochannels presented a near ohmic behavior due to their almost zero surface charge. The authors also showed a strong increment in the rectification efficiency caused by increasing the target complementary DNA sequence concentration. The increased rectification is due to the increment in the net surface charge, yielding a binding-type dependency of the rectification factor on the target concentration (Fig. 11(C)). The detection limit of this nanochannel sensor was 10 fM for target DNA. A remarkable feature of the device is its ability to discriminate complementary DNA (c-DNA) from non-complementary DNA (nc-DNA) and one-base mismatched DNA (1bm-DNA) samples with high specificity (Fig. 11(D) and (E)), even in real serum samples.

In general, the processes that mediate target recognition and signal transduction in biosensors are commonly based on different mechanisms [259]. In 2004 Dirks and Pierce discovered how binding of DNA to a substrate could accomplish both the role of recognition and signal amplification without external input [260]. They introduced the concept of Hybridization Chain Reaction (HCR), in which stable DNA monomers (hairpins H1 and H2) assemble only upon exposition to a target single-stranded DNA fragment. Hairpins act as monomer DNA building blocks that hybridize only when an initiator strand (target DNA) triggers a polymerization reaction into a nicked double helix. Moreover, the amplification of the initiator recognition event continues until H1 or H2 is completely consumed. Since its discovery, HCR represents a powerful technique as it allows the possibility of constructing biosensors solely from unmodified single-stranded DNA (or RNA). At the same time, it introduced the concept of triggered DNA-self-assembly into DNA nanostructures.

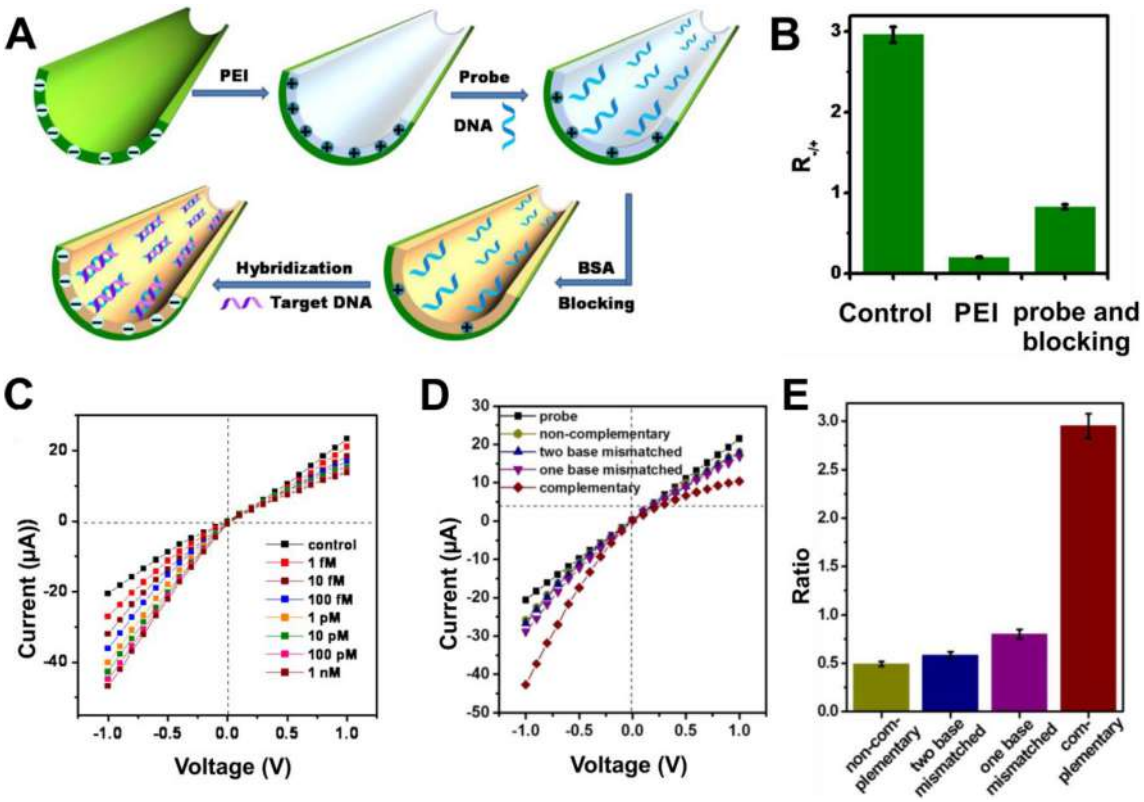

Fig. 11. **(A)** Schematic illustration of the probe DNA functionalized nanochannel biosensor for DNA detection. **(B)** Rectifying characteristics of the layer by layer assembly process on the conical nanochannel ($R_{-/+}$ is defined as the absolute value of the current at −1 V divided by the current at +1 V). **(C)** *I*–*V* curves of the nanochannel biosensor hybridized with c-DNA at a series of concentrations (1 fM–1 nM). **(D)** *I*–*V* curves of the nanochannels after being treated with 1 nM nc-DNA, 2bm-DNA, 1bm-DNA, and c-DNA for 1 h at 37°C, respectively. In this experiment, 0.1 M KCl, pH 7.0 acted as the control (black line), and **(E)** R−/+change ratios measured in 0.1 M KCl pH 7.0 of the modified nanochannel in the presence of 1 nM concentration of the above DNA strands. Reproduced with permission [258]. Copyright 2016, Elsevier.

Within this framework, Zhao et al. developed a DNA biosensor based on HCR in a label-free porous AAO membrane [261]. As the AAO membrane possesses symmetric cylindrical nanochannels, the approach was based on the measurement of ionic current decrease across the nanochannel membrane due to the steric blockage by the large DNA superstructure formed via the HCR process. The membrane was first appropriately functionalized with a thiol DNA capture probe (CP). After incubating the membranes with the target survivin messenger RNA (mRNA) solution, the designed DNA CP incorporated the target DNA via complementary hybridization. Finally, the membrane was incubated in the solution containing the H1 and H2 DNA hairpin probes and after HCR a large DNA superstructure was formed causing the blockage of the nanochannel. The developed nanochannel sensor achieved a sensitivity of 30 fM with a wide linear dynamic range from 0.1 to 10 pM, and good performance even in RNA extracts from different cultured cell lines.

7.1.2. *Detecting a type of non-coding RNAs: MicroRNAs*

Non-coding RNAs (ncRNAs) include multiple classes of RNA transcripts. Although they are not transcribed into proteins, they have been shown to regulate the transcription, stability, or translation of protein-coding genes in the mammalian genome [262,263]. MicroRNAs (miRNAs) are a type of ncRNA with ~21–24 nucleotides in length that are implicated in the post-transcriptional regulation of gene expression [264]. Commonly, miRNAs interact with specific mRNAs through complementary base-pairing to influence the translation or stability of the target mRNA molecule and thus reduce the final protein output. Furthermore, miRNAs have been shown to repress the expression of important cancer-related genes and might provide helpful strategies in the diagnosis and treatment of major diseases like cancer [265].

Although the term “hybridization” refers to the pair-based specific interaction between two DNA or RNA single strands, there also exist artificial synthetic templates that mimic the recognition of complementary DNA/RNA sequences that occurs in hybridization. Well-known examples of these artificial hybridizing templates are based on Peptide Nucleic Acids (PNAs) and Phosphorodiamidate Morpholino Oligomers (PMOs). PNA, whose backbone is composed of repeating N-(2-aminoethyl)-glycine units connected by peptide bonds, has proved to bind their complementary nucleic acid sequence with higher affinity and specificity compared with DNA probes [266]. In 2007, Jágerszki et al. reported for the first time the construction of PNA-functionalized gold nanotubes for the label-free quantification of complementary DNA sequences [267].

Phosphorodiamidate morpholino oligomer (PMO), discovered in 1985 by Summerton, belongs to the third generation of antisense oligonucleotides [268]. It is a synthetic DNA analogue with a neutral backbone of morpholine rings and displays a higher solubility in aqueous solutions and is more flexible in length compared with PNA.

Taking into account not only the relevance of miRNA but also the advantages of PMO as an artificial synthetic template for DNA recognition, Liao et al. built a hybrid artificial PET-PMO nanochannel-based biosensor that allows miRNA detection with good sequence specificity and sensitivity (Fig. 12) [269]. The PET conical nanochannel was first derivatized (via EDC/NHSS coupling reaction) with this synthetic DNA analogue PMO. Afterward, BSA was

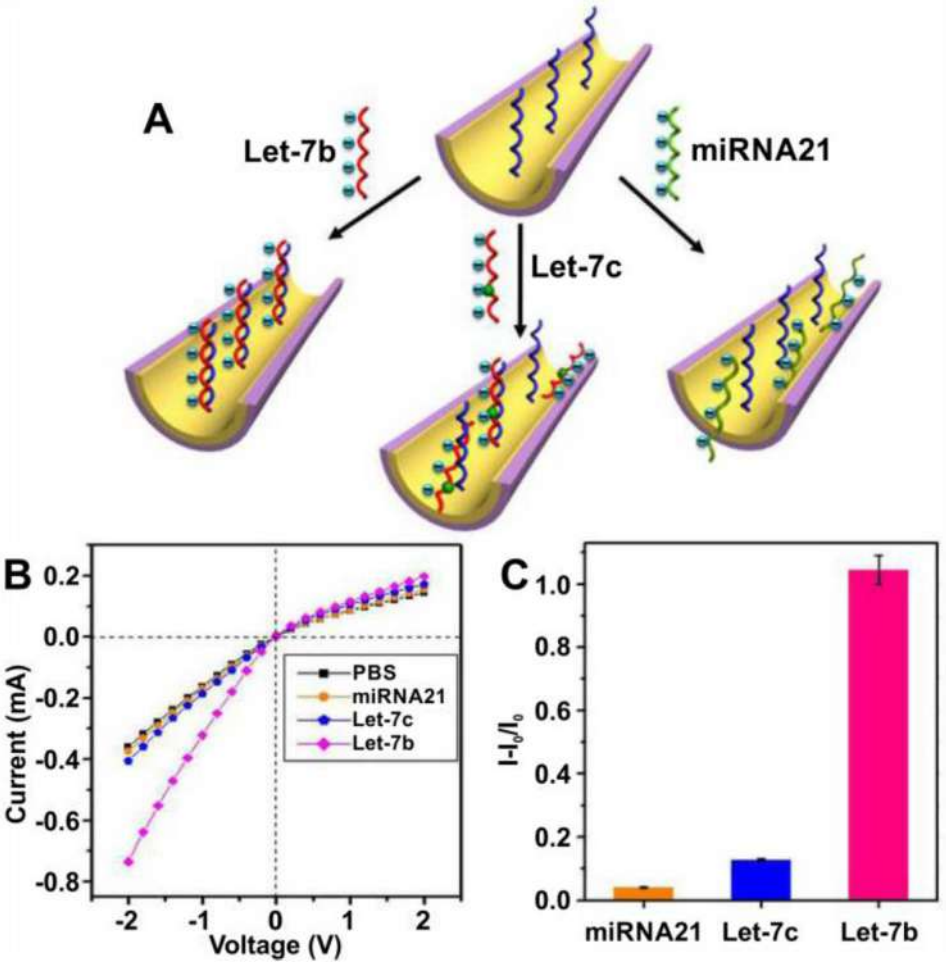

Fig. 12. **(A)** Schematic illustration showing the specificity of the nanochannel biosensor for miRNA detection. **(B)** *I*−*V* curves of the PMO functionalized nanochannel biosensor after treatment with 1 nM miR-21, Let-7c, and Let-7b, respectively. In this experiment, PBS solution pH 7.1 acted as the control (black line). **(C)** The relative ion current change ratios of the modified nanochannel in the presence of 1 nM concentration of the above-mentioned 3 miRNA strands. Reproduced with permission [269]. Copyright 2017, American Chemical Society.

employed to block the unmodified sites on the surface. Then, miRNA detection was realized by changes in ionic transport across the nanochannel caused by the PMO/miRNA hybridization process (Fig. 12(A)). The sensing principle relies on the changes in the nanochannel surface charge density that takes place as a consequence of the hybridization reaction. One of the attractive features of this sensing strategy relies on the fact that the hybridization efficiency between PMO and target miRNAs is enhanced by the neutral character of the PMO backbone and its high sequence-specific affinity. Also, the special 3D geometry of the nanochannels enlarges the surface area for the functionalization of the probe molecule and thus enhances the affinity between probe and target molecule. The authors showed that these sensing platforms are useful to detect target miRNAs in serum samples with a detection limit of 10 fM. The biosensors were capable of discerning complementary miRNAs (Let-7b) from non-complementary miRNAs (miR-21) and one-base mismatched miRNAs (Let-7c) (Fig. 12(B) and (C)).

In line with the importance of miRNA for clinical diagnosis and therapeutic evaluation of cancer, Zhang et al. recently developed a biomimetic solid-state nanochannel logic platform for the detection of miR-122, the most abundant miRNA in human adult liver cells [270]. Previous studies have shown that the expression of miR-122 is down-regulated in human hepatoma cells, the detection of miR-122 is thus closely related to the early diagnosis of liver cancer [271]. The authors created a new paradigm for the use of hybridization processes to detect DNA probes that combines the advantages of conical solid-state nanochannels with graphene oxide (GO) technology. Initially, the surface of PET-based single conical track-etched solid-state nanochannels was modified with polyethyleneimine (PEI) and Zr^{4+} to convert the surface charge from initially negative into positive. Additionally, a series of hairpin probes that are normally closely adsorbed onto the GO surface by π-π stacking forces were used to generate double-stranded DNA (*ds*-DNA) from mi-R122, which implied the detachment of the *ds*-DNA from the GO surface to the solution. Moreover, hairpins and miR-122 took part in a signal amplification strategy consisting of a mi-RNA catalyzed hairpin assembly (CHA) coupled to a hybridization chain reaction (HCR). The as generated ds-DNA in solution was accumulated at the positively charged PET-modified nanochannel surface using an external voltage and taking advantage of the affinity between Zr^{4+} and PO_4^{3-} groups of *ds*-DNA. The concentration of the added miRNA could be quantified from ICR curves to complete ultra-sensitive and label-free detection of the target miR-122, with a linear response between 100 aM and 10 pM of miR-122 and a limit of detection (LoD) of 97.2 aM. Additionally, the biosensor showed excellent selectivity for miR-122 detection over other randomly selected mi-RNAs and it displayed the capability of sensing miR-122 in a real human liver total RNA sample. Last but not least, the work reported an intelligent sensing system for the

simultaneous detection of multiple mi-RNAs that are overexpressed in hepatoma carcinoma cells.

7.2. Proteins and enzymes sensing

As the inner walls of the nanochannels offer an attractive surface to anchor a multiplicity of ligands/recognition elements, they have been used to inspire the detection of proteins using non-covalent interactions. In 2005 Siwy et al. reported a new type of protein nanosensor based on a single conical-shaped nanotube embedded within a PET membrane. A biochemical molecular-recognition agent (MRA) was immobilized at the small tip of the nanotube, which had a comparable size with the target proteins (streptavidin, immunoglobulin, and ricin protein). In terms of the ionic transport, this restriction in size was detected as a full shut-off of the current, which implies the complete blockage of the nanochannel triggered by the binding of the protein to its MRA in the nanochannel tip. Since then, many attempts have been made to create protein biosensors based on nanochannels [272–274].

In 2016 Lepoitevin et al. developed biosensors for glycoproteins like avidin and streptavidin based on their specific recognition reaction with biotin [275,276]. They fabricated silica-coated single cylindrical PET nanochannels by a combination of track-etching technology and atomic layer deposition. The silica surface was asymmetrically functionalized with a variety of spacers containing biotin, some of them based on PEG-polymers and the others of shorter length. By ionic transport measurements, the authors established that the short-length biotin-functionalized spacers were more suitable than the long-length spacers to discriminate avidin and streptavidin below pH 9 up to around 1 nM concentrations since with the small spacers the current rectification was a function of the protein charge. Finally, after the attachment of the glycoproteins, model biotinylated proteins such as IGg and BSA-anti-BSA were used to prove that binding sites of both avidin and streptavidin were still active and accessible in the nanochannels despite the confinement effects.

In both eukaryotes and prokaryotes, post-translational modification by protein phosphorylation is an essential mechanism for enzymatic and cellular regulation. Phosphoproteins are proteins that are usually phosphorylated by kinases. They may be part of signal transduction cascades in which one kinase phosphorylates one kinase (making it a phosphoprotein) or multiple kinases, to amplify and propagate a cellular signal. Furthermore, protein phosphorylation provides the cell a mechanism to switch ON/OFF many diverse processes such as metabolic pathways, membrane transport, gene transcription, and motor mechanisms, among others [277]. In this context, Nasir et al. developed a nanofluidic device for the label-free detection of phosphoprotein (PPn) analytes based on the combination of track-etching technology and post-grafting of the surface with a zinc (II) ion-chelator [278]. The surface-carboxylate groups of a single-pore PET SSN were first chemically modified (standard coupling chemistry) with dipicolylamine (DPA-NH_2). Then Zn^{2+} ion complexation was carried out by exposing the DPA-modified SSN to a $Zn(NO_3)_2$ solution. Every functionalization step was followed by ion-transport measurements at pH 7.4 and, as expected, the complexation of Zn^{2+} leads to the inversion of current rectification due to the switching from a cation-driven transport to an anion-driven regime. Regarding the sensing capability and the selectivity of the device, *I–V* measurements showed that the presence of non-phosphorylated proteins (lysozyme and dephospho-α-casein) did not alter the transmembrane ion-transport, whereas phosphorylated ones (albumin) produced a drastic decrease in the transmembrane ion current even at very low concentrations (1 nM). This indicates that bioconjugation had occurred in the nanochannel due to the specific coordination of Zn^{2+} ions with the phosphoryl moieties in the protein analyte. Also, for concentrations ≥100 nM a reduction/blockage of the ionic current was observed, which may be caused by a steric obstruction of the channel tip triggered by the presence of bioconjugates. In this line, phospho-α-casein was selected as a lower molecular weight phosphorylated protein compared to albumin to test if proteins having different molecular weights/chemical compositions could be identified based on the changes in the electrical response of the SSN. As phospho-α-casein is negatively charged at pH 7.4 (pI ~ 4.44), the ionic current rectification occurs in a cation-driven regime, and linear response of the current at +2 V with decreasing protein concentration was observed down to the nanomolar range (1–500 nM).

Human digestion involves breaking down macronutrients (fats, carbohydrates, and proteins) into their constituent parts (fatty acids, glycerol, monosaccharides, and amino acids). This occurs in the intestine, which then absorbs these nutrients into the blood [279]. Protein digestion involves the contribution of several enzymes and, for this aim, the pancreas secretes three endopeptidases (trypsin, chymotrypsin, and elastase) and two carboxypeptidases, CPA, and CPB, that cleave single amino acids off the free carboxyl ends of proteins. CPB hydrolyzes the C-terminal alkaline amino acid residues of the peptide, such as arginine, lysine, or ornithine, and it is considered an important indicator of acute pancreatitis [279]. The concentration of CPB in urine and plasma can reflect the severity of acute pancreatitis [280]. In 2019 Zhang et al. proposed a peptide-modified AAO nanochannel system for CPB activity detection (Fig. 13) [281]. For this, they carried out a chemical modification of the AAO nanochannels with APTS and glutaraldehyde in order to convert hydroxyl groups of AAO into aldehyde groups. A synthetic alkaline peptide ("peptide 1") was used to modify the inner walls of the nanochannel and study its effect on the transmembrane ion current (Fig. 13(A)).

Grafting with peptide 1 resulted in a severe decrease in the ion current, which could be explained by the formation of a dense peptide layer on the inner walls of the nanochannels leading to the distinct channel blocking effect (Fig. 13(B)). To evaluate the activity of CPB, peptide 1 was treated with the enzyme in solution and the resulted hydrolyzed alkaline peptides were assembled into the inner walls of the aldehyde-modified nanochannels. The channel size was small enough (~20 nm) to block the entrance of enzymes into the nanochannels, which led to the separation of CPB macromolecules from treated alkaline peptides that could enter the channel and react with the aldehyde groups immobilized on the walls by forming imino groups. As expected, when the CPB concentration increased, the ratio of the ion currents I_0/I decreased (I_0 and I are the ion currents values at −0.2 V before and after the peptide modification) (Fig. 13(C)). The different CPB levels obviously produce peptides of different lengths, resulting in different nanochannel blocking effects as quantified by the accurate current measurement. A linear relationship between I_0/I and the logarithm of CPB concentration from 0.01 to 10 U/ml was found, with a detection limit of 0.01 U/ml, a very low concentration compared with previous works (Fig. 13(D)). Also, the inhibition effects of EDTA, urea and ε-aminocaproic acid could be evaluated. The selectivity of the system was studied by detecting CPB, CPA, and trypsin under the same conditions. The experiments indicate excellent selectivity for CPB. Finally, enzyme activity measurements were performed by adding different concentrations of CPB to human serum solution, showing very accurate results.

7.3. Cells, cellular targets, and virus sensing

Cancer is a major cause of death that contributes to 15% of mortality worldwide providing 14 million estimated new cases per

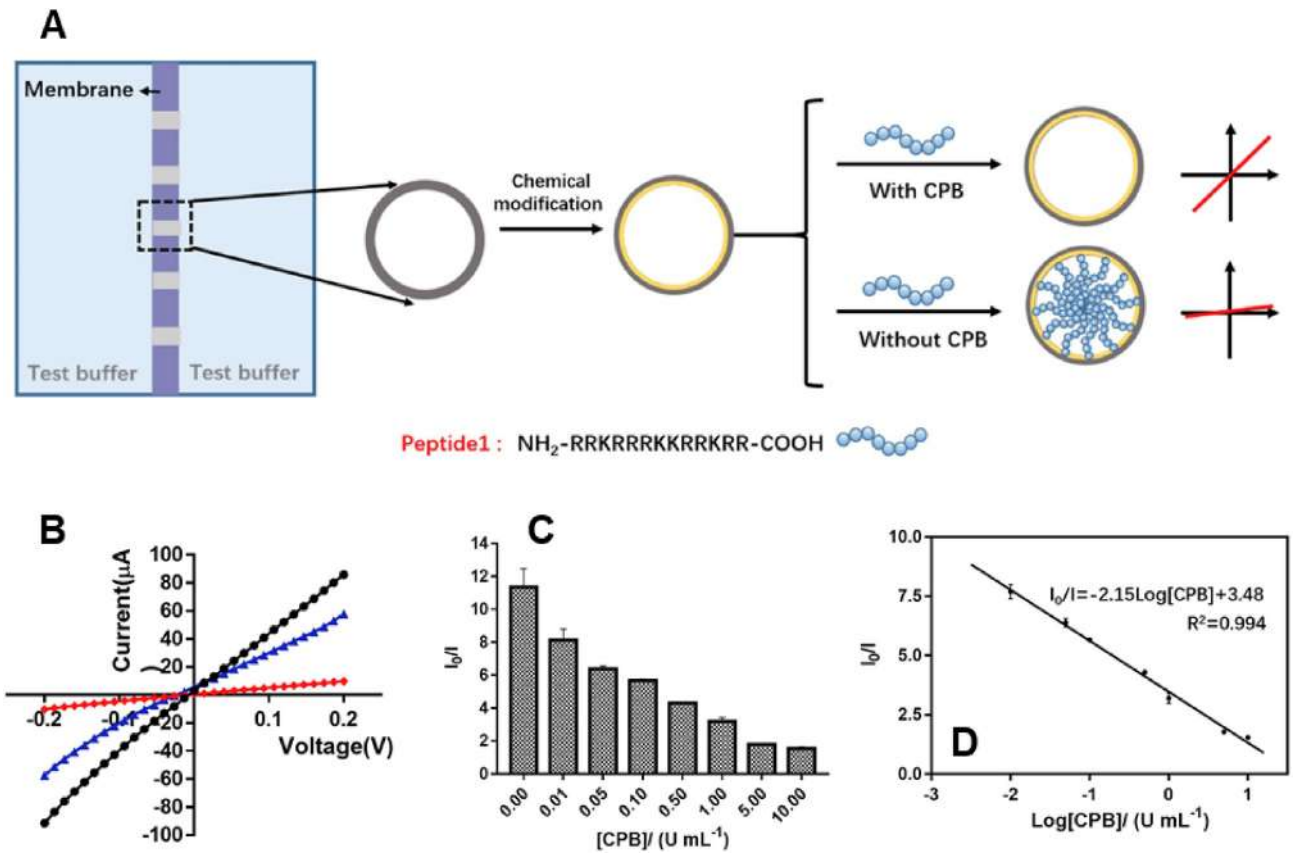

Fig. 13. **(A)** Schematic diagram of activity detection of carboxypeptidase B (CPB). Alkaline peptides are assembled in a chemically modified AAO membrane. In the presence of CPB, the peptides are hydrolyzed from the C-terminus to amino acids, which do not form a blockage inside the nanochannel. When there is no CPB in the system, the intact alkaline peptide can be attached to the inner wall of the nanochannel, resulting in a blocking effect. The blockage of the nanochannel is determined by the change of the *trans*-channel ion current. **(B)** The transmembrane ion current before (black curve), after (red curve) peptide modification, and after CPB treatment (blue curve) from −0.2 V to 0.2 V. The average diameter of the blank nanochannels is 22 ± 6 nm, the peptide1 concentration was 0.5 mg/ml, and the current-voltage detection was carried out using a buffer (5 mM tris-HCl, 100 mM KCl, pH 8.0). **(C)** I_0/I values corresponding to different activity units of CPB in the modification buffer. **(D)** The linear relationship between I_0/I values and the logarithm of CPB concentration. Reproduced with permission [281]. Copyright 2020, Elsevier B.V.

year [282]. In particular, metastases rather than primary tumors are responsible for most cancer deaths. During the past few years, many research groups have focused their attention on trying to elucidate a marker of poor prognosis not only in primary tumors but also in metastatic lesions that could predict the evolution of neoplasic disease. Most of this information has been used in discovery platforms to identify potential novel therapeutic targets [283]. Due to the relevance of cancer as a global health problem, improved ways to detect and treat metastatic diseases are still in profound need [284]. Regarding this, Cheng Wang's group of the China Pharmaceutical University in Nanjing has recently presented the construction of a novel nanofluidic platform based on a nanochannel-ion channel hybrid structure in order to address the detection and quantification of circulating tumor cells and cell surface glycans present in MCF-7 cells (Fig. 14). These authors reported for the first time the construction of a nanochannel-ion channel hybrid structure coupled with electrochemical detection for the capture and detection of circulating tumor cells (CTCs), which are cells that have been transferred from the primary tumor site into the peripheral blood [130]. The array was built using AAO clamped between two thin poly(dimethylsiloxane) (PDMS) films and placed between two halves of a customer-made electrochemical cell (Fig. 14(A)). The ion channel side of the hybrid membrane was chemically grafted with an aptamer specifically designed to bind to the transmembrane receptor protein tyrosine kinase 7 highly expressed on CCRF-CEM cell membrane (one type of CTCs) [285]. When exploring the *I*–*V* response, the aptamer-modified nanochannel-ion channel hybrid device showed a clear ionic rectification phenomenon due to the strong asymmetric nature of the array (Fig. 14(B)). In the presence of CCRF-CEM cells, the ionic current drastically dropped (Fig. 14(A)). By means of scanning electron microscopy (SEM), it was established that CCRF-CEM cells were trapped and covered the hybrid membrane surface, in line with the observed blocking of the ionic flow through the nanochannel-ion channel hybrid (Fig. 14(B)). Furthermore, experimental results with different cell lines showed excellent selectivity for the detection of CCRF-CEM cells. Also, a good linear correlation between the value of the ionic current drop and the cell concentration in the range of 100–1000 cells/ml was observed (Fig. 14(C)), and an excellent detection limit of 10 cells/100 μL was determined. Finally, the captured cells could be released by enzyme digestion affecting the cell viability only by 6%. This work provides a promising strategy for label-free detection of trace amounts of CTCs in a real-time format, which can be crucial for both the early diagnosis and treatment of cancer.

On the other hand, glycans might be the most abundant and diverse biopolymers in nature and are one of the four basic components of cells. Most of them exist as covalent linkages of saccharides often attached to proteins and lipids and constitute a significant amount of the mass and structural variation in biological systems. Glycans take part in many key biological processes such as cell adhesion, molecular trafficking and clearance, receptor

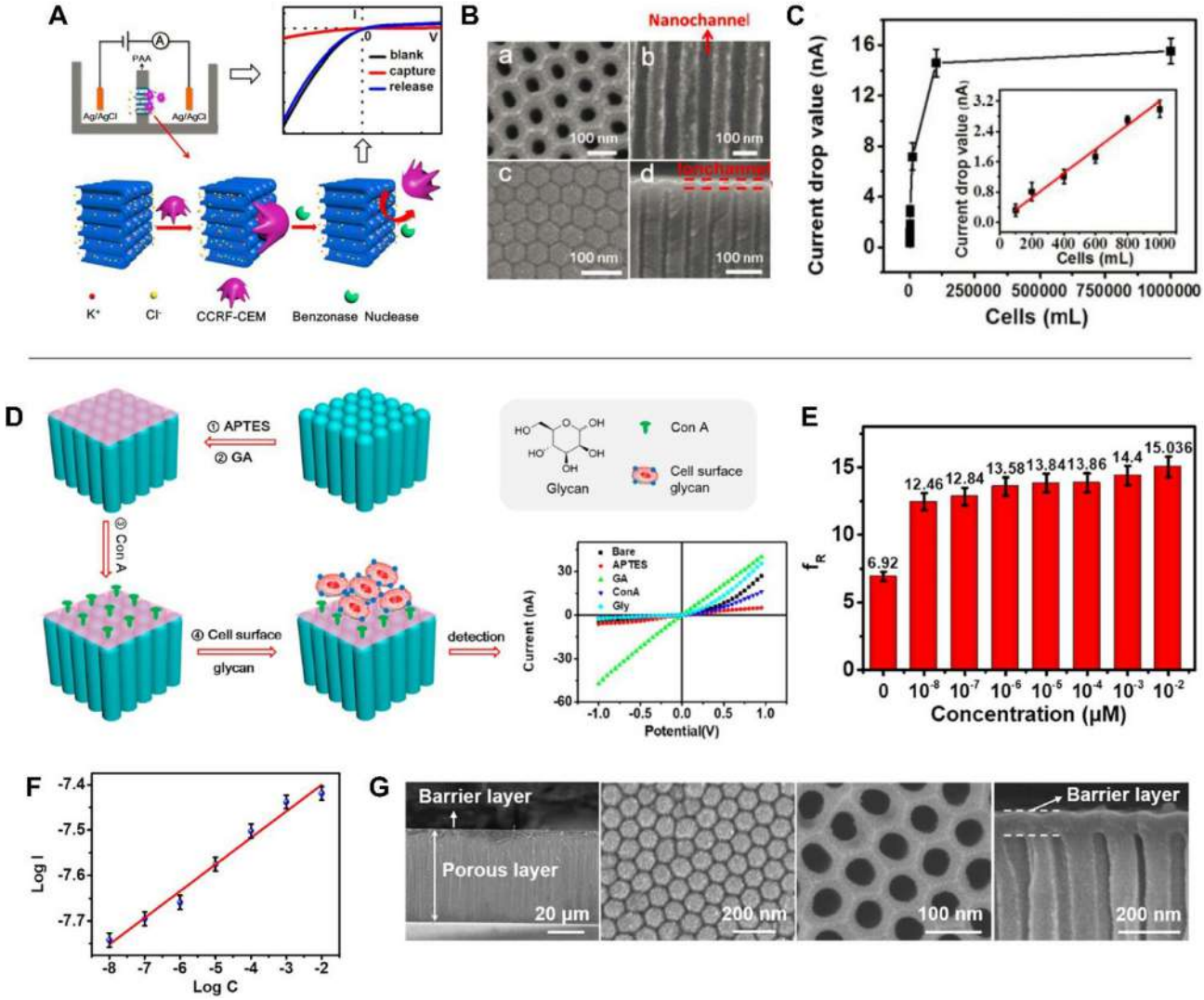

Fig. 14. **(A)** Diagrammatical Illustration of the CTCs Capture and Release Process on the Nanochannel–Ion Channel Hybrid representation of the Varied Electrochemical Responses Towards CTCs Capture and Release. **(B)** SEM images of PAA: (a) the porous layer; (b) the cross-section of the nanochannels; (c) the barrier layer; (d) the cross-section of the ion channel layer. **(C)** The current drop values at −1.0 V vs the CCRF-CEM cells concentration. Inset: the linear calibration plot at low cell concentrations. Adapted with permission [130]. Copyright 2017, American Chemical Society. **(D)** Illustration of the Electrochemical Detection Principle for Surface Modification and Glycan Detection on the Asymmetric PAA Membrane. (E) Rectification ratio (f_R) of the device versus glycan (mannose) concentration. **(F)** Calibration curve of Log I–Log C, I was the ionic current of hybrid after recognition with various concentrations of glycan. **(G)** SEM images of the fabricated nanochannel–ion-channel hybrid (From left to right: the whole cross-section, barrier layer, porous layer, cross-section with barrier layer). Reproduced with permission [288]. Copyright 2020, American Chemical Society.

activation, signal transduction, and endocytosis [286]. Glycosylation reactions are common post-translational modifications by which specific glycan structures are incorporated into proteins and lipid backbones [283]. In particular, the relation between glycosylation and its promoting or inhibiting tumor cell invasion and metastasis is of great importance in current cancer research [287].

Many recent studies revealed that changes in the glycosylation signature, not only of tumor cells themselves, but also of stromal cells, tumor-associated vascular cells, and immune cells, are characteristically defined in tumor transformation, metastasis, angiogenesis, and immune escape [283,287]. The differential glycosylation of cancer-associated versus healthy tissues is related to altered glycan expression in tumor cells or circulating glycoproteins and thus, it could be potentially used for diagnostic, prognostic, and therapeutic purposes [283]. Regarding this, Liu et al. reported in 2020 another asymmetric nanochannel-ion channel hybrid based on AAO, but this time for sensitive and label-free detection of mannose and cell surface glycans (Fig. 14) [288]. By SEM, the morphology of the hybrid array could be characterized (Fig. 14(G)). The whole thickness was ~50 μm, the ion channel side was connected with the nanochannels (diameter ~50 nm) through a barrier layer of about 65 nm. By using $[Ru(bpy)_3]^{2+}$ as a fluorescent probe, the pore diameter of the hybrid (ion-channel side) could be determined as less than 1.3 nm. By Fourier transform infrared spectroscopy (FTIR), the authors studied the postgrafting of the AAO ion-channel surface. The entire procedure involved the immobilization of amine groups by APTES hydrolysis and condensation, then glutaraldehyde (GA) modification and, finally, the attachment of concanavalin A (ConA) (Fig. 14(D)). As a lectin, ConA is a carbohydrate-binding protein and it endows the device with a specific recognition unit. In terms of ionic transport, the above-mentioned surface modification steps were monitored. The ionic current rectification at pH 7.4 showed a clear dependence on the surface charge. In particular, as the isoelectric point of Con A is ~5.0 [289], the outer surface of AAO must be

negatively charged after Con A binding at pH 7.4. Also, glycan detection was studied by ion transport measurements using mannose as a model molecule at various concentrations between 10 fM and 10 nM. An increment in the current at positive potentials and in the rectification factor was seen with higher mannose concentrations as the binding of mannose implies a higher negative surface charge (Fig. 14(E)). More specifically, a linear relationship was found between 10 fM and 10 nM (Fig. 14(F)), with a detection limit of 9.997 aM. Moreover, the device specificity for mannose detection was evaluated against glucose (Glu), chitosan (CTS), ascorbic acid (AA), bovine serum albumin (BSA), and cysteine (Cys). The current responses at +1.0 V remained nearly constant for mixtures of mannose and any interfering species, which implies a remarkable specificity of the prepared nanodevice toward mannose detection. Finally, different concentrations of MCF-7 cells were incubated on the ion-channel side of the hybrid AAO array in order to evaluate cell surface glycan detection. After 45 min of incubation, cells efficiently covered the outer surface of AAO, which resulted in a decreased current response. Also, the ionic current decreased continuously when the MCF-7 cell concentration increased from 10^2 to 10^6 cells ml^{-1}, meaning that the level of glycan expression in various cell concentrations could be directly reflected by monitoring the ionic current response after cell trapping.

Until now, in most cases, cellular target detection requires cell pre-treatment to extract the desired analytes. The detection of intracellular targets without sample pre-treatment process was accomplished with the insertion of nanoprobes into living cells using nanopore electrodes [290] and nanopipettes [291]. In other words, there is a great need for constructing SSNs to allow *in situ* and non-invasive detection of cellular targets, which would bring a whole world of possible applications in the biological field of living cells. Lou et al. presented recently a new solid-state nanochannel-based strategy to detect H_2O_2 released from living cells without insertion procedures [292]. For that aim, HeLa living cells were first incubated on a PET membrane containing cylindrical nanochannels. Then, the carboxyl groups provided by the hydrolysis of PET were functionalized by coupling chemistry with L-tyrosine in order to generate phenolic hydroxyl groups on the nanochannel surface. After that, the addition of an aggregation-induced emission luminogen called TT derived from tetraphenylethylene (TPE) in the presence of added horseradish peroxidase (HRP) and H_2O_2 released from living cells derived in the formation of di-tyrosine linkages and TT oligomerization, which induced a partial blocking of the ion transport pathway. Under optimized experimental conditions, a high sensitivity response to H_2O_2 was obtained: for 1 nM H_2O_2 a resistance of more than 100 kΩ was measured (+0.2 V). This response was supported by SEM images, showing that the average diameter of the nanochannels was 27 ± 3 nm (before testing) and 7 ± 1 nm (after testing). This implies that the decrease in the ionic current was due to the formation of TT oligomers. Concomitantly, confocal laser scanning microscopy showed that the fluorescence turned ON upon the addition of TT, H_2O_2, and HRP, which meant that TT aggregation provoked a TT fluorescence enhancement due to a restriction of the intramolecular motion process (RIM). In terms of selectivity, functionalized nanochannels exhibited a >70% current change ratio toward H_2O_2 over other ROS, including •OH,•ClO−,•TBHP, and •OtBu. Also, H_2O_2 extracts from HeLa cells were used to test the analytical performance of the functionalized nanochannels towards real samples. The current change ratios were enhanced gradually with increasing concentration of HeLa cells, validating the positive correlation between the current change ratios and the concentrations of H_2O_2. Finally, different cell lines including HeLa cells, RAW 264.7 cells, and A505 cells were utilized to study the kinetics of the detection procedure and to prove the effectiveness of the device.

This work is a major contribution in the field as it brings a new dual-signal output nanochannel strategy (ion-transport + fluorescence signal) in order to achieve non-invasive and *in situ* detection of H_2O_2 released from living cells.

The EIS method has also been shown to be an interesting alternative for the development of virus sensors. In 2016, Chaturvedi et al. reported the creation of a nanofluidic platform for the detection of MS2 bacteriophage viruses [179]. For this aim, an AAO membrane was modified with the MS2-phage polyclonal antibody in a three-step procedure that included the attachment of APTES onto the channel surface followed by the activation with glutaraldehyde, and the final antibody immobilization. When the antibody-modified membrane is exposed to the target virus, this is specifically bonded onto the surface promoting an abrupt change in the pore resistance that can be recorded via impedance measurements. By employing this strategy, the authors found a logarithmic dependence between the signal and MS2 bacteriophages in the concentration range of 10−2000 pfu (plaque-forming units)/ml with a limit of detection (LoD) of ~7 pfu/ml. Interestingly, this device could be accurately operated without a potentiostat by using a computer's sound card, which positions this development as a novel and promising strategy for the creation of point-of-care sensors.

8. Sensing and detection of small biomolecules and drugs

8.1. Detection of amino acids, carbohydrates, and other biologically relevant molecules

8.1.1. Amino acids

L-Tryptophan. In 2016 Ali et al. demonstrated an easy approach to create a tryptophan (L-Trp) sensor by immobilizing bovine serum albumin (BSA) on the surface of a single asymmetric PET nanochannel through mussel-inspired chemistry [293]. Immobilized BSA molecules served as chiral receptors since they have the ability to enantio-selectively recognize L-Trp over D-Trp isomer through specific BSA−tryptophan interactions. Firstly, dopamine (DA) was self-polymerized under alkaline conditions, allowing the deposit of a film of polydopamine (PDA) onto the channel surface. Then, BSA was immobilized on the PDA-coated channel surface by exploiting the Michael addition reaction [294]. The different functionalization steps promoted changes in the surface charge density of the pore which were monitored by conductometric measurements. In particular, the specific BSA−tryptophan interactions led to changes in the surface charge density that modulated the ionic transport through the nanochannel. Furthermore, the authors demonstrated that the as-constructed nanodevice is highly selective for L-Trp. Moreover, the nanochannel sensor successfully allowed L-Trp detection in the concentration range from 1.5 mM to 100 mM.

Arginine. Cao et al. developed an arginine (Arg) nanofluidic sensor by decorating a nanopore in a glass capillary with a thin film of BSA-protected Au nanocluster (BSA-Au NC) [119]. The conical glass nanopore was first modified with poly (ethylene imine) (PEI) and BSA via an electrostatic layer-by-layer deposition process. The attached BSA layer was capable of binding Au(III) ions allowing the *in-situ* generation of a structurally well-defined BSA-Au nanocluster (BSA-Au NC) film. Taking advantage of the well-known ability of BSA for discriminating enantiomers of amino acids and that the ionized carboxyl groups (-COO−) of BSA can interact with Arg via guanidinium groups, the device could be used directly for selective recognition of Arg enantiomers by monitoring the iontronic output. The added Arg selectively led to changes in the surface charge density, and concomitantly, in the ion transport properties of BSA-Au NC film-decorated glass nanopore. Thus, the ionic current response allowed the quantification of Arg with a

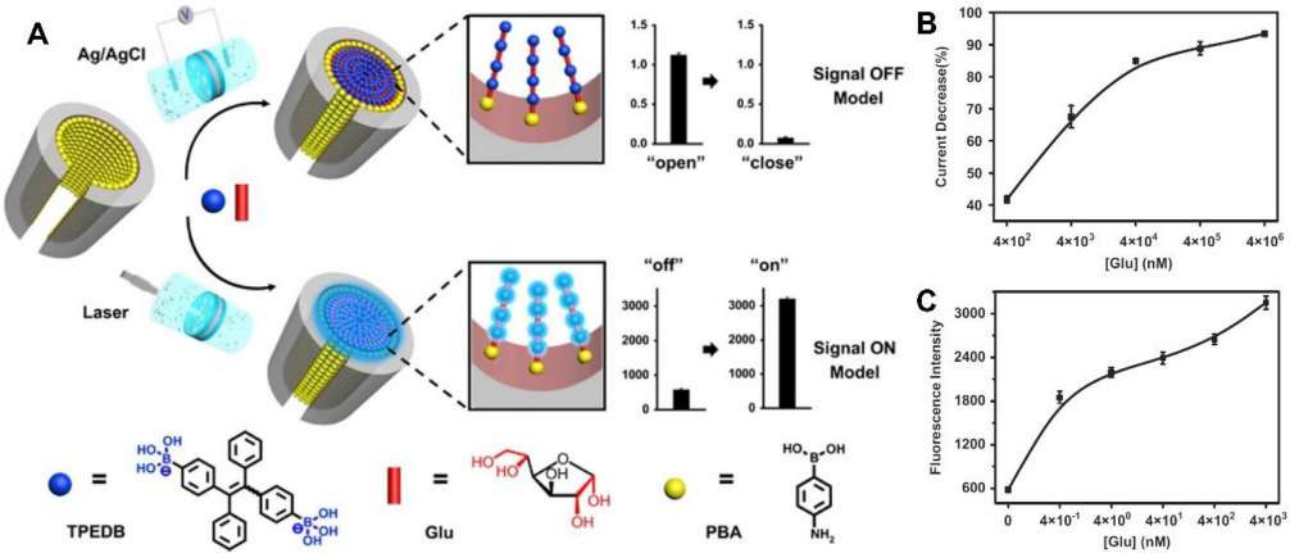

Fig. 15. **(A)** Scheme of PBA modified channel and the dual-output-signal recording. The exposition of PBA-modified channel to TPEDB and glucose triggered the oligomerization reaction on the channel walls that causes both a diminution in the current (close state) and an increment in the fluorescence intensity (ON). **(B)** Degree of current decreases as a function of glucose concentration. **(C)** Fluorescence intensity as a function of glucose concentration. Reproduced with permission [72]. Copyright 2016, Springer Nature Limited.

detection limit down to 1 fM, being more sensitive than the previously reported sensors.

8.1.2. Carbohydrates

Glucose. In 2016, Xu et al. developed a dual-signal-output glucose-sensor nanodevice based on PET nanochannels that allowed both the control of the ionic current and the fluorescence signal [72]. A cylindrical PET nanochannel was modified with the capture probe phenylboronic acid (PBA) via a two-step chemical reaction (Fig. 15(A)). When the PBA-modified channel was exposed to a mixture of glucose (d-Glu) and a previously synthesized aggregation-induced emission molecule 1,2-diphenylethene-1,2-diyl) bis (1,4-phenylene)-1,1′-diboronic acid (TPEDB), an oligomerization reaction between TPEDB and diol-contained glucose $(TPEDB\text{-}Glu)_n$ occurred on the surface of the nanochannel walls. As a consequence, the pathway for ion transport was blocked, resulting in a sharp decrease in the ionic current (closed state) (Fig. 15(B)). At the same time, when the TPEDB was oligomerized with glucose, the process of fluorogen was activated, and as a result, fluorescence turned ON (Fig. 15(C)). Thus, this specific oligomerization reaction and the combination of electric and optical signals in the nanochannel allowed the design of a highly sensitive and selective glucose-responsive nanodevice, which can act even in complex real samples.

In a similar way that those works summarized in Section 5.1, the host-guest supramolecular chemistry has been employed as a strategy for the development of sugar-responsive platforms [295]. For instance, Sun et al. reported a biomimetic glucose (Glu) enantiomer-driven ion gate device by means of the introduction of the chiral pillar [6]arene-based host-guest systems into a single conical PET nanochannel ("chiral" nanochannel) [296]. Basically, a previously synthesized chiral alanine-decorated pillar [6]arene (l-AP6) was associated with guest AZO moieties previously assembled to the PET nanochannel. The modification steps led to a decrease in the transmembrane current as a consequence of the decrease in negative surface charge and the increase in hydrophobicity. Moreover, when the modified channel was exposed to glucose, the current decreased further in the case of D-Glu (OFF state), while it remained almost unchanged in the case of L-Glu (ON state). The differences in the D-Glu and L-Glu responses were ascribed to the different binding strengths of chiral pillar [6]arene and glucose enantiomers. Glucose binding to the L-AP6-AZO complex is ten times more stable in the case of the D enantiomer. Also, D-glucose binding produces variations in the effective surface pKa, while the pKa remains practically the same after L-glucose binding. These variations in equilibrium constants suggested that the presence of D-Glu caused a diminution in the surface charge density of the channel that triggered an OFF state in the iontronic signal. Finally, after washing with water, the bound D-glucose is released and the ON state is recovered, with good reversibility.

Fructose. Taking advantage of the well-known borate-sugar specific interaction, a fructose-responsive nanofluidic diode by immobilizing poly(3-aminephenylboronic acid) (PAPBA) on a metalized single conical PC channel was described [137]. For this, an Au layer was sputtered onto the tip side of the PC membrane and then, the channel was modified with PAPBA by means of the electropolymerization of the monomer 3-amino-phenylboronic. At acid pH and in absence of fructose, the modified channel displayed a rectifying behavior due to the asymmetric geometry and the positively charged groups of PAPBA. However, the presence of fructose in solution promoted the formation of boronic acid-fructose complexes yielding negatively charged sites onto the surface which were transduced into changes in the iontronic output. This platform showed a sugar-regulated ion transport in a wide range of pH.

8.1.3. Neurotransmitters

Histamine. Neurotransmitters are considered chemical messengers that transmit neurological information as electrical signals within the cellular living system [297]. In particular, histamine (Hm) is a neurotransmitter that is naturally present in the human body in trace amounts and plays a key role in brain-controlled functions as neurotransmission, sleep, memory storage, thermoregulation, inflammation, secretion of hormones and gastric acid, food intake and cardiovascular control [68,298–301]. Ali et al. put their interest in Hm detection and designed a nanofluidic sensor based on a metal ion displacement mechanism [68]. In this nanodevice, the inner PET channel surface was decorated with N_α,N_α-

bis(carboxymethyl)-l-lysine (BCML) chains which expose nitrilotriacetic (NTA) moieties onto the surface. Subsequently, NTA-Ni^{2+} chelates complexes were formed by exposing the BCML-modified channel to a Ni^{2+} ion solution. When a certain amount of Hm is added, the Ni^{2+} present in the chelate is released forming stable Ni-Hm complexes. This process alters the surface charge density and concomitantly, the channel conductance, as evidenced by the *I–V* curves before and after the exposition of the nanochannel to the analyte. The proposed sensor was able to detect Hm at biologically relevant concentrations (~1 nM). On the contrary, other neurotransmitters such as glycine, serotonin, gamma-aminobutyric acid, and dopamine could not induce significant changes in the channel conductance due to their inability to displace and form stable complexes with Ni^{2+} ions. This nanochannel-based sensor exhibited high sensitivity, specificity, and reusability towards Hm detection.

Dopamine. This neurotransmitter from the catecholamine family has important functions in the human body (e.g. human metabolism, cardiovascular, central nervous, renal, and hormonal systems) [302]. Recently, Laucirica et al. presented the construction and functional evaluation of a highly sensitive dopamine-responsive iontronic device by functionalization of bullet-shaped track-etched single nanochannels in PET membranes with poly (3-aminobenzylamine) (PABA) (Fig. 16) [138]. Experimental results showed that the variety of basic groups in this amino-appended polyaniline derivative allowed programming the ion selectivity of the channel by setting the pH conditions. Furthermore, the amino-pendant groups of PABA allowed the selective chemical reaction with dopamine, leading to a change in the nanochannel surface charges (Fig. 16(A) and (B)). Thus, the exposition of the PABA-modified nanochannel to dopamine solutions selectively produced changes in the iontronic response. By rationally selecting the conditions for both the dopamine binding step and the iontronic reading, a correlation between rectification efficiency and dopamine concentration down to the nanomolar range was obtained, which was also successfully interpreted in terms of a simple binding model (Fig. 16(C) and (D)). Finally, the iontronic SSN response was selective to DA compared with other analytes such as urea and ascorbic acid.

8.1.4. Other small biologically relevant molecules

ATP. Recently, an extensive study about nanoconfined polyamine-phosphates interactions by modifying a PET single nanochannel with polyallylamine (PAH) was presented [85]. There,

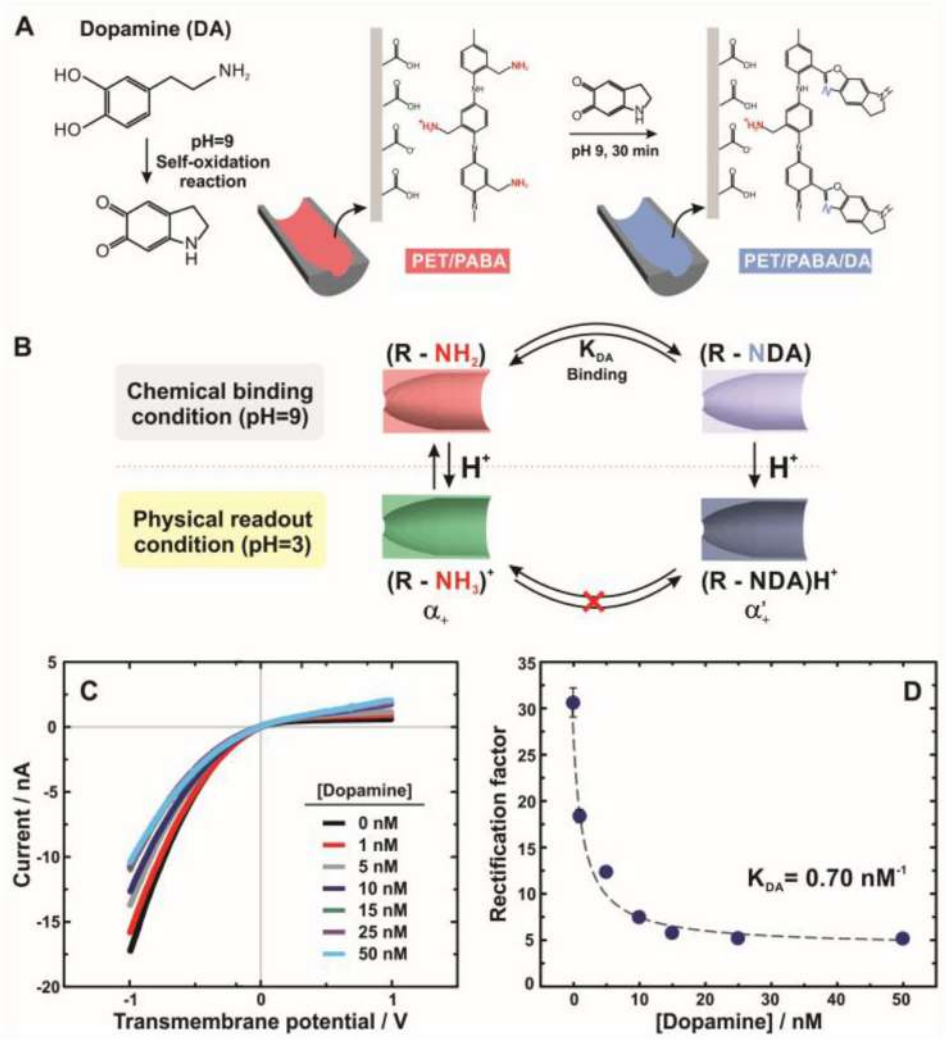

Fig. 16. **(A)** Scheme of reaction between DA and PET/PABA. **(B)** Scheme depicting the chemical species and steps at each pH condition for interpreting the DA-responsiveness in terms of a simple binding model. **(C)** *I–V* curves of PET/PABA SSN after the exposition to different DA concentrations. **(D)** Changes in f_{rec} for different DA concentrations. The dashed line corresponds to fit with the binding model to the experimental data. Reproduced from Ref. [138] with permission from the Royal Society of Chemistry.

the transmembrane current behavior was studied as a function of the bulk concentration of phosphates-based molecules at different pHs. The presence of phosphate-based molecules such as ATP promotes the formation of amine-phosphate complexes that cause variations in the surface charge density and therefore in the transmembrane current. At physiological pH, the system revealed a selective ATP-modulated response in the micromolar concentration range. The sensitivity of the iontronic response of asymmetric SSN to changes in the surface charge allowed the interpretation of the experimental results in terms of a binding model.

In 2018, Li and coworkers assembled a photo-controlled DNA-aptamer-based system to selectively and repetitively capture and release ATP from a PI single nanochannel [303]. The key component of this system is accomplished by introducing the photo-responsive Azo-groups into the ATP aptamer, which generates changes in the folding-unfolding states by undergoing light-induced isomerization. Then, Azo-DNA switches between refolding and unfolding states, along with capturing and releasing ATP molecules (Fig. 17(A)). After Azo-modification, the transmembrane ion conductance of the nanochannels decreased drastically due to the blockage of DNA strands. When the system was treated with visible-light and ATP (>1 pM), the stretched DNA captured ATP molecules to form a stable hairpin structure which increased the effective pore size of the nanochannel and correspondingly ionic current (capture state) (Fig. 17(B) and (C)). After exposure to UV light, ATP molecules are released from the hairpin structures and the DNA conformation recovers to the random single-stranded structure. This partially blocked the nanochannels and decreased the ionic current (release state). Additionally, the photo-controlled folding and unfolding process of the DNA was shown to be reversible and allowed the repeated capture-release processing of ATP molecules in the nanochannels, which endowed the ATP transmembrane transport by the continuously capturing and releasing process (Fig. 17(D)).

Urea. The manipulation of specificity and selectivity of SSNs by functionalization with enzymatic architectures that catalyze specific biochemical reactions has attracted considerable attention. In this framework, Pérez-Mitta et al. reported a seminal work that focuses on a mechanism for sensing urea by using a urease-modified single PET nanochannel [61]. To build this nanodevice, firstly, the electrostatic assembly of poly (allylamine) (PAH) on the etched bullet-shaped PET nanochannels was performed, and then urease was electrostatically adsorbed on the PAH-modified channel (Fig. 18(A)). Urease catalyzes the hydrolysis of urea into ammonia and carbon dioxide causing a local pH increase and, consequently, a decrease in the protonation degree of the PAH, reducing the positive surface charge density in the channel. Thus, the local pH change is amplified for the use of the weak polyelectrolyte and revealed by changes in the ionic current. This mechanism was demonstrated to be reversible and reproducible and the developed biosensing device was able to reach a limit of detection of 1 nM (Fig. 18(B) and (C)).

Aldehydes and fatty acids. Lu et al. developed an electrochemical impedance biosensor based on AAO nanochannels by anchoring human odorant-binding proteins (hOBPs) to detect

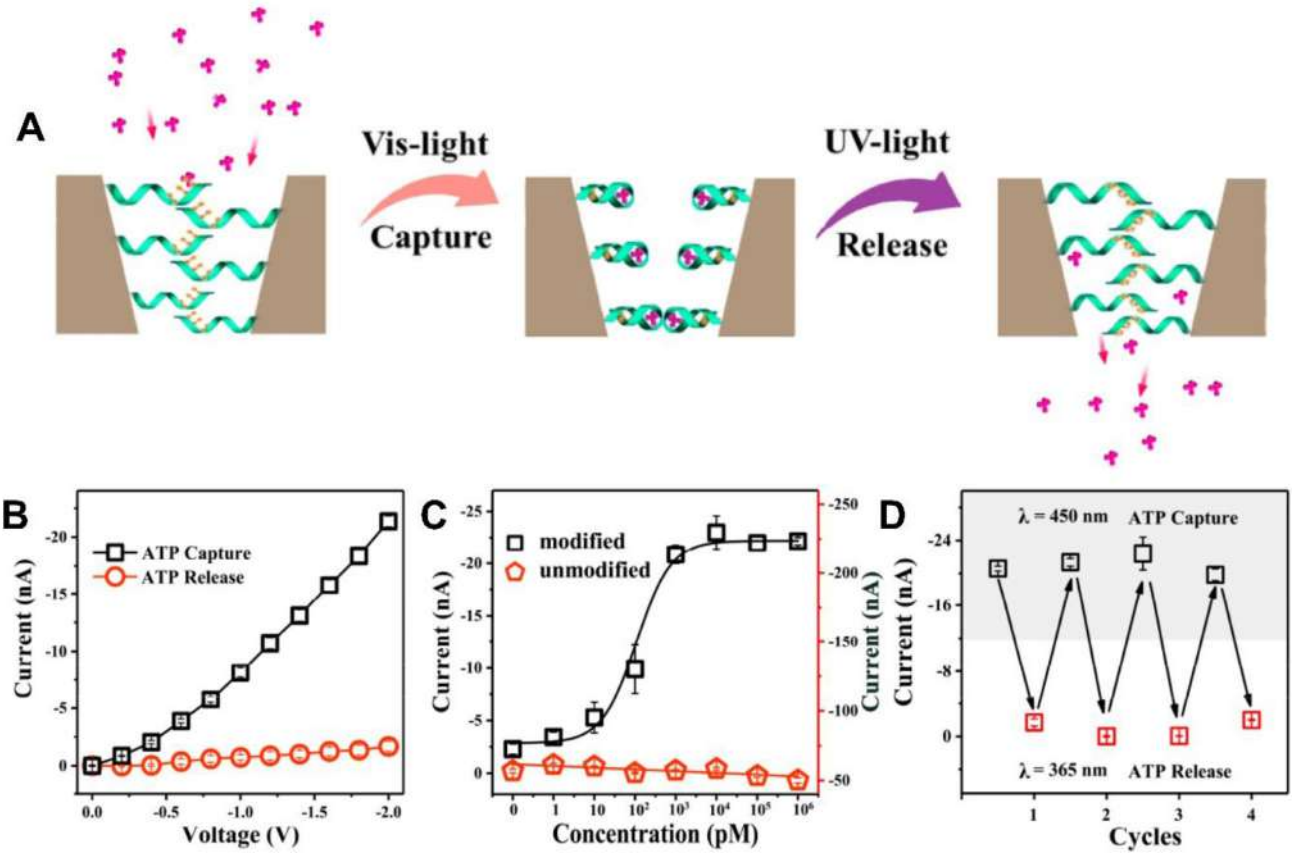

Fig. 17. **(A)** Scheme of the functioning mechanism of the light-driven ATP sensor. In the presence of Vis-light, the Azo-aptamer modified channel captures the ATP producing an increment in the effective size. Subsequent irradiation with UV-light promotes the release of ATP and restoring to the initial condition of the device. **(B)** *I*–*V* curves of the functional nanochannel in the ATP capture and release states, respectively. The capture of ATP triggers a clear increment in the ionic current. **(C)** Relationship between the current (at −2 V) and the concentration of ATP before and after aptamer modification. **(D)** Reversibility between the capture and release states. Reproduced with permission [303]. Copyright 2018, American Chemical Society.

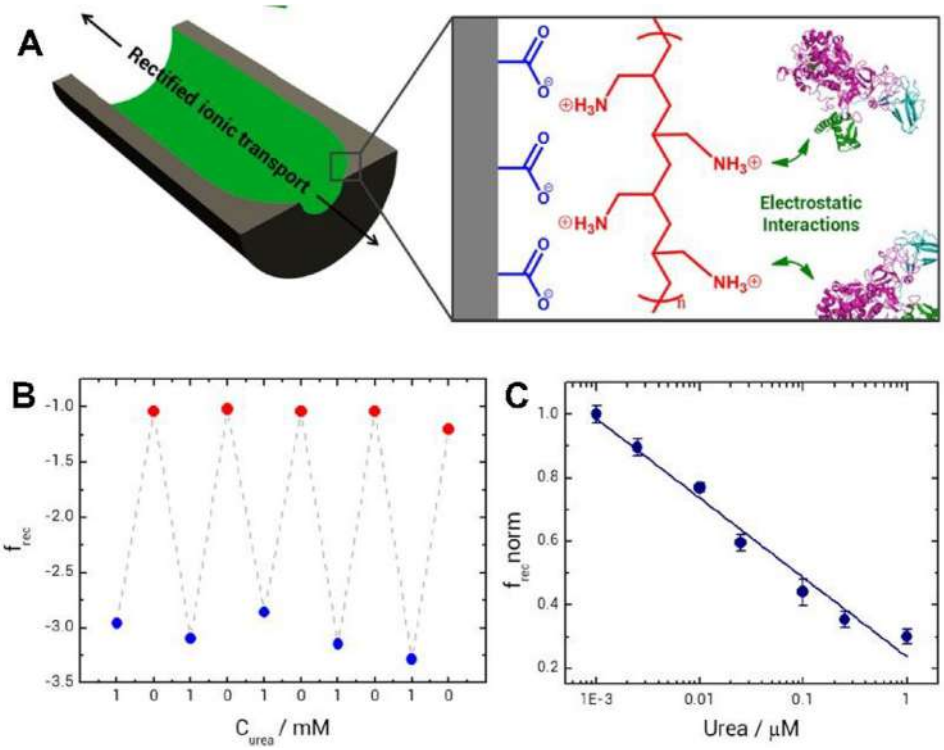

Fig. 18. **(A)** Scheme of the urease-modified single PET nanochannel. The attachment of urease by electrostatic interactions granted urea-responsiveness to the sensor. **(B)** The reversibility of the different states of the artificial nanochannel by measuring the rectification factor in the presence and absence of urea alternately. **(C)** Calibration curve in terms of normalized rectification factor vs urea concentration. The device displayed a limit of detection of 1 nM. Reproduced with permission [61]. Copyright 2018, American Chemical Society.

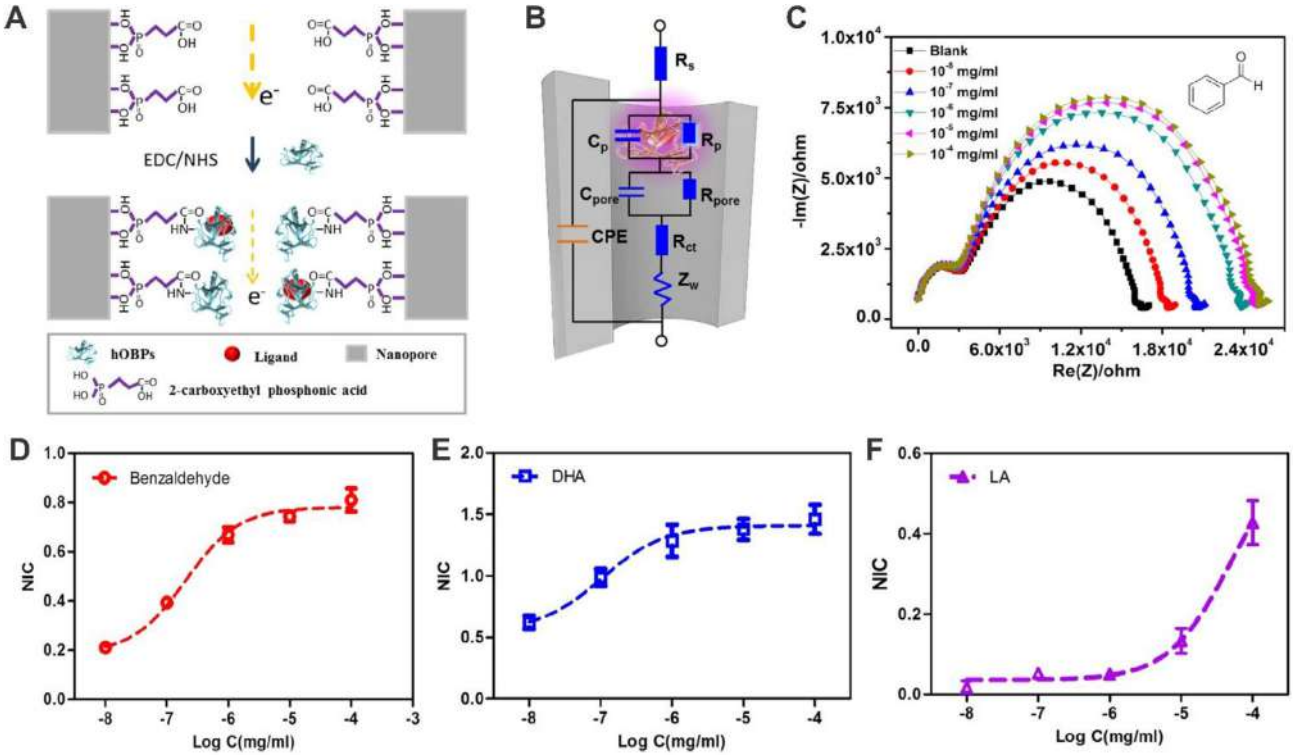

Fig. 19. (A) Schematic illustration of the construction of the hOBPs-modified nanodevice. (B) Equivalent circuit of the hOBPs-modified channels. (C) Impedance spectra of the channel for different benzaldehyde concentrations. (D), (E) and (F) Normalized impedance changes (NIC) in terms of the concentration of benzaldehyde, docosahexaenoic (DHA), and lauric acid (LA), respectively. Adapted with permissions from Ref. [42]. Copyright © 2015 Elsevier B.V. All rights reserved.

biomolecular ligands related to diseases, specifically benzaldehyde, docosahexaenoic and lauric acids (Fig. 19(A)) [42]. The hOBPs present a hydrophobic cavity in their structure that can host different lipophilic ligands to form a "protein-ligand" complex [304,305]. In a nanochannel, this "protein-ligand" interaction could induce changes in protein folding, increasing the resistance to the transmembrane ionic transport. Following this concept, the nanodevice resistances in an impedance circuit could be represented by the protein structure of hOBPs on the surface (R_p), the channel walls (R_{pore}), the solution (R_s), and an additional charge transfer resistance (R_{ct}) which was selected to indicate the efficiency of ion blockage (Fig. 19(B)). By impedance spectroscopy measurements of the different ligand treatments, the authors showed that the exposition to the analytes increases only the series resistance of R_{pore} and R_p, which are related to the interactions between hOBPs on the pore walls and their ligands (Fig. 19(C)). Also, the authors demonstrated that the impedance increment can be related to the ligand concentrations, reaching detection limits lower than 10^{-8} mg/ml (Fig. 19(D), (E) and (F)).

8.2. Drugs and contaminants sensors based on SSN

Naproxen. Nonsteroidal anti-inflammatory drugs (NSAIDs) are the most widely used analgesic medications in the world owing to their ability to reduce pain and inflammation [306]. Naproxen ((S)-6-methoxy-α-methyl-2-naproxen-phthalene acetic acid) is one of the best-known NSAIDs, commonly used for the treatment of osteo- and rheumatoid arthritis, among other pain generating conditions. As the (S)-enantiomer of naproxen (Npx) has greater pharmacological activity than (R)-Npx, Boussouar et al. designed an innovative strategy for detecting chiral drugs with label-free conical track-etched SSNs [307]. In their approach, N-acetyl-L-cysteine capped gold nanoparticles (NALC-AuNP) behave as chiral selectors for the enantioselective recognition of S-Npx in the presence of R-Npx. More specifically, when the nanochannel is exposed to a working solution containing NALC-AuNP and S-Npx or R-Npx, the ionic current noticeably decreases in the presence of S-Npx. The transmembrane ionic current gradually decreases upon increasing S-Npx concentration (0–1 mM), whereas it remains almost constant when the same experiment is carried out in the presence of R-Npx. Furthermore, the authors suggested that the chiral recognition might be associated with a differential stabilization provided by the hydrogen bonds between the ligand N-acetyl-L-cysteine capped on the AuNP surface and S-Npx. By Dynamic light scattering measurements, it could be shown that, when S-Npx was used, these interactions reduced the surface charge of AuNP causing a pronounced aggregation. This phenomenon would be responsible for the rapid blocking of the nanochannel and the concomitant decrease in the transmembrane current. The detection limit achieved by this method was 1 nM for S-Npx and the device showed a reversible modulation between alternative exposure to S-Npx/NALC−AuNP solution and solutions of NALC−AuNP without S-Npx. Finally, a current response to S-Npx with good selectivity was observed in both serum and urine samples.

Inositol-phosphate. Building biomimetic InsP-responsive nanochannels have emerged as a significant strategy in order to acquire a better understanding of the Ca^{2+}-related cellular signal pathways [234,308]. In this line, a biomimetic inositol phosphate-responsive nanochannel device was built on PAA (porous anodic alumina) membranes (Fig. 20(A)) [309]. PAA nanochannels were chemically modified with a copolymer PNI-*co*-ATBA (N-isopropylacrylamide-*co*-4-(3-acryloylthioureido) benzoic acid copolymer) by surface-initiated atom transfer radical polymerization (SI-ATRP). ATBA played as the core inositol phosphate (InsP) recognition unit and the flexible PNI offered a smart hydrogen bonding network in order to modulate the movement of polymer chains due to external stimuli [310]. The copolymer immobilized on the inner surface of the nanochannels becomes expanded by complexation with InsP in the nanomolar range, leading to a sharp decrease in the size of nanochannels, which further decreased the transmembrane ionic current (ohmic behavior) (Fig. 20(B)). With this device, a clear discrimination between InsP and other phosphate species ($InsP_2$, $InsP_3$, and $InsP_6$) could be achieved.

Cocaine. More recently, Wang et al. reported an aptamer-based strategy for further developing diverse nanochannel molecular biosensors with ultrahigh sensitivity and real-time monitoring properties for efficient drug detections (Fig. 21) [311]. In their work, bullet-shaped PET single nanochannel walls were modified by anchoring a C-aptamer which was then recognized by cocaine and other target DNA aptamer (T-aptamer) (Fig. 21(A)). In the presence of cocaine and T-aptamer, a remarkable change in the iontronic output is detected, while when just one of them is present, no changes in the rectification behavior occurred (Fig. 21(B) and (C)). From a microscopic point of view, the complexation of cocaine between the aptamers led to a significant decrease in the effective pore size, thereby decreasing the transmembrane ionic current and the rectification factor (Fig. 21(D) and (E)). Indeed, for a fixed concentration of T-aptamer, a linear response was observed between the transmembrane current at +2 V and the logarithm of the cocaine concentration in the range from 1 nM to 500 μM (Fig. 21(E)). Moreover, the inherent selectivity of aptamers for the target molecule was demonstrated by evaluating the iontronic response of the device in the presence of other closely related drugs as atropine and tropinone.

Oversulfated chondroitin (OSCS). The oversulfated chondroitin (OSCS) is a known heparin contaminant. Heparin (HEP) is commonly used as an anticoagulant agent to treat several clotting disorders [312]. In the last decade, small OSCS concentrations in HEP were shown to cause death in a group of patients around the world [313]. In this context, Ma et al. proposed a label-free reusable sensor to detect OSCS in HEP samples [314]. The nanodevice is based on a PET conical nanochannel functionalized with poly-L-lysine (PLL) and HEP. Initially, the modification of the PET nanochannel with PLL produces a characteristic rectification of an asymmetrical channel with positive surface charge density. The subsequent exposition to HEP triggers an inversion in the polarity of the surface charge density which inverts the rectification properties. This fact has been ascribed to the great affinity between the negatively charged HEP and the PLL-modified surface. Taking advantage of this behavior, the authors introduced a reusable HEP sensor that is able to detect HEP in the concentration range from 25 ng/ml to 3 μg/ml. On the other hand, when the PLL-modified channel was exposed to HEP pretreated with the enzyme heparinase, only a slight change in the iontronic signal was observed which was attributed to the low affinity between the degraded HEP and the PLL. However, in the presence of OSCS, the heparinase is inhibited and the HEP is less degraded. The long chains of heparin have a better affinity with the PLL inducing more efficient charge compensation characterized by a rectification factor decrease. Thus, the rectification factor value decreased with the OSCS concentration. Taking into account that OSCS contaminant has the ability to inhibit HEP degradation promoted by heparinase, the authors presented an OSCS sensor. This platform was sensitive to the inhibition of heparinase by OSCS until a concentration of 200 pg/ml representing 0.01% in weight of HEP. This resolution is one order of magnitude lower than the one obtained by liquid chromatography.

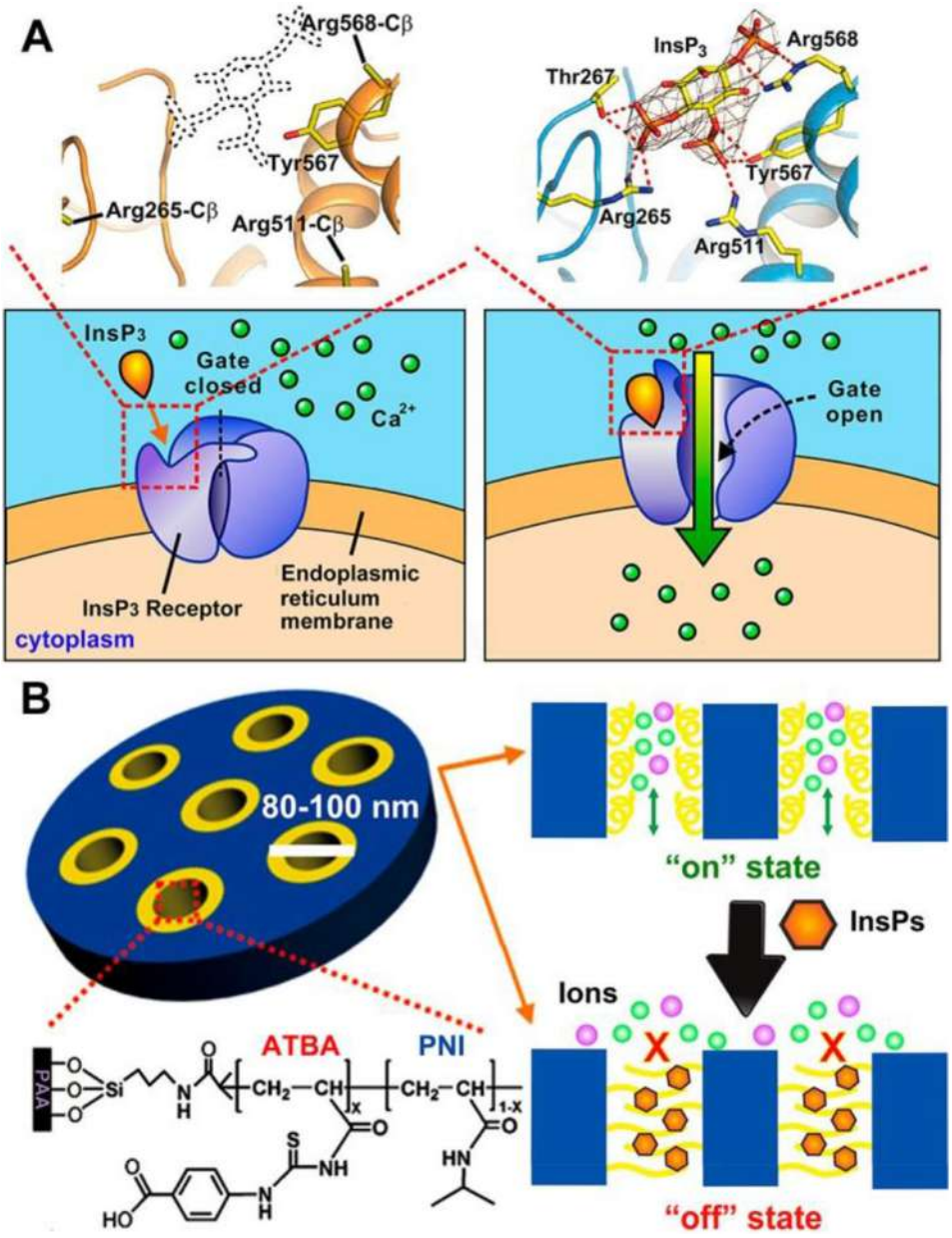

Fig. 20. Inositol-phosphate. (A) Building biomimetic inositol phosphate (InsP)-bonding interactions among $InsP_3$ and specific amino acid residues located on the $InsP_3$ receptor protein ($InsP_3R$), $InsP_3$ is bound to the receptor protein and triggers the conformational switching of $InsP_3R$, which opens the Ca^{2+} channels on the endoplasmic reticulum membrane, leading to a sharp increase in Ca^{2+} concentration in the cytoplasm. **(B)** shows that our biomimetic InsP-responsive ion channels are constructed by modifying InsP-responsive copolymer PNI-co-$ATBA_{0.2}$ on the AAO membrane. The copolymer chains can undergo a remarkable globule-to-coil transition upon exposure to InsPs in ultralow concentrations (at the nanomolar level), which significantly decreases the diameter of the nanochannels and obstructs ion transport across the nanochannels. Reproduced with permission [309]. Copyright 2017, American Chemical Society.

9. Discussion and upcoming challenges

So far, recent works related to the development of SSN-based (bio)sensors have been addressed. In those reports, researchers displayed a broad repertoire of strategies and notions for the development of (bio)sensing platforms compatible with the detection of different analytes such as drugs, ions, nucleic acids, proteins, amino-acids, cells, etc. Regardless of the type of analyte, the key concept that rules the construction of this kind of (bio) sensor is the integration of different recognition elements that, in presence of the analyte, generate predictable changes in the channel properties and thus, a readable variation in the iontronic signal. The ability to transduce different biological, physical, or chemical changes under confinement into iontronic (or electrochemical) signals offers the possibility to detect analyte concentrations with a high sensibility using relatively simple and inexpensive equipment. However, with the purpose of making further progress in this topic and transferring it into technological platforms with tangible applications several issues should be considered.

After the creation of the SSNs, the integration of the recognition element into them is the first critical step in the development of SSNs-based (bio)sensors. As discussed in the previous sections, the current state of this topic shows that there exists mature technical know-how to successfully integrate chemical and biological recognition elements into SSNs through different experimental

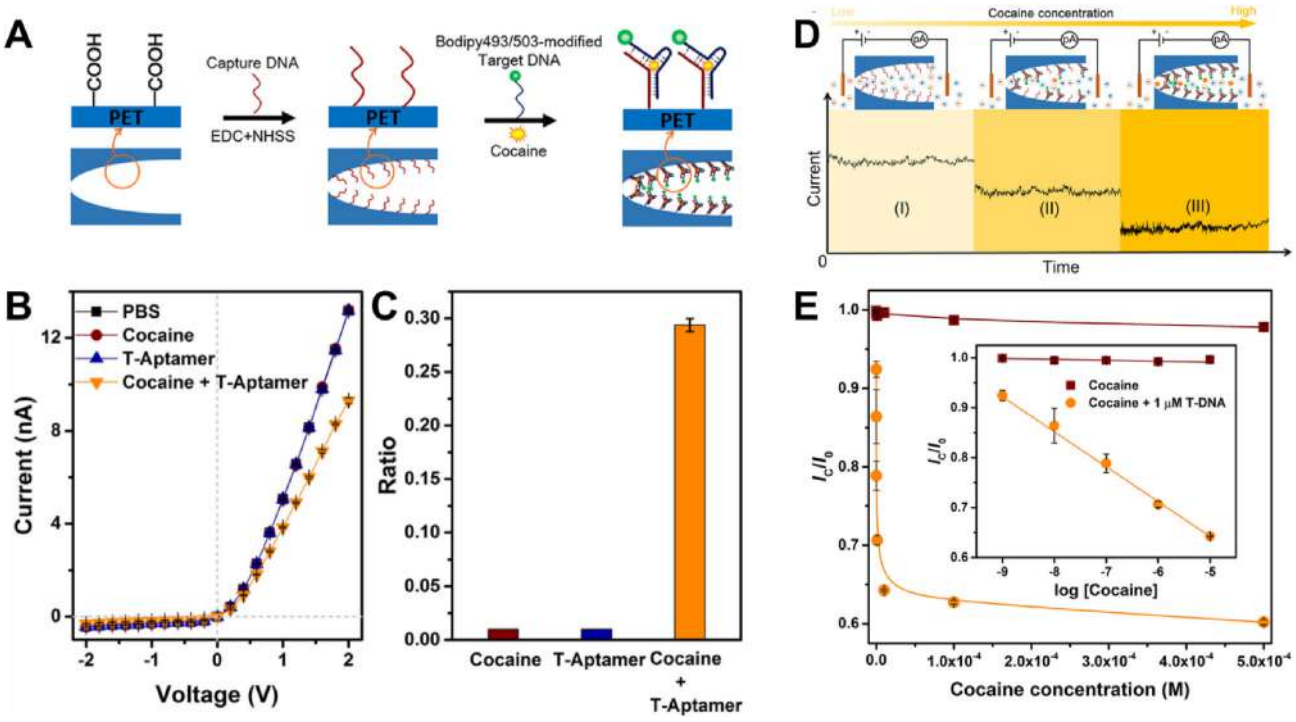

Fig. 21. **(A)** Schematic Representation of a High-Sensitive Aptamer-Based Cocaine Detector Using an Engineered Single Nanochannel; Discriminating property of 1 μM target cocaine in the single-nanochannel-based platform without or with the addition of 1 μM target aptamers, as labeled. **(B)** *I*–*V* curves measured in 0.01 M PBS (pH = 7.4) with or without T-aptamer at a scanning voltage varied from −2 to +2 V with a 21 s period. **(C)** Comparison of the current change ratios, $(I_0-I)/I_0$, recorded at +2 V with 1 μM target cocaine in the proposed platform with or without T-aptamer, where I_0 and I are the current measured in the absence and presence of target analytes. **(D)** Cocaine recognition with a DNA-aptamer-modified single bullet-shaped nanochannel-based platform. Schematic representation of the cocaine detection mechanism with (I) non-cocaine-bound C-aptamer, and (II, III) cocaine-bound states of C-aptamers, forming cocaine-aptamer complexes. Cocaine could be directly detected by monitoring ionic current signals, and the current decreases as the cocaine concentration increases. **(E)** Comparison of the current ratio I_c/I_0 recorded at +2 V with different concentrations of target cocaine in the proposed platform with or without T-aptamer, where I_c is the ionic current measured at different cocaine concentrations, and I_0 is the current measured in the absence of cocaine. Reproduced with permission [311]. Copyright 2018, American Chemical Society.

protocols. The most common integration strategies involve (1) covalent grafting onto the channel surface and (2) deposition via non-covalent assembly [13,16]. Covalent grafting is usually achieved via chemical reactions (for example, coupling with EDC/NHS or post-grafting with organosilanes in silica-coated surfaces) which provide high chemical stability due to the covalent bonds [13,67,145,160]. As an example, the EDC/NHS enables the anchoring of recognition elements onto the surface through the combination of primary amine and carboxylic acid groups. As these chemical groups are common in several receptors, proteins, or even synthesized aptamers, this protocol is widely used for both biofunctionalizations and integration of molecular recognition elements (e.g. crown ethers and pillarenes) [152]. However, in some cases, chemical covalent modifications can be subjected to complex protocols [309]. On the other hand, non-covalent bonding is usually achieved by electrostatic self-assembly and the LbL method and offers simplicity as its main strength. Taking advantage of the charged nature of pristine nanochannels, this technique has been widely exploited for the immobilization of polyelectrolytes [23,85,138]. Also, the possibility to modulate the final charged state of the surface enables the subsequent integration of different recognition elements such as enzymes and proteins [61,119]. In contrast to covalent bonding, non-covalent bonding drawback is related to the stability of the final assemblies, which can be strongly compromised by environmental conditions [16,197].

Based on the state of the art of this field, we can say the adequate selection of the recognition elements is one of the keys in the development of SSN-based (bio)sensors since it determines not only the analyte and its sensing mechanism but also the integration strategy, selectivity, environmental conditions, and stability. Considering the recognition elements addressed in this review, host-guest supramolecular systems from crown-ether, calixarene, pillarene, and other macrocyclic families provide the possibility to create reproducible and robust platforms for a wide variety of analytes such as ions, drugs, and sugars [212,296,315,317,318]. Also, due to the non-covalent nature of the supramolecular host-guest interactions, the reusability in aqueous solutions showed not to be a challenge. Furthermore, some of the host-guest-based sensors introduced in this review have evidenced a low limit of detection (nM range or lower) [216,219,295]. All these features added to not only the large pool of macrocyclic receptors commercially available but also the possibility to design and prepare the recognition element according to the analytical problem position these kinds of sensors as sensing platforms with unlimited potential [317]. However, to paraphrase Prof. Otto S. Wolfbeis [319], sensors are much more than only the probe molecules, and therefore, the careful choice of the integration method and the structural properties of the channel (e.g. size and geometry) result crucial in order to be able to transduce selective host-guest events into readable iontronic signals in a sensitive way. In the case of macrocyclic probes, their integration onto the surface usually involves different covalent chemical reactions and, in some cases, these can be very challenging from an organically synthetic point of view [317].

Beyond the host-guest supramolecular compounds, throughout the review, several sensing platforms based on nanochannels modified with different non-biological recognition elements such as polymers and organic molecules were introduced. Depending on the specific recognition elements, the methods of integration can vary

from covalent grafting (e.g. via EDC/NHS reaction) to non-covalent deposition (e.g. electrostatic self-assembly) [129,239,245]. In contrast to the macrocyclic-modified channels, the sensing mechanisms can include both non-covalent and covalent interactions which opens the door to a wide range of strategies and target compounds. Well-known examples are the use of boronic acid-sugar interactions and the equilibrium between transition metals and their ligands [72,137,232,239]. While the opportunities to create sensing platforms by exploiting different interactions are almost unlimited, the generation of selective devices remains the main challenge. Also, in the case of systems employing covalent interactions as sensing mechanisms, the reusability (associated with reversibility) of the sensor is not a trivial issue.

As already discussed in this work, biomolecules such as nucleic acids, enzymes, proteins, and aptamers are used as valuable recognition elements when integrated into SSNs. Depending on the identity of the recognition element, the integration method and sensing mechanism present marked differences. Usually, biomolecules such as aptamers, nucleic acids, proteins, and enzymes, can be grafted on the surface by covalent chemical reactions or deposited via electrostatic self-assembly (or LbL) [61,197,258,269,311,316]. In both cases, the method must assure the attachment of biomolecules onto the nanochannel surface without appreciable loss of activity, which is particularly critical in the case of enzymes. Additionally, the nature of the recognition element determines the operation conditions of the device. For instance, the activity of enzymes depends on temperature, ionic strength, and pH, which restricts the sensor operation to certain environmental conditions [320]. While the delicate nature of some biological recognition elements is the major drawback of biofunctionalized sensors, they offer high selectivity (even specificity) and the possibility to amplify the signal which positions it as one of the preferred molecular systems for the development of SSNs-based sensors [25,26].

SSNs-based devices capable of quantifying target molecules under very low concentration conditions have been reported in several works (Tables 1–4). Nevertheless, much effort is needed to transform these valuable findings into commercial applications. In this line, we believe that there are at least two main challenges to tackle in the immediate future. On the one hand, variability arising not only from the nanofabrication technique but also from the integration of the recognition elements can be a determinant factor. The implementation of different straightforward chemical routes for the development of SSNs-based sensors can be a key to improve reproducibility. In this regard, some examples show that the previous functionalization of the channel surface with SiO_2 (via ALD) or Au (via sputtering) offers several simple chemical routes with high stability for the molecular probe integration which can be an interesting alternative to reinforce the reproducibility [137,145,160]. Also, advances in nanofabrication technologies will play a crucial role in this point. On the other hand, while some examples are showing sensitive and selective performances even in real samples such as serum, urine, or cells, most of the reported works have been tested in ideal aqueous solutions prepared in the laboratory [252,281,295,307]. It is widely known that exposure to real samples can severely affect the sensing capabilities because different chemical and biological compounds present in the complex matrix can adsorb unspecifically onto the surface of the channel (or membrane) generating negative effects on the performance [36,321]. Considering these effects, long-term stability can be also a critical issue, and therefore, searching for different alternatives to mitigate this phenomenon acquires a great relevance.

Last, but not least, as in other areas of (bio)sensing, the research compartmentalization can become a barrier to be broken down [317]. The construction of (bio)sensors with real applications requires a multidisciplinary approach involving backgrounds in biology, chemistry, physics, materials science, engineering, and medicine. In order to move ahead, the synergistic combination and coordination of actors from different areas will be crucial.

10. Concluding remarks and perspectives

Accurate and reliable sensing of chemical and biological species is of paramount relevance in multiple aspects of our daily lives. For example, sensitive detection of biomarkers is a prerequisite for identifying at-risk patients as early as possible during the disease process. Meeting the increasing demand for sensors with high

Table 1
Detection of target ionic analytes with nanochannel-based sensors by employing different strategies.

Target analyte	Nanochannel material	Recognition element	Limit of detection (LoD)	Reference
Borate	PET	N-(3-triethoxysilylpropyl)-gluconamide	0.1 nM	[145]
Ca^{+2}	AAO	Heptapeptide-based copolymer	10 pM	[224]
Cs^{+}	PET	p-tert-butylcalix [4]arene-crown	1 mM	[213]
Cu^{+2}	PET	dsDNA (DNAzyme)	10 nM	[221]
Cu^{+2}	PET	Peptide	10 fM	[222]
Cu^{+2}	AAO	Polyglutamic acid	0.3 fM	[129]
F^{-}	PET	tert-butyldiphenylsilyl-fluoresceine	0.1 mM	[242]
Hg^{+2}	PET	Mercaptoacetic acidpillar [5]arene	10 μM	[218]
HSO_3^{-}	PET	4-aminophenyl-phenyl-Methanone	1 μM	[241]
K^{+}	PET	4-Aminobenzo-18-crown-6	1 fM	[216]
K^{+}	PET	Amine-terminated bis-podand	10 μM	[217]
K^{+}	PET	DNA hydrogel	50 mM	[223]
Li^{+}	PET	Aminoethyl-benzo-12-crown-4	1 μM	[212]
NO_2^{-}	PET	p-phenylecediamine	10 pM	[240]
O_2^{*-}	Quartz nanopipette	Cyt C	0.2 μM	[226]
Pb^{+2}	PET	4-Aminobenzo-18-crown-6	1 fM	[214]
Pb^{+2}	PET	4-Aminobenzo-18-crown-6	1 μM	[215]
Pyrophosphate	PI	Isozianid functionalized calix [4]arene	10 nM	[219]
Pyrophosphate	PET	Di(2-picolyl)amine	10 pM	[229]
Pyrophosphate	PET	N′–(4–((2,2′:6′,2″–terpyridine)–4–yl)benzyl)ethane–1,2–diamine/Zn^{+2}	1 μM	[232]
S^{-2}	TiO_2	Bovine serum albumin/Cu	1 nM	[47]
UO^{+2}	PI	4-aminobenzamidoxine	1 fM	[239]
Zn^{+2}	PET	DNA supersandwich (DNAzyme)	1 nM	[73]
Zn^{+2}	PET	N′–(4–((2,2′:6′,2″–terpyridine)–4–yl)benzyl)ethane–1,2–diamine	1 nM	[232]

Table 2
Detection of gases with nanochannels-based sensors by different strategies.

Target analyte	Nanochannel material	Recognition element	Detection limit/range	Matrix	Reference
Carbon dioxide	PI	APTE (1-(4-amino-phenyl)-2,2,2-trifluoro-ethanone)	–	aq	[245]
Nitric oxide	PET	2,3-diaminobenzene acid	10^{-3}-10^{-7} Mm	aq	[251]
Nitric oxide	PET	Rhodamine 6G	35.3 fM	endothelial cells	[252]
Formaldehyde	PET	Ethylenediamine	10^{-9}-10^{-6} mg/ml	aq	[255]

Table 3
Detection of nucleic acids, proteins, cells, cellular targets, and viruses with nanochannel-based biosensors.

Target analyte	Nanochannel material	Recognition element	Limit of detection (LoD)/ range	Matrix	Reference
7.1. Nucleic acids sensing using the hybridization strategy					
DNA	PET	Complementary DNA	10 fM	serum	[258]
m-RNA	AAO	Thiol-DNA capture probe	30 fM; DLR: 0.1–10 pM.	RNA extracts from cultured cell lines	[261]
mi-RNA	PET	PMO	10 fM	aq	[269]
mi-R122	PET/GO	Zr^{4+}/PO_4^{3-}-dsDNA	LoD = 97.2 aM; DLR: 10 aM-10 pM	Human liver total RNA sample.	[270]
7.2. Proteins and enzymes					
Avidin/Streptavidin	PET/SiO_2	Biotin functionalized spacers	1 nM	aq	[275]
Carboxypeptidase B activity (CPB)	AAO	Specific alkaline peptide	LoD = 0.01 U/ml; DLR: 0.01–10 U/ml	Human serum solution	[281]
Phosphoprotein analytes (PPn)	PET	Dipicolyamine (DPA)-Zn^{2+}	1–50 nM (phospho-α-casein)	aq	[278]
7.3. Sensing cells, cellular targets, or viruses with nanochannel-based sensors					
Circulating tumour cells (CTCs)	AAO	Specific aptamer	LoD = 10 cells/μl; LDR: 100–1000 cells/ml.	Cells aq. Solution.	[130]
H_2O_2 released from cells	PET	L-tyrosine	–	–	[292]
Mannose/Cells surface glycans	AAO	Concavalin A	Mannose: LoD = 9.997 aM, DLR: 10 fM-10 mM; MCF-7 Cells: 10^2-10^6 Cells/ml.	aq. Solution/Cells aq. solution	[288]
MS2 bacteriophage	AAO	MS2-phage polyclonal antibody	LoD = 7 pfu/ml	aq	[179]

Table 4
Detection of small biomolecules and drugs with nanochannels-based biosensors by different strategies.

Target analyte	Nanochannel material	Recognition element	Limit of detection (LoD)/range	Matrix	Reference
Adamantanamine	PET	Cucurbit [7]uril	4.54 nM	chicken samples	[315]
Adenosine	PET	Aptamer	–	aq	[316]
Arginine	Glass	BSA-Au nanocluster	1 fM	aq	[119]
ATP	PI	Azo-DNA aptamer	0.25–104 pM	aq	[303]
ATP	PET	polyallylamine	0.5–2 μM	aq	[85]
Benzaldehyde, Docosahexaenoic acid, Lauric acid	AAO	human odorant-binding proteins	10^{-8} mg/ml	aq	[42]
Cocaine	PET	DNA-Aptamer	1 nM	aq	[311]
Dopamine	PET	poly (3-aminobenzylamine)	1–50 nM	aq	[138]
Fructose	PC	poly(3-aminephenylboronic acid)	10 mM	aq	[137]
Glucose	PET	(1,2-diphenylethene-1,2-diyl) bis (1,4-phenylene)-1, 1′-diboronic acid	0.4 μM	urine	[72]
Glucose	PET	Chiral pillar [6]arene decorated with L-alanine	1 mM	aq	[296]
Histamine	PET	Nα,Nα-bis(carboxymethyl)-l-lysine	1–106 nM	aq	[68]
Inositol-phosphate	AAO	copolymer PNI-co-ATBA	1 nM	aq	[309]
L-Tryptophan	PET	bovine serum albumin (BSA)	1.5–100 mM	wheat samples	[293]
N-acetylglucosamine	PET	Tryptophan pillararene	10^{-6} M	serum	[295]
Naproxen	PET	N-acetyl-L-cysteine capped gold nanoparticles	1 nM	aq, serum and urine	[307]
Ochratoxin A	Glass	DNA-aptamer	5 nM	wheat samples	[120]
Oversulfated chondroitin	PET	poly-L-lysine	25 ng/ml - 3 μg/ml	aq	[314]
Urea	PET	Polyallylamine/urease enzyme	1 nM	aq	[61]

sensitivity, high selectivity, and rapid detection presents many challenges. In the last decade, sensors based on nanoporous platforms, such as biomimetic nanochannels, glass nanopipettes, or nanoporous alumina, have been widely studied due to their high sensitivity, rapid detection, and simple test procedure. Part of the appeal of nanochannel-based (bio)sensors relies on the tremendous potential for the detection of a wide range of analytes which is mainly attributed to the unique transport properties of these nanoarchitectures.

We should also bear in mind that the integration of receptors, macromolecular ligands, or biological entities into nanochannels may lead to very interesting and useful ensemble properties

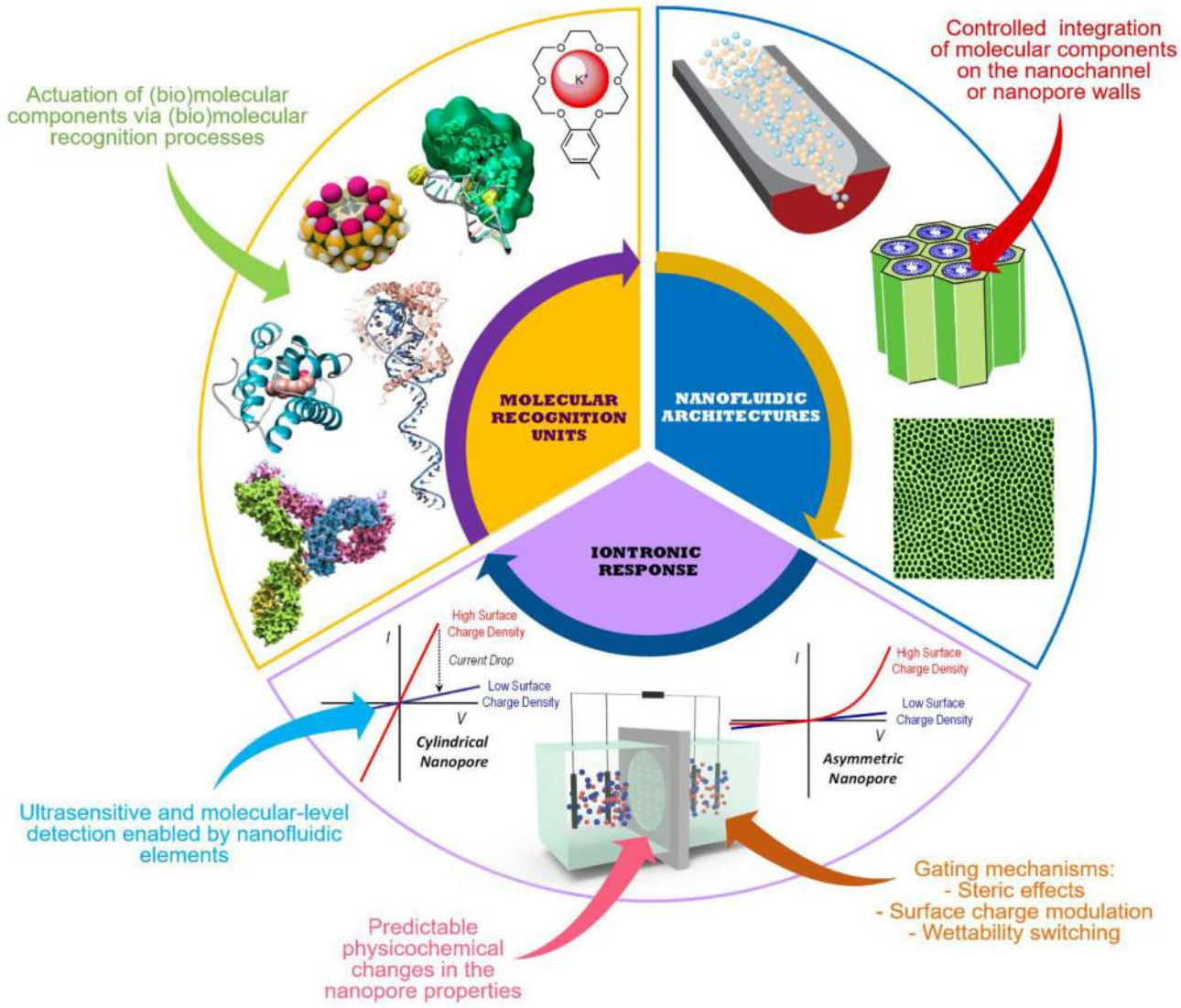

Fig. 22. Illustration describing the combination of molecular recognition units and nanochannel architectures in order to design nanofluidic architectures capable of transducing biological, chemical, and physical stimuli into predictable "iontronic" signals.

emanating directly from nanoconfinement effects (Fig. 22). Physical, chemical, and biological processes that occur in the constrained spaces of nanochannels deserve particular attention for they are a fundamental part of the "iontronic" transduction process of the nanoporous platform. In a physically constrained environment, interfacial interactions can play a dominant role in determining the physicochemical characteristics of the nanochannel walls, with a concomitant effect on the ionic transport properties. This is particularly relevant in the context of the biosensing applications of nanochannels. The biosensing capabilities of these nanochannels depend sensitively on the surface characteristics of their inner walls to achieve the desired functionality of the nanofluidic system. When a target molecule diffuses into the nanochannel, it can react with specific binding groups located on the inner surface of the nanochannel, thus inducing the sensing effect, or the physical or chemical changes, due to a detection event.

Due to the fact that nanochannels have dimensions comparable to the size of biological molecules, depending on the size of the target molecule, the molecular recognition process can cause a decrease in the effective diameter of the nanochannel. However, depending on the chemical nature of the target molecule and the binding sites, the recognition process can also lead to changes in the surface charge density or the wettability of the confined space of the nanochannels. The fundamental notion here is that in either of the above cases the recognition process carries with it predictable physicochemical transformations of the nanochannel environment, which ultimately result in measurable transmembrane ionic current changes (Fig. 22).

It is clear today that nanoscale control over the shape and surface chemistry of the nanochannels not only enables new modalities for biosensing but also plays a crucial role in biosensing performance. Engineered nanochannels of varying geometries, and fabricated in different materials, can generate predictable ionic signals in the presence of specific chemical and biological targets, as a result of the electrostatic and/or steric effects stemming from the recognition process. The orchestration of electrostatic, steric, and nanoconfinement effects is key to the fabrication of highly sensitive, selective, and fast-responding nanochannel biosensors, making them promising candidates for clinical applications.

What is important here is that the integration of precisely assembled biomolecular and supramolecular machinery into nanochannels has opened the path for the detection and quantification of targets of varying structural and functional complexity, ranging from small molecules to circulating tumor cells.

Further, synergistically enhanced ionic signals have been achieved through the concertation of different functions into the nanochannels. One clear example of this strategy is the "iontronic" detection of analytes through enzymatic processes taking place in charged nanochannels.

A careful look at the recent literature reveals that the "iontronic" characteristics of the engineered nanochannels enable precise and reliable quantitative analysis for various target analytes with remarkable sensitivities, breaking through the limits of other detection methods. In the last decade, nanochannel-based sensors have gained relevance in the detection of biomolecules for disease diagnosis, the detection of contaminants for water quality assessment, and the detection of chemical analytes for the evaluation of physiological activity. Recent trends in both scientific research and business development indicate a growing interest in nanopore and nanochannel sensors with the ultimate goal of developing a broad range of reliable, inexpensive, high-performance biomedical devices, and intelligent platforms, which can be easily interfaced with digital electronics for biomedical diagnostics. In fact, the increasing number of patent applications filed by large companies reflects the eagerness of the industry to convert novel innovations in nanopore sensors into commercial products. At present, companies such as IBM [322,323], Intel [324], Agilent Technologies [325,326], Roche [327], and Samsung [328] have filed patent applications related to fabrication, functionalization, measurement, and applications of solid-state nanopores and nanochannels.

The creativity of chemists and materials scientists provided a means for developing a wide variety of functional nanoporous platforms with unprecedented functional properties. Most of this progress stemmed from looking to nature's blueprints for intentional, creative direction, as many sensing mechanisms or the design of many nanopore and nanochannel sensors are based on the features of their biological counterparts.

The new frontiers for nanochannel (bio)sensors are rapidly advancing and the future offers the prospect of many developments as researchers show an increased mastery in the precise incorporation of active elements into nanochannels and nanopores. Looking at the ongoing developments, we can say today that significant progress on nanochannel sensors is being made in the nanoscience community. And, undoubtedly, the progress made in these research activities has taken the field to a new level of maturity.

The purpose of this work was to provide comprehensive coverage of current and emerging technologies of nanochannel sensing, explaining the principles of the sensor design and discussing new trends in the field. It is our hope that this work will form a foundation (and indeed a motivation) for new researchers in the area as well as also being useful - as a quick overview of major findings - to experienced researchers.

Declaration of competing interest

The authors declare that they have no known competing financial interests or personal relationships that could have appeared to influence the work reported in this paper.

Acknowledgements

G. L. and Y. T. T. acknowledge a scholarship from CONICET. G.L. also acknowledges a scholarship for a short-term research stay from DAAD and the support of GET_INvolved programme of GSI. V.M.C acknowledges postdoctoral financial support from Universidad Nacional de La Plata. M. L. C., W. A. M., and O. A. are CONICET fellows and acknowledge financial support from Universidad Nacional de La Plata (PPID-X867), CONICET (PIP-0370), and ANPCyT (PICT-2017-1523 and PICT2016-1680). C. T. and M. E. T. M. acknowledge support by the LOEWE project iNAPO funded by the Hessen State Ministry of Higher Education, Research and Arts.

References

[1] A. Gleich, C. Pade, U. Petschow, E. Pissarskoi, Potentials and Trends in Biomimetics, first ed., Springer Berlin Heidelberg, Berlin, Heidelberg, 2010. https://doi.org/10.1007/978-3-642-05246-0.
[2] M. Tagliazucchi, I. Szleifer, Transport mechanisms in nanopores and nanochannels: can we mimic nature? Mater. Today 18 (2015) 131–142. https://doi.org/10.1016/j.mattod.2014.10.020.
[3] X. Hou, L. Jiang, Learning from nature: building bio-inspired smart nanochannels, ACS Nano 3 (2009) 3339–3342. https://doi.org/10.1021/nn901402b.
[4] G. Pérez-Mitta, A.G. Albesa, C. Trautmann, M.E. Toimil-Molares, O. Azzaroni, Bioinspired integrated nanosystems based on solid-state nanopores: "iontronic" transduction of biological, chemical and physical stimuli, Chem. Sci. 8 (2017) 890–913. https://doi.org/10.1039/c6sc04255d.
[5] C. Dekker, Solid-state nanopores, Nat. Nanotechnol. 2 (2007) 209–215. https://doi.org/10.1142/9789814287005_0007.
[6] G. Xie, L. Wen, L. Jiang, Biomimetic smart nanochannels for power harvesting, Nano Res. 9 (2016) 59–71. https://doi.org/10.1007/s12274-016-0993-1.
[7] K. Xiao, L. Jiang, M. Antonietti, Ion transport in nanofluidic devices for energy harvesting, Joule 3 (2019) 2364–2380. https://doi.org/10.1016/j.joule.2019.09.005.
[8] X. Hou, W. Guo, L. Jiang, Biomimetic smart nanopores and nanochannels, Chem. Soc. Rev. 40 (2011) 2385–2401. https://doi.org/10.1039/c0cs00053a.
[9] L.T. Sexton, L.P. Horne, C.R. Martin, Developing synthetic conical nanopores for biosensing applications, Mol. Biosyst. 3 (2007) 667–685. https://doi.org/10.1039/b708725j.
[10] A. de la Escosura-Muñiz, A. Merkoçi, Nanochannels preparation and application in biosensing, ACS Nano 6 (2012) 7556–7583. https://doi.org/10.1021/nn301368z.
[11] K. Xiao, L. Wen, L. Jiang, Biomimetic solid-state nanochannels: from fundamental research to practical applications, Small 12 (2016) 2810–2831. https://doi.org/10.1002/smll.201600359.
[12] G. Pérez-Mitta, M.E. Toimil-Molares, C. Trautmann, W.A. Marmisollé, O. Azzaroni, Molecular design of solid-state nanopores: fundamental concepts and applications, Adv. Mater. 31 (2019) 1901483. https://doi.org/10.1002/adma.201901483.
[13] M. Tagliazucchi, I. Szleifer, Chemically Modified Nanopores and Nanochannels, first ed., Elsevier, 2016.
[14] R. Spohr, Ion Tracks and Microtechnology, first ed., Vieweg, Wiesbaden, 1990. https://doi.org/10.1007/978-3-322-83103-3.
[15] B. Hille, Ion Channels of Excitable Membranes, third ed., Sinauer Associates, Sunderland, 2001.
[16] X. Hou, H. Zhang, L. Jiang, Building bio-inspired artificial functional nanochannels: from symmetric to asymmetric modification, Angew. Chem. Int. Ed. 51 (2012) 5296–5307. https://doi.org/10.1002/anie.201104904.
[17] Y.-B. Zheng, S. Zhao, S.-H. Cao, S.-L. Cai, X.-H. Cai, Y.-Q. Li, A temperature, pH and sugar triple-stimuli-responsive nanofluidic diode, Nanoscale 9 (2017) 433–439. https://doi.org/10.1039/C6NR07339E.
[18] S. Nasir, M. Ali, W. Ensinger, Thermally controlled permeation of ionic molecules through synthetic nanopores functionalized with amine-terminated polymer brushes, Nanotechnology 23 (2012) 225502. https://doi.org/10.1088/0957-4484/23/22/225502.
[19] M. Zhang, X. Hou, J. Wang, Y. Tian, X. Fan, J. Zhai, L. Jiang, Light and pH cooperative nanofluidic diode using a spiropyran- functionalized single nanochannel, Adv. Mater. 24 (2012) 2424–2428. https://doi.org/10.1002/adma.201104536.
[20] G. Laucirica, V.M. Cayón, Y. Toum Terrones, M.L. Cortez, M.E. Toimil-Molares, C. Trautmann, W.A. Marmisollé, O. Azzaroni, Electrochemically addressable nanofluidic devices based on PET nanochannels modified with electropolymerized poly- o -aminophenol films, Nanoscale 12 (2020) 6002–6011. https://doi.org/10.1039/C9NR10336H.
[21] G. Pérez-Mitta, W.A. Marmisollé, C. Trautmann, M.E. Toimil-Molares, O. Azzaroni, An all-plastic field-effect nanofluidic diode gated by a conducting polymer layer, Adv. Mater. 29 (2017) 1700972. https://doi.org/10.1002/adma.201700972.
[22] P. Li, G. Xie, X.Y. Kong, Z. Zhang, K. Xiao, L. Wen, L. Jiang, Light-controlled ion transport through biomimetic DNA-based channels, Angew. Chem. Int. Ed. 55 (2016) 15637–15641. https://doi.org/10.1002/anie.201609161.
[23] G. Pérez-Mitta, A. Albesa, F.M. Gilles, M.E. Toimil-Molares, C. Trautmann, O. Azzaroni, Noncovalent approach toward the construction of nanofluidic diodes with pH-reversible rectifying properties: insights from theory and

experiment, J. Phys. Chem. C 121 (2017) 9070–9076. https://doi.org/10.1021/acs.jpcc.7b01639.
[24] Z. Long, S. Zhan, P. Gao, Y. Wang, X. Lou, F. Xia, Recent advances in solid nanopore/channel analysis, Anal. Chem. 90 (2018) 577–588. https://doi.org/10.1021/acs.analchem.7b04737.
[25] D. Ding, P. Gao, Q. Ma, D. Wang, F. Xia, Biomolecule-functionalized solid-state ion nanochannels/nanopores: features and techniques, Small 15 (2019) 1804878. https://doi.org/10.1002/smll.201804878.
[26] R.E. Gyurcsányi, Chemically-modified nanopores for sensing, TrAC Trends Anal. Chem. (Reference Ed.) 27 (2008) 627–639. https://doi.org/10.1016/j.trac.2008.06.002.
[27] S. Howorka, Z. Siwy, Nanopore analytics: sensing of single molecules, Chem. Soc. Rev. 38 (2009) 2360–2384. https://doi.org/10.1039/b813796j.
[28] W.H. Coulter, Means for Counting Particles Suspended in a Fluid, U.S. Patent, 1953. No. 2656508.
[29] B.N. Miles, A.P. Ivanov, K.A. Wilson, F. Doğan, D. Japrung, J.B. Edel, Single molecule sensing with solid-state nanopores: novel materials, methods, and applications, Chem. Soc. Rev. 42 (2013) 15–28. https://doi.org/10.1039/C2CS35286A.
[30] W. Shi, A.K. Friedman, L.A. Baker, Nanopore sensing, Anal. Chem. 89 (2017) 157–188. https://doi.org/10.1021/acs.analchem.6b04260.
[31] L. Xue, H. Yamazaki, R. Ren, M. Wanunu, A.P. Ivanov, J.B. Edel, Solid-state nanopore sensors, Nat. Rev. Mater. 5 (2020) 931–951. https://doi.org/10.1038/s41578-020-0229-6.
[32] Y. Goto, R. Akahori, I. Yanagi, K. Takeda, Solid-state nanopores towards single-molecule DNA sequencing, J. Hum. Genet. 65 (2020) 69–77. https://doi.org/10.1038/s10038-019-0655-8.
[33] L. Restrepo-Pérez, C. Joo, C. Dekker, Paving the way to single-molecule protein sequencing, Nat. Nanotechnol. 13 (2018) 786–796. https://doi.org/10.1038/s41565-018-0236-6.
[34] Y. He, M. Tsutsui, Y. Zhou, X.-S. Miao, Solid-state nanopore systems: from materials to applications, NPG Asia Mater. 13 (2021) 48. https://doi.org/10.1038/s41427-021-00313-z.
[35] M. Rahman, M.J.N. Sampad, A. Hawkins, H. Schmidt, Recent advances in integrated solid-state nanopore sensors, Lab Chip (2021). https://doi.org/10.1039/D1LC00294E.
[36] Q. Ma, Z. Si, Y. Li, D. Wang, X. Wu, P. Gao, F. Xia, Functional solid-state nanochannels for biochemical sensing, TrAC Trends Anal. Chem. (Reference Ed.) 115 (2019) 174–186. https://doi.org/10.1016/j.trac.2019.04.014.
[37] J.-H. Han, K.B. Kim, H.C. Kim, T.D. Chung, Ionic circuits based on polyelectrolyte diodes on a microchip, Angew. Chem. Int. Ed. 48 (2009) 3830–3833. https://doi.org/10.1002/anie.200900045.
[38] J.-H. Han, K.B. Kim, J.H. Bae, B.J. Kim, C.M. Kang, H.C. Kim, T.D. Chung, Ion flow crossing over a polyelectrolyte diode on a microfluidic chip, Small 7 (2011) 2629–2639. https://doi.org/10.1002/smll.201100827.
[39] R.B. Schoch, J. Han, P. Renaud, Transport phenomena in nanofluidics, Rev. Mod. Phys. 80 (2008) 839–883. https://doi.org/10.1103/RevModPhys.80.839.
[40] R.B. Schoch, H. van Lintel, P. Renaud, Effect of the surface charge on ion transport through nanoslits, Phys. Fluids 17 (2005) 100604. https://doi.org/10.1063/1.1896936.
[41] N. Li, S. Yu, C.C. Harrell, C.R. Martin, Conical nanopore membranes. Preparation and transport properties, Anal. Chem. 76 (2004) 2025–2030. https://doi.org/10.1021/ac035402e.
[42] Y. Lu, D. Zhang, Q. Zhang, Y. Huang, S. Luo, Y. Yao, S. Li, Q. Liu, Impedance spectroscopy analysis of human odorant binding proteins immobilized on nanopore arrays for biochemical detection, Biosens. Bioelectron. 79 (2016) 251–257. https://doi.org/10.1016/j.bios.2015.12.047.
[43] A.J. Bard, L.R. Faulkner, Electrochemical Methods. Fundamentals and Applications, second ed., Wiley, USA, 2001.
[44] J.N. Israelachvili, Intermolecular and Surface Forces, third ed., Elsevier, 2011. https://doi.org/10.1016/C2011-0-05119-0.
[45] R.B. Schoch, P. Renaud, Ion transport through nanoslits dominated by the effective surface charge, Appl. Phys. Lett. 86 (2005) 253111. https://doi.org/10.1063/1.1954899.
[46] C. Lee, L. Joly, A. Siria, A.-L. Biance, R. Fulcrand, L. Bocquet, Large apparent electric size of solid-state nanopores due to spatially extended surface conduction, Nano Lett. 12 (2012) 4037–4044. https://doi.org/10.1021/nl301412b.
[47] J. Guo, L. Yang, H. Xu, C. Zhao, Z. Dai, Z. Gao, Y. Song, Biomineralization-driven ion gate in TiO 2 nanochannel arrays for cell H 2 S sensing, Anal. Chem. 91 (2019) 13746–13751. https://doi.org/10.1021/acs.analchem.9b03119.
[48] Z.S. Siwy, Ion-current rectification in nanopores and nanotubes with broken symmetry, Adv. Funct. Mater. 16 (2006) 735–746. https://doi.org/10.1002/adfm.200500471.
[49] P. Ramírez, P.Y. Apel, J. Cervera, S. Mafé, Pore structure and function of synthetic nanopores with fixed charges: tip shape and rectification properties, Nanotechnology 19 (2008). https://doi.org/10.1088/0957-4484/19/31/315707.
[50] G. Laucirica, W.A. Marmisollé, M.E. Toimil-Molares, C. Trautmann, O. Azzaroni, Redox-driven reversible gating of solid-state nanochannels, ACS Appl. Mater. Interfaces 11 (2019) 30001–30009. https://doi.org/10.1021/acsami.9b05961.
[51] W. Guo, Y. Tian, L. Jiang, Asymmetric ion transport through ion-channel-mimetic solid-state nanopores, Acc. Chem. Res. 46 (2013) 2834–2846. https://doi.org/10.1021/ar400024p.
[52] X. Huang, X.-Y. Kong, L. Wen, L. Jiang, Bioinspired ionic diodes: from unipolar to bipolar, Adv. Funct. Mater. 28 (2018) 1801079. https://doi.org/10.1002/adfm.201801079.
[53] Z.S. Siwy, S. Howorka, Engineered voltage-responsive nanopores, Chem. Soc. Rev. 39 (2010) 1115–1132. https://doi.org/10.1039/b909105j.
[54] L. Yang, P. Liu, C. Zhu, Y. Zhao, M. Yuan, X.-Y. Kong, L. Wen, L. Jiang, Ion transport regulation through triblock copolymer/PET asymmetric nanochannel membrane: model system establishment and rectification mapping, Chin. Chem. Lett. 32 (2021) 822–825. https://doi.org/10.1016/j.cclet.2020.04.047.
[55] S. Tseng, S.-C. Lin, C. Lin, J. Hsu, Influences of cone angle and surface charge density on the ion current rectification behavior of a conical nanopore, J. Phys. Chem. C 120 (2016) 25620–25627. https://doi.org/10.1021/acs.jpcc.6b08588.
[56] Q.H. Nguyen, M. Ali, S. Nasir, W. Ensinger, Transport properties of track-etched membranes having variable effective pore-lengths, Nanotechnology 26 (2015) 485502. https://doi.org/10.1088/0957-4484/26/48/485502.
[57] J. Cervera, B. Schiedt, R. Neumann, S. Mafé, P. Ramírez, Ionic conduction, rectification, and selectivity in single conical nanopores, J. Chem. Phys. 124 (2006) 104706. https://doi.org/10.1063/1.2179797.
[58] G. Pérez-Mitta, A.G. Albesa, M.E. Toimil-Molares, C. Trautmann, O. Azzaroni, The influence of divalent anions on the rectification properties of nanofluidic diodes: insights from experiments and theoretical simulations, ChemPhysChem 17 (2016) 2718–2725. https://doi.org/10.1002/cphc.201600370.
[59] G. Laucirica, M.E. Toimil-Molares, C. Trautmann, W.A. Marmisollé, O. Azzaroni, Polyaniline for improved blue energy harvesting: highly rectifying nanofluidic diodes operating in hypersaline conditions via one-step functionalization, ACS Appl. Mater. Interfaces 12 (2020) 28148–28157. https://doi.org/10.1021/acsami.0c05102.
[60] G. Pérez-Mitta, J.S. Tuninetti, W. Knoll, C. Trautmann, M.E. Toimil-Molares, O. Azzaroni, Polydopamine meets solid-state nanopores: a bioinspired integrative surface chemistry approach to tailor the functional properties of nanofluidic diodes, J. Am. Chem. Soc. 137 (2015) 6011–6017. https://doi.org/10.1021/jacs.5b01638.
[61] G. Pérez-Mitta, A.S. Peinetti, M.L. Cortez, M.E. Toimil-Molares, C. Trautmann, O. Azzaroni, Highly sensitive biosensing with solid-state nanopores displaying enzymatically reconfigurable rectification properties, Nano Lett. 18 (2018) 3303–3310. https://doi.org/10.1021/acs.nanolett.8b01281.
[62] J.H. Wang, C.R. Martin, A new drug-sensing paradigm based on ion-current rectification in a conically shaped nanopore, Nanomedicine 3 (2008) 13–20. https://doi.org/10.2217/17435889.3.1.13.
[63] S.N. Bush, T.T. Volta, C.R. Martin, Chemical sensing and chemoresponsive pumping with conical-pore polymeric membranes, Nanomaterials 10 (2020) 571. https://doi.org/10.3390/nano10030571.
[64] J. Wang, M. Zhang, J. Zhai, L. Jiang, Theoretical simulation of the ion current rectification (ICR) in nano-pores based on the Poisson-Nernst-Planck (PNP) model, Phys. Chem. Chem. Phys. 16 (2014) 23–32. https://doi.org/10.1039/c3cp51712h.
[65] F.M. Gilles, M. Tagliazucchi, O. Azzaroni, I. Szleifer, Ionic conductance of polyelectrolyte-modified nanochannels: nanoconfinement effects on the coupled protonation equilibria of polyprotic brushes, J. Phys. Chem. C 120 (2016) 4789–4798. https://doi.org/10.1021/acs.jpcc.5b11788.
[66] P. Ramírez, V. Gómez, J. Cervera, B. Schiedt, S. Mafé, Ion transport and selectivity in nanopores with spatially inhomogeneous fixed charge distributions, J. Chem. Phys. 126 (2007) 1–10. https://doi.org/10.1063/1.2735608.
[67] G. Pérez-Mitta, A.G. Albesa, W. Knoll, C. Trautmann, M.E. Toimil-Molares, O. Azzaroni, Host–guest supramolecular chemistry in solid-state nanopores: potassium-driven modulation of ionic transport in nanofluidic diodes, Nanoscale 7 (2015) 15594–15598. https://doi.org/10.1039/C5NR04645A.
[68] M. Ali, P. Ramirez, I. Duznovic, S. Nasir, S. Mafe, W. Ensinger, Label-free histamine detection with nanofluidic diodes through metal ion displacement mechanism, Colloids Surf. B Biointerfaces 150 (2017) 201–208. https://doi.org/10.1016/j.colsurfb.2016.11.038.
[69] J.-P. Hsu, Y.-C. Chen, C.-T. Wu, Detection of the trace level of heavy metal ions by pH-regulated conical nanochannels, J. Taiwan Inst. Chem. Eng. 109 (2020) 145–152. https://doi.org/10.1016/j.jtice.2020.02.015.
[70] G. Laucirica, A.G. Albesa, M.E. Toimil-Molares, C. Trautmann, W.A. Marmisollé, O. Azzaroni, Shape matters: enhanced osmotic energy harvesting in bullet-shaped nanochannels, Nanomater. Energy 71 (2020) 104612. https://doi.org/10.1016/j.nanoen.2020.104612.
[71] B. Yameen, M. Ali, R. Neumann, W. Ensinger, W. Knoll, O. Azzaroni, Ionic transport through single solid-state nanopores controlled with thermally nanoactuated macromolecular gates, Small 5 (2009) 1287–1291. https://doi.org/10.1002/smll.200801318.
[72] X. Xu, W. Zhao, P. Gao, H. Li, G. Feng, Z. Zhao, X. Lou, Coordination of the electrical and optical signals revealing nanochannels with an 'onion-like' gating mechanism and its sensing application, NPG Asia Mater. 8 (2016) e234. https://doi.org/10.1038/am.2015.138.
[73] N. Liu, R. Hou, P. Gao, X. Lou, F. Xia, Sensitive Zn 2+ sensor based on bio-functionalized nanopores via combination of DNAzyme and DNA

supersandwich structures, Analyst 141 (2016) 3626–3629. https://doi.org/10.1039/C6AN00171H.
[74] M. Tagliazucchi, I. Szleifer, Stimuli-responsive polymers grafted to nanopores and other nano-curved surfaces: structure, chemical equilibrium and transport, Soft Matter 8 (2012) 7292. https://doi.org/10.1039/c2sm25777g.
[75] M. Tagliazucchi, O. Azzaroni, I. Szleifer, Responsive polymers end-tethered in solid-state nanochannels: when nanoconfinement really matters, J. Am. Chem. Soc. 132 (2010) 12404–12411. https://doi.org/10.1021/ja104152g.
[76] R. Brilmayer, S. Kübelbeck, A. Khalil, M. Brodrecht, U. Kunz, H. Kleebe, G. Buntkowsky, G. Baier, A. Andrieu-Brunsen, Influence of nanoconfinement on the pKa of polyelectrolyte functionalized silica mesopores, Adv. Mater. Interfaces 7 (2020) 1901914. https://doi.org/10.1002/admi.201901914.
[77] M. Ali, B. Yameen, J. Cervera, P. Ramírez, R. Neumann, W. Ensinger, W. Knoll, O. Azzaroni, Layer-by-Layer assembly of polyelectrolytes into ionic current rectifying solid-state nanopores: insights from theory and experiment, J. Am. Chem. Soc. 132 (2010) 8338–8348. https://doi.org/10.1021/ja101014y.
[78] R. Nap, P. Gong, I. Szleifer, Weak polyelectrolytes tethered to surfaces: effect of geometry, acid–base equilibrium and electrical permittivity, J. Polym. Sci., Part B: Polym. Phys. 44 (2006) 2638–2662. https://doi.org/10.1002/polb.20896.
[79] D. Wang, R.J. Nap, I. Lagzi, B. Kowalczyk, S. Han, B.A. Grzybowski, I. Szleifer, How and why nanoparticle's curvature regulates the apparent pKa of the coating ligands, J. Am. Chem. Soc. 133 (2011) 2192–2197. https://doi.org/10.1021/ja108154a.
[80] C. Pfeiffer, C. Rehbock, D. Hühn, C. Carrillo-Carrion, D.J. de Aberasturi, V. Merk, S. Barcikowski, W.J. Parak, Interaction of colloidal nanoparticles with their local environment: the (ionic) nanoenvironment around nanoparticles is different from bulk and determines the physico-chemical properties of the nanoparticles, J. R. Soc. Interface 11 (2014) 20130931. https://doi.org/10.1098/rsif.2013.0931.
[81] Y. Toum Terrones, F. Coluccio Leskow, A.V. Bordoni, S.L. Acebedo, C.C. Spagnuolo, A. Wolosiuk, A silica supported tricarbocyanine based pH nanosensor with a large Stokes shift and a near infrared fluorescence response: performance in vitro and in live cells, J. Mater. Chem. B. 5 (2017) 4031–4034. https://doi.org/10.1039/C7TB00622E.
[82] G. Laucirica, W.A. Marmisollé, O. Azzaroni, Dangerous liaisons: anion-induced protonation in phosphate-polyamine interactions and their implications for the charge states of biologically relevant surfaces, Phys. Chem. Chem. Phys. 19 (2017) 8612–8620. https://doi.org/10.1039/c6cp08793k.
[83] S. Patra, A.K. Pandey, S.K. Sarkar, A. Goswami, Wonderful nanoconfinement effect on redox reaction equilibrium, RSC Adv. 4 (2014) 33366–33369. https://doi.org/10.1039/C4RA05104A.
[84] A.B. Grommet, M. Feller, R. Klajn, Chemical reactivity under nanoconfinement, Nat. Nanotechnol. 15 (2020) 256–271. https://doi.org/10.1038/s41565-020-0652-2.
[85] G. Laucirica, G. Pérez-Mitta, M.E.M.E. Toimil-Molares, C. Trautmann, W.A.W.A. Marmisollé, O. Azzaroni, Amine-phosphate specific interactions within nanochannels: binding behavior and nanoconfinement effects, J. Phys. Chem. C 123 (2019) 28997–29007. https://doi.org/10.1021/acs.jpcc.9b07977.
[86] C. Wang, D.-K. Ye, Y.-Y. Wang, T. Lu, X.-H. Xia, Insights into the “free state” enzyme reaction kinetics in nanoconfinement, Lab Chip 13 (2013) 1546. https://doi.org/10.1039/c3lc41319e.
[87] C. Wang, Z.-H. Sheng, J. Ouyang, J.-J. Xu, H.-Y. Chen, X.-H. Xia, Nano-confinement effects: glucose oxidase reaction kinetics in nanofluidics, ChemPhysChem 13 (2012) 762–768. https://doi.org/10.1002/cphc.201100842.
[88] H. Dai, Y. Li, Y. Fu, Y. Li, Enzyme catalysis induced polymer growth in nanochannels: a new approach to regulate ion transport and to study enzyme kinetics in nanospace, Electroanalysis 30 (2018) 328–335. https://doi.org/10.1002/elan.201700703.
[89] A.M. Downs, C. McCallum, S. Pennathur, Confinement effects on DNA hybridization in electrokinetic micro- and nanofluidic systems, Electrophoresis 40 (2019) 792–798. https://doi.org/10.1002/elps.201800356.
[90] L. Rubinovich, M. Polak, The intrinsic role of nanoconfinement in chemical equilibrium: evidence from DNA hybridization, Nano Lett. 13 (2013) 2247–2251. https://doi.org/10.1021/nl4008198.
[91] M.J. Shon, A.E. Cohen, Mass action at the single-molecule level, J. Am. Chem. Soc. 134 (2012) 14618–14623. https://doi.org/10.1021/ja3062425.
[92] G. Pérez-Mitta, W.A. Marmisollé, C. Trautmann, M.E. Toimil-Molares, O. Azzaroni, Nanofluidic diodes with dynamic rectification properties stemming from reversible electrochemical conversions in conducting polymers, J. Am. Chem. Soc. 137 (2015) 15382–15385. https://doi.org/10.1021/jacs.5b10692.
[93] G. Pérez-Mitta, L. Burr, J.S. Tuninetti, C. Trautmann, M.E. Toimil-Molares, O. Azzaroni, Noncovalent functionalization of solid-state nanopores via self-assembly of amphipols, Nanoscale 8 (2016) 1470–1478. https://doi.org/10.1039/c5nr08190d.
[94] P.Y. Apel, D. Fink, Ion-track etching, in: D. Fink (Editor), Transp. Process. Ion-Irradiated Polym., Springer-Verlag Berlin Heidelberg, 2004, pp. 147–202.
[95] G. Pérez-Mitta, C. Trautmann, M.E. Toimil-Molares, O. Azzaroni, Single ion track-etched nanochannels for analytical applications, in: M. Tagliazucchi, I. Szleifer (Editors), Chem. Modif. Nanopores Nanochannels, Elsevier, 2017, pp. 61–83. https://doi.org/10.1016/B978-0-323-40182-1.00003-8.
[96] A. Hadley, C. Notthoff, P. Mota-Santiago, U.H. Hossain, N. Kirby, M.E. Toimil-Molares, C. Trautmann, P. Kluth, Etched ion tracks in amorphous SiO 2 characterized by small angle x-ray scattering: influence of ion energy and etching conditions, Nanotechnology 30 (2019) 274001. https://doi.org/10.1088/1361-6528/ab10c8.
[97] M.E. Toimil-Molares, Characterization and properties of micro- and nanowires of controlled size, composition, and geometry fabricated by electrodeposition and ion-track technology, Beilstein J. Nanotechnol. 3 (2012) 860–883. https://doi.org/10.3762/bjnano.3.97.
[98] C. Trautmann, Micro- and nanoengineering with ion tracks, in: R. Hellborg, H.J. Whitlow, Y. Zhang (Editors), Ion Beams Nanosci. Technol., Springer-Verlag Berlin Heidelberg, 2009, pp. 369–387.
[99] P. Apel, A. Schulz, R. Spohr, C. Trautmann, V. Vutsadakis, Tracks of very heavy ions in polymers, Nucl. Instrum. Methods Phys. Res. Sect. B Beam Interact. Mater. Atoms 131 (1997) 55–63. https://doi.org/10.1016/S0168-583X(97)00389-3.
[100] D. Fink, Fundamentals of Ion-Irradiated Polymers, Springer Berlin Heidelberg, Berlin, Heidelberg, 2004. https://doi.org/10.1007/978-3-662-07326-1.
[101] Y. Sun, Z. Zhu, Z. Wang, Y. Jin, J. Liu, M. Hou, Q. Zhang, Swift heavy ion induced amorphisation and chemical modification in polycarbonate, Nucl. Instrum. Methods Phys. Res. Sect. B Beam Interact. Mater. Atoms 209 (2003) 188–193. https://doi.org/10.1016/S0168-583X(02)02027-X.
[102] F. Dehaye, E. Balanzat, E. Ferain, R. Legras, Chemical modifications induced in bisphenol A polycarbonate by swift heavy ions, Nucl. Instrum. Methods Phys. Res. Sect. B Beam Interact. Mater. Atoms 209 (2003) 103–112. https://doi.org/10.1016/S0168-583X(02)02048-7.
[103] M. Toulemonde, C. Trautmann, E. Balanzat, K. Hjort, A. Weidinger, Track formation and fabrication of nanostructures with MeV-ion beams, Nucl. Instrum. Methods Phys. Res. Sect. B Beam Interact. Mater. Atoms 216 (2004) 1–8. https://doi.org/10.1016/j.nimb.2003.11.013.
[104] R. Spohr, Method for Producing Nuclear Traces or Microholes Originating from Nuclear Traces of an Individual Ion, 1983. US4369370A.
[105] P. Apel, Track etching technique in membrane technology, Radiat. Meas. 34 (2001) 559–566. https://doi.org/10.1016/S1350-4487(01)00228-1.
[106] Z. Siwy, Y. Gu, H.A. Spohr, D. Baur, A. Wolf-Reber, R. Spohr, P. Apel, Y.E. Korchev, Rectification and voltage gating of ion currents in a nanofabricated pore, Europhys. Lett. 60 (2002) 349–355. https://doi.org/10.1209/epl/i2002-00271-3.
[107] Z. Siwy, P. Apel, D. Baur, D.D. Dobrev, Y.E. Korchev, R. Neumann, R. Spohr, C. Trautmann, K.O. Voss, Preparation of synthetic nanopores with transport properties analogous to biological channels, Surf. Sci. 532–535 (2003) 1061–1066. https://doi.org/10.1016/S0039-6028(03)00448-5.
[108] P.Y. Apel, I.V. Blonskaya, N.E. Lizunov, K. Olejniczak, O.L. Orelovitch, B.A. Sartowska, S.N. Dmitriev, Asymmetrical nanopores in track membranes: fabrication, the effect of nanopore shape and electric charge of pore walls, promising applications, Russ. J. Electrochem. 53 (2017) 58–69. https://doi.org/10.1134/s1023193517010037.
[109] P.Y. Apel, I.V. Blonskaya, A.Y. Didyk, S.N. Dmitriev, O.L. Orelovitch, D. Root, L.I. Samoilova, V.A. Vutsadakis, Surfactant-enhanced control of track-etch pore morphology, Nucl. Instrum. Methods Phys. Res. Sect. B Beam Interact. Mater. Atoms 179 (2001) 55–62. https://doi.org/10.1016/S0168-583X(00)00691-1.
[110] P.Y. Apel, I.V. Blonskaya, O.L. Orelovitch, S.N. Dmitriev, Diode-like ion-track asymmetric nanopores: some alternative methods of fabrication, Nucl. Instrum. Methods Phys. Res. Sect. B Beam Interact. Mater. Atoms 267 (2009) 1023–1027. https://doi.org/10.1016/j.nimb.2009.02.012.
[111] Z. Siwy, P. Apel, D. Dobrev, R. Neumann, R. Spohr, C. Trautmann, K. Voss, Ion transport through asymmetric nanopores prepared by ion track etching, Nucl. Instrum. Methods Phys. Res. Sect. B Beam Interact. Mater. Atoms 208 (2003) 143–148. https://doi.org/10.1016/S0168-583X(03)00884-X.
[112] Z. Siwy, D. Dobrev, R. Neumann, C. Trautmann, K. Voss, Electro-responsive asymmetric nanopores in polyimide with stable ion-current signal, Appl. Phys. Mater. Sci. Process 76 (2003) 781–785. https://doi.org/10.1007/s00339-002-1982-7.
[113] C. Trautmann, W. Brüchle, R. Spohr, J. Vetter, N. Angert, Pore geometry of etched ion tracks in polyimide, Nucl. Instrum. Methods Phys. Res. Sect. B Beam Interact. Mater. Atoms 111 (1996) 70–74. https://doi.org/10.1016/0168-583X(95)01264-8.
[114] S. Karim, W. Ensinger, S.A. Mujahid, K. Maaz, E.U. Khan, Effect of etching conditions on pore shape in etched ion-track polycarbonate membranes, Radiat. Meas. 44 (2009) 779–782. https://doi.org/10.1016/j.radmeas.2009.10.022.
[115] B. Zhang, Y. Zhang, H.S. White, The nanopore electrode, Anal. Chem. 76 (2004) 6229–6238. https://doi.org/10.1021/ac049288r.
[116] G. Wang, A.K. Bohaty, I. Zharov, H.S. White, Photon gated transport at the glass nanopore electrode, J. Am. Chem. Soc. 128 (2006) 13553–13558. https://doi.org/10.1021/ja064274j.
[117] B. Zhang, J. Galusha, P.G. Shiozawa, G. Wang, A.J. Bergren, R.M. Jones, R.J. White, E.N. Ervin, C.C. Cauley, H.S. White, Bench-top method for fabricating glass-sealed nanodisk electrodes, glass nanopore electrodes, and glass nanopore membranes of controlled size, Anal. Chem. 79 (2007) 4778–4787. https://doi.org/10.1021/ac070609j.
[118] J.H. Shim, J. Kim, G.S. Cha, H. Nam, R.J. White, H.S. White, R.B. Brown, Glass Nanopore-Based Ion-Selective Electrodes, Anal. Chem. 79 (2007) 3568–3574. https://doi.org/10.1021/ac061984z.

[119] S. Cao, S. Ding, Y. Liu, A. Zhu, G. Shi, Biomimetic mineralization of gold nanoclusters as multifunctional thin films for glass nanopore modification, characterization, and sensing, Anal. Chem. 89 (2017) 7886–7892. https://doi.org/10.1021/acs.analchem.7b00802.
[120] S. Zhang, H. Chai, K. Cheng, L. Song, W. Chen, L. Yu, Z. Lu, B. Liu, Y.-D. Zhao, Ultrasensitive and regenerable nanopore sensing based on target induced aptamer dissociation, Biosens. Bioelectron. 152 (2020) 112011. https://doi.org/10.1016/j.bios.2020.112011.
[121] L.A. Baker, P. Jin, C.R. Martin, Biomaterials and biotechnologies based on nanotube membranes, Crit. Rev. Solid State Mater. Sci. 30 (2005) 183–205. https://doi.org/10.1080/10408430500198169.
[122] J. Domagalski, E. Xifre-Pérez, L.F. Marsal, Recent advances in nanoporous anodic alumina: principles, engineering, and applications, Nanomaterials 11 (2021) 430. https://doi.org/10.3390/nano1102430.
[123] R.C. Furneaux, W.R. Rigby, A.P. Davidson, The formation of controlled-porosity membranes from anodically oxidized aluminium, Nature 337 (1989) 147–149. https://doi.org/10.1038/337147a0.
[124] A. Ruiz-Clavijo, O. Caballero-Calero, M. Martín-González, Revisiting anodic alumina templates: from fabrication to applications, Nanoscale 13 (2021) 2227–2265. https://doi.org/10.1039/D0NR07582E.
[125] J.W. Diggle, T.C. Downie, C.W. Goulding, Anodic oxide films on aluminum, Chem. Rev. 69 (1969) 365–405. https://doi.org/10.1021/cr60259a005.
[126] D. Kowalski, D. Kim, P. Schmuki, TiO2 nanotubes, nanochannels and mesosponge: self-organized formation and applications, Nano Today 8 (2013) 235–264. https://doi.org/10.1016/j.nantod.2013.04.010.
[127] J.H. Yuan, F.Y. He, D.C. Sun, X.H. Xia, A simple method for preparation of through-hole porous anodic alumina membrane, Chem. Mater. 16 (2004) 1841–1844. https://doi.org/10.1021/cm049971u.
[128] Y. Lin, Q. Lin, X. Liu, Y. Gao, J. He, W. Wang, Z. Fan, A highly controllable electrochemical anodization process to fabricate porous anodic aluminum oxide membranes, Nanoscale Res. Lett. 10 (2015) 495. https://doi.org/10.1186/s11671-015-1202-y.
[129] X.-P. Zhao, S.-S. Wang, M.R. Younis, X.-H. Xia, C. Wang, Asymmetric nanochannel–ionchannel hybrid for ultrasensitive and label-free detection of copper ions in blood, Anal. Chem. 90 (2018) 896–902. https://doi.org/10.1021/acs.analchem.7b03818.
[130] J. Cao, X.P. Zhao, M.R. Younis, Z.Q. Li, X.H. Xia, C. Wang, Ultrasensitive capture, detection, and release of circulating tumor cells using a nanochannel-ion channel hybrid coupled with electrochemical detection technique, Anal. Chem. 89 (2017) 10957–10964. https://doi.org/10.1021/acs.analchem.7b02765.
[131] W. Chen, B. Jin, Y.-L. Hu, Y. Lu, X.-H. Xia, Entrapment of protein in nanotubes formed by a nanochannel and ion-channel hybrid structure of anodic alumina, Small 8 (2012) 1001–1005. https://doi.org/10.1002/smll.201102117.
[132] D. Brüggemann, Nanoporous aluminium oxide membranes as cell interfaces, J. Nanomater. 2013 (2013) 460870. https://doi.org/10.1155/2013/460870.
[133] U. Diebold, The surface science of titanium dioxide, Surf. Sci. Rep. 48 (2003) 53–229. https://doi.org/10.1016/S0167-5729(02)00100-0.
[134] J. Wang, Z. Lin, Freestanding TiO 2 nanotube Arrays with ultrahigh aspect ratio via electrochemical anodization, Chem. Mater. 20 (2008) 1257–1261. https://doi.org/10.1021/cm7028917.
[135] G.D. Sulka, J. Kapusta-Kołodziej, A. Brzózka, M. Jaskuła, Fabrication of nanoporous TiO2 by electrochemical anodization, Electrochim. Acta 55 (2010) 4359–4367. https://doi.org/10.1016/j.electacta.2009.12.053.
[136] G. Liu, K. Du, K. Wang, Surface wettability of TiO2 nanotube arrays prepared by electrochemical anodization, Appl. Surf. Sci. 388 (2016) 313–320. https://doi.org/10.1016/j.apsusc.2016.01.010.
[137] G. Pérez-Mitta, W.A. Marmisolle, L. Burr, M.E. Toimil-Molares, C. Trautmann, O. Azzaroni, Proton-gated rectification regimes in nanofluidic diodes switched by chemical effectors, Small 14 (2018) 1703144. https://doi.org/10.1002/smll.201703144.
[138] G. Laucirica, Y. Toum Terrones, V.M. Cayón, M.L. Cortez, M.E. Toimil-Molares, C. Trautmann, W.A. Marmisollé, O. Azzaroni, High-sensitivity detection of dopamine by biomimetic nanofluidic diodes derivatized with poly(3-aminobenzylamine), Nanoscale 12 (2020) 18390–18399. https://doi.org/10.1039/D0NR03634J.
[139] Z. Zhang, L. Wen, L. Jiang, Bioinspired smart asymmetric nanochannel membranes, Chem. Soc. Rev. 47 (2018) 322–356. https://doi.org/10.1039/C7CS00688H.
[140] V.P. Menon, C.R. Martin, Fabrication and evaluation of nanoelectrode ensembles, Anal. Chem. 67 (1995) 1920–1928. https://doi.org/10.1021/ac00109a003.
[141] M. De Leo, F.C. Pereira, L.M. Moretto, P. Scopece, S. Polizzi, P. Ugo, Towards a better understanding of gold electroless deposition in track-etched templates, Chem. Mater. 19 (2007) 5955–5964. https://doi.org/10.1021/cm071703j.
[142] F. Muench, U. Kunz, C. Neetzel, S. Lauterbach, H.-J. Kleebe, W. Ensinger, 4-(Dimethylamino)pyridine as a powerful auxiliary reagent in the electroless synthesis of gold nanotubes, Langmuir 27 (2011) 430–435. https://doi.org/10.1021/la104015a.
[143] N. Ulrich, A. Spende, L. Burr, N. Sobel, I. Schubert, C. Hess, C. Trautmann, M.E. Toimil-Molares, Conical nanotubes synthesized by atomic layer deposition of Al2O3, TiO2, and SiO2 in etched ion-track nanochannels, Nanomaterials 11 (2021) 1874. https://doi.org/10.3390/nano11081874.
[144] A. Spende, N. Sobel, M. Lukas, R. Zierold, J.C. Riedl, L. Gura, I. Schubert, J.M.M. Moreno, K. Nielsch, B. Stühn, C. Hess, C. Trautmann, M.E. Toimil-Molares, TiO 2 , SiO 2 , and Al 2 O 3 coated nanopores and nanotubes produced by ALD in etched ion-track membranes for transport measurements, Nanotechnology 26 (2015) 335301. https://doi.org/10.1088/0957-4484/26/33/335301.
[145] V.M. Cayón, G. Laucirica, Y. Toum Terrones, M.L. Cortez, G. Pérez-Mitta, J. Shen, C. Hess, M.E. Toimil-Molares, C. Trautmann, W.A. Marmisollé, O. Azzaroni, Borate-driven ionic rectifiers based on sugar-bearing single nanochannels, Nanoscale 13 (2021) 11232–11241. https://doi.org/10.1039/D0NR07733J.
[146] M. Ritala, M. Leskelä, Atomic layer deposition, in: Handb. Thin Film, Elsevier, 2002, pp. 103–159. https://doi.org/10.1016/B978-012512908-4/50005-9.
[147] S.M. George, Atomic layer deposition: an overview, Chem. Rev. 110 (2010) 111–131. https://doi.org/10.1021/cr900056b.
[148] M.S. Sander, M.J. Côté, W. Gu, B.M. Kile, C.P. Tripp, Template-Assisted fabrication of dense, aligned arrays of titania nanotubes with well-controlled dimensions on substrates, Adv. Mater. 16 (2004) 2052–2057. https://doi.org/10.1002/adma.200400446.
[149] N. Sobel, C. Hess, M. Lukas, A. Spende, B. Stühn, M.E. Toimil-Molares, C. Trautmann, Conformal SiO 2 coating of sub-100 nm diameter channels of polycarbonate etched ion-track channels by atomic layer deposition, Beilstein J. Nanotechnol. 6 (2015) 472–479. https://doi.org/10.3762/bjnano.6.48.
[150] V. Romero, V. Vega, J. García, R. Zierold, K. Nielsch, V.M. Prida, B. Hernando, J. Benavente, Changes in morphology and ionic transport induced by ALD SiO 2 coating of nanoporous alumina membranes, ACS Appl. Mater. Interfaces 5 (2013) 3556–3564. https://doi.org/10.1021/am400300r.
[151] J.S. Ponraj, G. Attolini, M. Bosi, Review on atomic layer deposition and applications of oxide thin films, Crit. Rev. Solid State Mater. Sci. 38 (2013) 203–233. https://doi.org/10.1080/10408436.2012.736886.
[152] M. Yüce, H. Kurt, How to make nanobiosensors: surface modification and characterisation of nanomaterials for biosensing applications, RSC Adv. 7 (2017) 49386–49403. https://doi.org/10.1039/C7RA10479K.
[153] O. Azzaroni, M.H. Fonticelli, G. Benítez, P.L. Schilardi, R. Gago, I. Caretti, L. Vázquez, R.C. Salvarezza, Direct nanopatterning of metal surfaces using self-assembled molecular films, Adv. Mater. 16 (2004) 405–409. https://doi.org/10.1002/adma.200306190.
[154] O. Azzaroni, M. Mir, W. Knoll, Supramolecular architectures of streptavidin on biotinylated self-assembled monolayers. Tracking biomolecular reorganization after bioconjugation, J. Phys. Chem. B 111 (2007) 13499–13503. https://doi.org/10.1021/jp076707q.
[155] M. Fonticelli, O. Azzaroni, G. Benítez, M.E. Martins, P. Carro, R.C. Salvarezza, Molecular self-assembly on ultrathin metallic surfaces: alkanethiolate monolayers on Ag(1 × 1)–Au(111), J. Phys. Chem. B 108 (2004) 1898–1905. https://doi.org/10.1021/jp0359384.
[156] S. Nasir, M. Ali, P. Ramirez, V. Gómez, B. Oschmann, F. Muench, M.N. Tahir, R. Zentel, S. Mafe, W. Ensinger, Fabrication of single cylindrical Au-coated nanopores with non-homogeneous fixed charge distribution exhibiting high current rectifications, ACS Appl. Mater. Interfaces 6 (2014) 12486–12494. https://doi.org/10.1021/am502419j.
[157] K.B. Jirage, J.C. Hulteen, C.R. Martin, Effect of thiol chemisorption on the transport properties of gold nanotubule membranes, Anal. Chem. 71 (1999) 4913–4918. https://doi.org/10.1021/ac990615i.
[158] S.B. Lee, C.R. Martin, Controlling the transport properties of gold nanotubule membranes using chemisorbed thiols, Chem. Mater. 13 (2001) 3236–3244. https://doi.org/10.1021/cm0101071.
[159] X. Xu, H. He, Y. Jin, Facile one-step photochemical fabrication and characterization of an ultrathin gold-decorated single glass nanopipette, Anal. Chem. 87 (2015) 3216–3221. https://doi.org/10.1021/ac5034165.
[160] C.C. Harrell, P. Kohli, Z. Siwy, C.R. Martin, DNA - nanotube artificial ion channels, J. Am. Chem. Soc. 126 (2004) 15646–15647. https://doi.org/10.1021/ja044948v.
[161] B.Y. Kim, C.B. Swearingen, J.A. Ho, E.V. Romanova, P.W. Bohn, J.V. Sweedler, Direct immobilization of fab‘ in nanocapillaries for manipulating mass-limited samples, J. Am. Chem. Soc. 129 (2007) 7620–7626. https://doi.org/10.1021/ja070041w.
[162] B. Yameen, M. Ali, M. Álvarez, R. Neumann, W. Ensinger, W. Knoll, O. Azzaroni, A facile route for the preparation of azide-terminated polymers. “Clicking” polyelectrolyte brushes on planar surfaces and nanochannels, Polym. Chem. 1 (2010) 183–192. https://doi.org/10.1039/B9PY00201D.
[163] O. Azzaroni, S.E. Moya, A.A. Brown, Z. Zheng, E. Donath, W.T.S. Huck, Polyelectrolyte brushes as ink nanoreservoirs for microcontact printing of ionic species with poly(dimethyl siloxane) stamps, Adv. Funct. Mater. 16 (2006) 1037–1042. https://doi.org/10.1002/adfm.200500702.
[164] S.E. Moya, O. Azzaroni, T. Kelby, E. Donath, W.T.S. Huck, Explanation for the apparent absence of collapse of polyelectrolyte brushes in the presence of bulky ions, J. Phys. Chem. B 111 (2007) 7034–7040. https://doi.org/10.1021/jp071026g.
[165] A.A. Brown, O. Azzaroni, L.M. Fidalgo, W.T.S. Huck, Polymer brush resist for responsive wettability, Soft Matter 5 (2009) 2738. https://doi.org/10.1039/b902179e.
[166] A. Andrieu-Brunsen, S. Micoureau, M. Tagliazucchi, I. Szleifer, O. Azzaroni, G.J.A.A. Soler-Illia, Mesoporous hybrid thin film membranes with PMETAC@ silica architectures: controlling ionic gating through the tuning of

polyelectrolyte density, Chem. Mater. 27 (2015) 808–821. https://doi.org/10.1021/cm5037953.
[167] P. Zucca, E. Sanjust, Inorganic materials as supports for covalent enzyme immobilization: methods and mechanisms, Molecules 19 (2014) 14139–14194. https://doi.org/10.3390/molecules190914139.
[168] H.H. Weetall, Preparation of immobilized proteins covalently coupled through silane coupling agents to inorganic supports, Appl. Biochem. Biotechnol. 41 (1993) 157–188. https://doi.org/10.1007/BF02916421.
[169] A. de la Escosura-Muñiz, A. Merkoçi, Nanochannels for electrical biosensing, TrAC Trends Anal. Chem. (Reference Ed.) 79 (2016) 134–150. https://doi.org/10.1016/j.trac.2015.12.003.
[170] A.C. Marques, P.J. Costa, S. Velho, M.H. Amaral, Functionalizing nanoparticles with cancer-targeting antibodies: a comparison of strategies, J. Contr. Release 320 (2020) 180–200. https://doi.org/10.1016/j.jconrel.2020.01.035.
[171] P. Liu, G. Xie, P. Li, Z. Zhang, L. Yang, Y. Zhao, C. Zhu, X.-Y. Kong, L. Jiang, L. Wen, A universal tunable nanofluidic diode via photoresponsive host–guest interactions, NPG Asia Mater. 10 (2018) 849–857. https://doi.org/10.1038/s41427-018-0079-5.
[172] G. Hou, H. Zhang, G. Xie, K. Xiao, L. Wen, S. Li, Y. Tian, L. Jiang, Ultratrace detection of glucose with enzyme-functionalized single nanochannels, J. Mater. Chem. A. 2 (2014) 19131–19135. https://doi.org/10.1039/C4TA05013D.
[173] M. Ali, M.N. Tahir, Z. Siwy, R. Neumann, W. Tremel, W. Ensinger, Hydrogen peroxide sensing with horseradish peroxidase-modified polymer single conical nanochannels, Anal. Chem. 83 (2011) 1673–1680. https://doi.org/10.1021/ac102795a.
[174] E.T. Acar, S.F. Buchsbaum, C. Combs, F. Fornasiero, Z.S. Siwy, Biomimetic potassium-selective nanopores, Sci. Adv. 5 (2019), eaav2568. https://doi.org/10.1126/sciadv.aav2568.
[175] M. Shen, J.F. Rusling, C.K. Dixit, Site-selective orientated immobilization of antibodies and conjugates for immunodiagnostics development, Methods 116 (2017) 95–111. https://doi.org/10.1016/j.ymeth.2016.11.010.
[176] J. Conde, J.T. Dias, V. Grazú, M. Moros, P.V. Baptista, J.M. de la Fuente, Revisiting 30 years of biofunctionalization and surface chemistry of inorganic nanoparticles for nanomedicine, Front. Chem. 2 (2014). https://doi.org/10.3389/fchem.2014.00048.
[177] O. Barbosa, C. Ortiz, Á. Berenguer-Murcia, R. Torres, R.C. Rodrigues, R. Fernandez-Lafuente, Glutaraldehyde in bio-catalysts design: a useful crosslinker and a versatile tool in enzyme immobilization, RSC Adv. 4 (2014) 1583–1600. https://doi.org/10.1039/C3RA45991H.
[178] I. Migneault, C. Dartiguenave, M.J. Bertrand, K.C. Waldron, Glutaraldehyde: behavior in aqueous solution, reaction with proteins, and application to enzyme crosslinking, Biotechniques 37 (2004) 790–802. https://doi.org/10.2144/04375RV01.
[179] P. Chaturvedi, S.D. Rodriguez, I. Vlassiouk, I.A. Hansen, S.N. Smirnov, Simple and versatile detection of viruses using anodized alumina membranes, ACS Sens. 1 (2016) 488–492. https://doi.org/10.1021/acssensors.6b00003.
[180] J. Tu, Z. Zhou, Y. Liu, T. Li, S. Lu, L. Xiao, P. Xiao, G. Zhang, Z. Sun, Nanochannel-based sensor for the detection of lead ions in traditional Chinese medicine, RSC Adv. 11 (2021) 3751–3758. https://doi.org/10.1039/D0RA10157E.
[181] C. Wang, D. Jin, Y. Yu, L. Tang, Y. Sun, Z. Sun, G.-J. Zhang, A dual antibody-modified nanochannel biosensor for capture and identification of exosomes, Sensor. Actuator. B Chem. 314 (2020) 128056. https://doi.org/10.1016/j.snb.2020.128056.
[182] S. Zhang, G. Liu, H. Chai, Y. Zhao, L. Yu, W. Chen, Electrochemistry Communications Detection of alkaline phosphatase activity with a functionalized nanopipette, Electrochem. Commun. 99 (2019) 71–74. https://doi.org/10.1016/j.elecom.2019.01.008.
[183] J. Irigoyen, S.E. Moya, J.J. Iturri, I. Llarena, O. Azzaroni, E. Donath, Specific ζ-potential response of layer-by-layer coated colloidal particles triggered by polyelectrolyte ion interactions, Langmuir 25 (2009) 3374–3380. https://doi.org/10.1021/la803360n.
[184] M. Coustet, J. Irigoyen, T.A. Garcia, R.A. Murray, G. Romero, M. Susana Cortizo, W. Knoll, O. Azzaroni, S.E. Moya, Layer-by-layer assembly of polymersomes and polyelectrolytes on planar surfaces and microsized colloidal particles, J. Colloid Interface Sci. 421 (2014) 132–140. https://doi.org/10.1016/j.jcis.2014.01.038.
[185] E. Diamanti, N. Muzzio, D. Gregurec, J. Irigoyen, M. Pasquale, O. Azzaroni, M. Brinkmann, S.E. Moya, Impact of thermal annealing on wettability and antifouling characteristics of alginate poly-l-lysine polyelectrolyte multilayer films, Colloids Surf. B Biointerfaces 145 (2016) 328–337. https://doi.org/10.1016/j.colsurfb.2016.05.013.
[186] E. Piccinini, S. Alberti, G.S. Longo, T. Berninger, J. Breu, J. Dostalek, O. Azzaroni, W. Knoll, Pushing the boundaries of interfacial sensitivity in graphene FET sensors: polyelectrolyte multilayers strongly increase the Debye screening length, J. Phys. Chem. C 122 (2018) 10181–10188. https://doi.org/10.1021/acs.jpcc.7b11128.
[187] T. Berninger, C. Bliem, E. Piccinini, O. Azzaroni, W. Knoll, Cascading reaction of arginase and urease on a graphene-based FET for ultrasensitive, real-time detection of arginine, Biosens. Bioelectron. 115 (2018) 104–110. https://doi.org/10.1016/j.bios.2018.05.027.
[188] M.L. Cortez, A. Lorenzo, W.A. Marmisollé, C. von Bilderling, E. Maza, L. Pietrasanta, F. Battaglini, M. Ceolín, O. Azzaroni, Highly-organized stacked multilayers via layer-by-layer assembly of lipid-like surfactants and polyelectrolytes. Stratified supramolecular structures for (bio)electrochemical nanoarchitectonics, Soft Matter 14 (2018) 1939–1952. https://doi.org/10.1039/C8SM00052B.
[189] E. Maza, J.S. Tuninetti, N. Politakos, W. Knoll, S. Moya, O. Azzaroni, pH-responsive ion transport in polyelectrolyte multilayers of poly(-diallyldimethylammonium chloride) (PDADMAC) and poly(4-styrenesulfonic acid-co-maleic acid) (PSS-MA) bearing strong- and weak anionic groups, Phys. Chem. Chem. Phys. 17 (2015) 29935–29948. https://doi.org/10.1039/C5CP03965G.
[190] G.E. Fenoy, E. Maza, E. Zelaya, W.A. Marmisollé, O. Azzaroni, Layer-by-layer assemblies of highly connected polyelectrolyte capped-Pt nanoparticles for electrocatalysis of hydrogen evolution reaction, Appl. Surf. Sci. 416 (2017) 24–32. https://doi.org/10.1016/j.apsusc.2017.04.086.
[191] T.D. Lazzara, K.H.A. Lau, A.I. Abou-Kandil, A.-M. Caminade, J.-P. Majoral, W. Knoll, Polyelectrolyte layer-by-layer deposition in cylindrical nanopores, ACS Nano 4 (2010) 3909–3920. https://doi.org/10.1021/nn1007594.
[192] P. Actis, B. Vilozny, R.A. Seger, X. Li, O. Jejelowo, M. Rinaudo, N. Pourmand, Voltage-controlled metal binding on polyelectrolyte-functionalized nanopores, Langmuir 27 (2011) 6528–6533. https://doi.org/10.1021/la2005612.
[193] Y. Teng, X.-Y. Kong, P. Liu, Y. Qian, Y. Hu, L. Fu, W. Xin, L. Jiang, L. Wen, A universal functionalization strategy for biomimetic nanochannel via external electric field assisted non-covalent interaction, Nano Res. 14 (2021) 1421–1428. https://doi.org/10.1007/s12274-020-3192-z.
[194] Y. Wang, V. Bansal, A.N. Zelikin, F. Caruso, Templated synthesis of single-component polymer capsules and their application in drug delivery, Nano Lett. 8 (2008) 1741–1745. https://doi.org/10.1021/nl080877c.
[195] Y. Wang, A.S. Angelatos, D.E. Dunstan, F. Caruso, Infiltration of macromolecules into nanoporous silica particles, Macromolecules 40 (2007) 7594–7600. https://doi.org/10.1021/ma071125s.
[196] G. Decher, J.D. Hong, J. Schmitt, Buildup of ultrathin multilayer films by a self-assembly process: III. Consecutively alternating adsorption of anionic and cationic polyelectrolytes on charged surfaces, Thin Solid Films 210–211 (1992) 831–835. https://doi.org/10.1016/0040-6090(92)90417-A.
[197] M. Lepoitevin, B. Jamilloux, M. Bechelany, E. Balanzat, J.M. Janot, S. Balme, Fast and reversible functionalization of a single nanopore based on layer-by-layer polyelectrolyte self-assembly for tuning current rectification and designing sensors, RSC Adv. 6 (2016) 32228–32233. https://doi.org/10.1039/c6ra03698h.
[198] T. Ma, P. Gaigalas, M. Lepoitevin, I. Plikusiene, M. Bechelany, J. Janot, E. Balanzat, S. Balme, Impact of polyelectrolyte multilayers on the ionic current rectification of conical nanopores, Langmuir 34 (2018) 3405–3412. https://doi.org/10.1021/acs.langmuir.8b00222.
[199] Y. Cho, C. Lee, J. Hong, Pore size effect on the formation of polymer nanotubular structures within nanoporous templates, Colloids Surf. A: Physicochem. Eng. Asp. 443 (2014) 195–200. https://doi.org/10.1016/j.colsurfa.2013.11.013.
[200] C.J. Roy, C. Dupont-Gillain, S. Demoustier-Champagne, A.M. Jonas, J. Landoulsi, Growth mechanism of confined polyelectrolyte multilayers in nanoporous templates, Langmuir 26 (2010) 3350–3355. https://doi.org/10.1021/la903121e.
[201] J.-M.Y. Carrillo, A.V. Dobrynin, Layer-by-Layer assembly of charged nanoparticles on porous substrates: molecular dynamics simulations, ACS Nano 5 (2011) 3010–3019. https://doi.org/10.1021/nn200065q.
[202] L. Järup, Hazards of heavy metal contamination, Br. Med. Bull. 68 (2003) 167–182. https://doi.org/10.1093/bmb/ldg032.
[203] O. Barbier, G. Jacquillet, M. Tauc, M. Cougnon, P. Poujeol, Effect of heavy metals on, and handling by, the kidney, Nephron. Physiol. 99 (2005) 105–110. https://doi.org/10.1159/000083981.
[204] A. Cockburn, G. Brambilla, M.-L. Fernández, D. Arcella, L.R. Bordajandi, B. Cottrill, C. van Peteghem, J.-L. Dorne, Nitrite in feed: from Animal health to human health, Toxicol. Appl. Pharmacol. 270 (2013) 209–217. https://doi.org/10.1016/j.taap.2010.11.008.
[205] M. Ghittorelli, L. Lingstedt, P. Romele, N.I. Craciun, Z.M. Kovács-Vajna, P.W.M. Blom, F. Torricelli, High-sensitivity ion detection at low voltages with current-driven organic electrochemical transistors, Nat. Commun. 9 (2018) 1441. https://doi.org/10.1038/s41467-018-03932-3.
[206] S. Li, C. Zhang, S. Wang, Q. Liu, H. Feng, X. Ma, J. Guo, Electrochemical microfluidics techniques for heavy metal ion detection, Analyst 143 (2018) 4230–4246. https://doi.org/10.1039/C8AN01067F.
[207] B. Bansod, T. Kumar, R. Thakur, S. Rana, I. Singh, A review on various electrochemical techniques for heavy metal ions detection with different sensing platforms, Biosens. Bioelectron. 94 (2017) 443–455. https://doi.org/10.1016/j.bios.2017.03.031.
[208] S. Zhang, I. Boussouar, H. Li, Selective sensing and transport in bionic nanochannel based on macrocyclic host-guest chemistry, Chin. Chem. Lett. 32 (2021) 642–648. https://doi.org/10.1016/j.cclet.2020.06.035.
[209] T. Ogoshi, S. Kanai, S. Fujinami, T. Yamagishi, Y. Nakamoto, para -Bridged Symmetrical Pillar[5]arenes: their Lewis Acid Catalyzed Synthesis and Host–Guest Property, J. Am. Chem. Soc. 130 (2008) 5022–5023. https://doi.org/10.1021/ja711260m.
[210] E. Blasius, D.J. Cram, K.-P. Janzen, W.M. Müller, H. Sieger, K.N. Trueblood, F. Vögtle, E. Weber, Host Guest Complex Chemistry I, Springer Berlin Heidelberg, Berlin, Heidelberg, 1981. https://doi.org/10.1007/BFb0111244.
[211] Q. Liu, K. Xiao, L. Wen, H. Lu, Y. Liu, X.-Y. Kong, G. Xie, Z. Zhang, Z. Bo, L. Jiang, Engineered ionic gates for ion conduction based on sodium and potassium

activated nanochannels, J. Am. Chem. Soc. 137 (2015) 11976–11983. https://doi.org/10.1021/jacs.5b04911.
[212] M. Ali, I. Ahmed, P. Ramirez, S. Nasir, S. Mafe, C.M. Niemeyer, W. Ensinger, Lithium ion recognition with nanofluidic diodes through host-guest complexation in confined geometries, Anal. Chem. 90 (2018) 6820–6826. https://doi.org/10.1021/acs.analchem.8b00902.
[213] M. Ali, I. Ahmed, P. Ramirez, S. Nasir, J. Cervera, S. Mafe, C.M. Niemeyer, W. Ensinger, Cesium-induced ionic conduction through a single nanofluidic pore modified with calixcrown moieties, Langmuir 33 (2017) 9170–9177. https://doi.org/10.1021/acs.langmuir.7b02368.
[214] Y. Qian, Z. Zhang, W. Tian, L. Wen, L. Jiang, A Pb 2+ ionic gate with enhanced stability and improved sensitivity based on a 4′-aminobenzo-18-crown-6 modified funnel-shaped nanochannel, Faraday Discuss 210 (2018) 101–111. https://doi.org/10.1039/C8FD00025E.
[215] X. Wu, J. Experton, W. Xu, C.R. Martin, Chemoresponsive nanofluidic pump that turns off in the presence of lead ion, Anal. Chem. 90 (2018) 7715–7720. https://doi.org/10.1021/acs.analchem.8b01623.
[216] K. Wu, K. Xiao, L. Chen, R. Zhou, B. Niu, Y. Zhang, L. Wen, Biomimetic voltage-gated ultrasensitive potassium-activated nanofluidic based on a solid-state nanochannel, Langmuir 33 (2017) 8463–8467. https://doi.org/10.1021/acs.langmuir.7b01705.
[217] M. Ali, I. Ahmed, S. Nasir, I. Duznovic, C.M. Niemeyer, W. Ensinger, Potassium-induced ionic conduction through a single nanofluidic pore modified with acyclic polyether derivative, Anal. Chim. Acta 1039 (2018) 132–139. https://doi.org/10.1016/j.aca.2018.07.056.
[218] F. Zhang, J. Ma, Y. Sun, I. Boussouar, D. Tian, H. Li, L. Jiang, Fabrication of a mercaptoacetic acid pillar[5]arene assembled nanochannel: a biomimetic gate for mercury poisoning, Chem. Sci. 7 (2016) 3227–3233. https://doi.org/10.1039/C5SC04726A.
[219] F. Zhu, G. Yang, M.K. Dhinakaran, R. Wang, M. Song, H. Li, A pyrophosphate-activated nanochannel inspired by a TRP ion channel, Chem. Commun. 55 (2019) 12833–12836. https://doi.org/10.1039/C9CC06615B.
[220] J. Lei, H. Ju, Signal amplification using functional nanomaterials for biosensing, Chem. Soc. Rev. 41 (2012) 2122–2134. https://doi.org/10.1039/c1cs15274b.
[221] Y. Chen, D. Zhou, Z. Meng, J. Zhai, An ion-gating multinanochannel system based on a copper-responsive self-cleaving DNAzyme, Chem. Commun. 52 (2016) 10020–10023. https://doi.org/10.1039/C6CC03943J.
[222] L.K. Müller, I. Duznovic, D. Tietze, W. Weber, M. Ali, V. Stein, W. Ensinger, A.A. Tietze, Ultrasensitive and selective copper(II) detection: introducing a bioinspired and robust sensor, Chem. Eur J. 26 (2020) 8511–8517. https://doi.org/10.1002/chem.202001160.
[223] Y. Wu, D. Wang, I. Willner, Y. Tian, L. Jiang, Smart DNA hydrogel integrated nanochannels with high ion flux and adjustable selective ionic transport, Angew. Chem. Int. Ed. 57 (2018) 7790–7794. https://doi.org/10.1002/anie.201803222.
[224] Y. Li, Y. Xiong, D. Wang, X. Li, Z. Chen, C. Wang, H. Qin, J. Liu, B. Chang, G. Qing, Smart polymer-based calcium-ion self-regulated nanochannels by mimicking the biological Ca2+-induced Ca2+ release process, NPG Asia Mater. 11 (2019) 46. https://doi.org/10.1038/s41427-019-0148-4.
[225] M.D. Hartle, M.D. Pluth, A practical guide to working with H2S at the interface of chemistry and biology, Chem. Soc. Rev. 45 (2016) 6108–6117. https://doi.org/10.1039/C6CS00212A.
[226] R.E. Ozel, G. Bulbul, J. Perez, N. Pourmand, Functionalized quartz nanopipette for intracellular superoxide sensing: a tool for monitoring reactive oxygen species levels in single living cell, ACS Sens. 3 (2018) 1316–1321. https://doi.org/10.1021/acssensors.8b00185.
[227] K. Zhan, Z. Li, J. Chen, Y. Hou, J. Zhang, R. Sun, Z. Bu, L. Wang, M. Wang, X. Chen, X. Hou, Tannic acid modified single nanopore with multivalent metal ions recognition and ultra-trace level detection, Nano Today 33 (2020) 100868. https://doi.org/10.1016/j.nantod.2020.100868.
[228] C. Zhao, H. Zhang, J. Hou, R. Ou, Y. Zhu, X. Li, L. Jiang, H. Wang, Effect of anion species on ion current rectification properties of positively charged nanochannels, ACS Appl. Mater. Interfaces 12 (2020) 28915–28922. https://doi.org/10.1021/acsami.0c08263.
[229] M. Ali, I. Ahmed, P. Ramirez, S. Nasir, C.M. Niemeyer, S. Mafe, W. Ensinger, Label-free pyrophosphate recognition with functionalized asymmetric nanopores, Small 12 (2016) 2014–2021. https://doi.org/10.1002/smll.201600160.
[230] Q. Liu, L. Wen, K. Xiao, H. Lu, Z. Zhang, G. Xie, X.Y. Kong, Z. Bo, L. Jiang, A biomimetic voltage-gated chloride nanochannel, Adv. Mater. 28 (2016) 3181–3186. https://doi.org/10.1002/adma.201505250.
[231] X. Xu, R. Hou, P. Gao, M. Miao, X. Lou, B. Liu, F. Xia, Highly robust nanopore-based dual-signal-output ion detection system for achieving three successive calibration curves, Anal. Chem. 88 (2016) 2386–2391. https://doi.org/10.1021/acs.analchem.5b04388.
[232] Y. Zhang, R. Zhou, Z. Zhao, X.-Y. Kong, G. Xie, Q. Liu, P. Li, Z. Zhang, K. Xiao, Z. Liu, L. Wen, L. Jiang, Sequential recognition of zinc and pyrophosphate ions in a terpyridine-functionalized single nanochannel, ChemPhysChem 18 (2017) 253–259. https://doi.org/10.1002/cphc.201600923.
[233] B. Niu, K. Xiao, X. Huang, Z. Zhang, X.-Y.Y. Kong, Z. Wang, L. Wen, L. Jiang, High-sensitivity detection of iron(III) by dopamine-modified funnel-shaped nanochannels, ACS Appl. Mater. Interfaces 10 (2018) 22632–22639. https://doi.org/10.1021/acsami.8b05686.
[234] G. Pérez-Mitta, W.A. Marmisollé, A.G. Albesa, M.E. Toimil-Molares, C. Trautmann, O. Azzaroni, Phosphate-responsive biomimetic nanofluidic diodes regulated by polyamine-phosphate interactions: insights into their functional behavior from theory and experiment, Small 14 (2018) 1702131. https://doi.org/10.1002/smll.201702131.
[235] X. Wang, Y. Chen, Z. Meng, Q. Zhang, J. Zhai, Effect of trivalent “calcium-like” cations on ionic transport behaviors of artificial calcium-responsive nanochannels, J. Phys. Chem. C 122 (2018) 24863–24870. https://doi.org/10.1021/acs.jpcc.8b08662.
[236] X. Liu, Q. Zeng, C. Liu, J. Yang, L. Wang, Experimental and finite element method studies for femtomolar cobalt ion detection using a DHI modified nanochannel, Analyst 144 (2019) 6118–6127. https://doi.org/10.1039/C9AN01344J.
[237] Y. Sun, F. Zhang, Z. Sun, M. Song, D. Tian, H. Li, Zn 2+ and EDTA cooperative switchable nanofluidic diode based on asymmetric modification of single nanochannel, Chem. Eur J. 22 (2016) 4355–4358. https://doi.org/10.1002/chem.201504616.
[238] Y. Li, L. Tu, X. Ma, H. Chen, Y. Fan, Q. Zhou, Y. Sun, Engineering a smart nanofluidic sensor for high-performance peroxynitrite sensing through a spirocyclic ring open/close reaction strategy, ACS Sens. 6 (2021) 808–814. https://doi.org/10.1021/acssensors.0c01719.
[239] L. Yang, Y. Qian, X.-Y. Kong, M. Si, Y. Zhao, B. Niu, X. Zhao, Y. Wei, L. Jiang, L. Wen, Specific recognition of uranyl ion employing a functionalized nanochannel platform for dealing with radioactive contamination, ACS Appl. Mater. Interfaces 12 (2020) 3854–3861. https://doi.org/10.1021/acsami.9b19544.
[240] Y. Qian, Z. Zhang, X.Y. Kong, W. Tian, L. Wen, L. Jiang, Engineered artificial nanochannels for nitrite ion harmless conversion, ACS Appl. Mater. Interfaces 10 (2018) 30852–30859. https://doi.org/10.1021/acsami.8b09749.
[241] H. Chen, L. Xu, W. Tuo, X. Chen, J. Huang, X. Zhang, Y. Sun, Fabrication of a smart nanofluidic biosensor through a reversible covalent bond strategy for high-efficiency bisulfite sensing and removal, Anal. Chem. 92 (2020) 4131–4136. https://doi.org/10.1021/acs.analchem.0c00131.
[242] M. Ali, I. Ahmed, P. Ramirez, S. Nasir, J. Cervera, C.M. Niemeyer, W. Ensinger, Fluoride-induced modulation of ionic transport in asymmetric nanopores functionalized with “caged” fluorescein moieties, Nanoscale 8 (2016) 8583–8590. https://doi.org/10.1039/C6NR00292G.
[243] S.L. Turner, N. Li, T. Guda, J. Githure, R.T. Cardé, A. Ray, Ultra-prolonged activation of CO2-sensing neurons disorients mosquitoes, Nature 474 (2011) 87–91. https://doi.org/10.1038/nature10081.
[244] M.T. Gillies, The role of carbon dioxide in host-finding by mosquitoes (Diptera: Culicidae): a review, Bull. Entomol. Res. 70 (1980) 525–532. https://doi.org/10.1017/S0007485300007811.
[245] X. Shang, G. Xie, X.-Y. Kong, Z. Zhang, Y. Zhang, W. Tian, L. Wen, L. Jiang, An artificial CO 2 -driven ionic gate inspired by olfactory sensory neurons in mosquitoes, Adv. Mater. 29 (2017) 1603884. https://doi.org/10.1002/adma.201603884.
[246] S. Firestein, How the olfactory system makes sense of scents, Nature 413 (2001) 211–218. https://doi.org/10.1038/35093026.
[247] L. Zwiebel, W. Takken, Olfactory regulation of mosquito–host interactions, Insect Biochem. Mol. Biol. 34 (2004) 645–652. https://doi.org/10.1016/j.ibmb.2004.03.017.
[248] M. Ma, Encoding olfactory signals via multiple chemosensory systems, Crit. Rev. Biochem. Mol. Biol. 42 (2007) 463–480. https://doi.org/10.1080/10409230701693359.
[249] D. Fukumura, S. Kashiwagi, R.K. Jain, The role of nitric oxide in tumour progression, Nat. Rev. Canc. 6 (2006) 521–534. https://doi.org/10.1038/nrc1910.
[250] M. Delledonne, Y. Xia, R.A. Dixon, C. Lamb, Nitric oxide functions as a signal in plant disease resistance, Nature 394 (1998) 585–588. https://doi.org/10.1038/29087.
[251] Y. Han, Z. Sun, Z. Sun, X. Chen, Y. Zhang, Y. Sun, H. Li, Engineering a NO-regulated nanofluidic sensor through the cyclization reaction strategy, Chem. Eur J. 26 (2020) 11099–11103. https://doi.org/10.1002/chem.202001089.
[252] L. Ge, J. Wu, C. Wang, F. Zhang, Z. Liu, Engineering artificial switchable nanochannels for selective monitoring of nitric oxide release from living cells, Biosens. Bioelectron. 169 (2020) 112606. https://doi.org/10.1016/j.bios.2020.112606.
[253] K. Lu, W. Ye, L. Zhou, L.B. Collins, X. Chen, A. Gold, L.M. Ball, J.A. Swenberg, Structural characterization of formaldehyde-induced cross-links between amino acids and deoxynucleosides and their oligomers, J. Am. Chem. Soc. 132 (2010) 3388–3399. https://doi.org/10.1021/ja908282f.
[254] A. Songur, O.A. Ozen, M. Sarsilmaz, The Toxic Effects of Formaldehyde on the Nervous System, 2010, pp. 105–118. https://doi.org/10.1007/978-1-4419-1352-4_3.
[255] K. Wu, X. Kong, K. Xiao, Y. Wei, C. Zhu, R. Zhou, M. Si, J. Wang, Y. Zhang, L. Wen, Engineered smart gating nanochannels for high performance in formaldehyde detection and removal, Adv. Funct. Mater. 29 (2019) 1807953. https://doi.org/10.1002/adfm.201807953.
[256] D. Khodakov, C. Wang, D.Y. Zhang, Diagnostics based on nucleic acid sequence variant profiling: PCR, hybridization, and NGS approaches, Adv. Drug Deliv. Rev. 105 (2016) 3–19. https://doi.org/10.1016/j.addr.2016.04.005.

[257] I. Vlassiouk, P. Takmakov, S. Smirnov, Sensing DNA hybridization via ionic conductance through a nanoporous electrode, Langmuir 21 (2005) 4776–4778. https://doi.org/10.1021/la0471644.
[258] Z. Sun, T. Liao, Y. Zhang, J. Shu, H. Zhang, G.J. Zhang, Biomimetic nanochannels based biosensor for ultrasensitive and label-free detection of nucleic acids, Biosens. Bioelectron. 86 (2016) 194–201. https://doi.org/10.1016/j.bios.2016.06.059.
[259] D. Evanko, Hybridization chain reaction, Nat. Methods 1 (2004) 186–187. https://doi.org/10.1038/nmeth1204-186a.
[260] R.M. Dirks, N.A. Pierce, Triggered amplification by hybridization chain reaction, Proc. Natl. Acad. Sci. Unit. States Am. 101 (2004) 15275–15278. https://doi.org/10.1073/pnas.0407024101.
[261] T. Zhao, H.S. Zhang, H. Tang, J.H. Jiang, Nanopore biosensor for sensitive and label-free nucleic acid detection based on hybridization chain reaction amplification, Talanta 175 (2017) 121–126. https://doi.org/10.1016/j.talanta.2017.07.024.
[262] J.S. Mattick, The genetic signatures of noncoding RNAs, PLoS Genet. 5 (2009), e1000459. https://doi.org/10.1371/journal.pgen.1000459.
[263] D.P. Bartel, MicroRNAs: target recognition and regulatory functions, Cell 136 (2009) 215–233. https://doi.org/10.1016/j.cell.2009.01.002.
[264] H. Ling, M. Fabbri, G.A. Calin, MicroRNAs and other non-coding RNAs as targets for anticancer drug development, Nat. Rev. Drug Discov. 12 (2013) 847–865. https://doi.org/10.1038/nrd4140.
[265] A. Esquela-Kerscher, F.J. Slack, Oncomirs - MicroRNAs with a role in cancer, Nat. Rev. Canc. 6 (2006) 259–269. https://doi.org/10.1038/nrc1840.
[266] M. Egholm, O. Buchardt, L. Christensen, C. Behrens, S.M. Freier, D.A. Driver, R.H. Berg, S.K. Kim, B. Norden, P.E. Nielsen, PNA hybridizes to complementary oligonucleotides obeying the Watson-Crick hydrogen-bonding rules, Nature 365 (1993) 566–568. https://doi.org/10.1038/365566a0.
[267] G. Jágerszki, R.E. Gyurcsányi, L. Höfler, E. Pretsch, Hybridization-modulated ion fluxes through peptide-nucleic-acid- functionalized gold nanotubes. A new approach to quantitative label-free DNA analysis, Nano Lett. 7 (2007) 1609–1612. https://doi.org/10.1021/nl0705438.
[268] J. Summerton, D. Weller, Morpholino antisense oligomers: design, preparation, and properties, Antisense Nucleic Acid Drug Dev. 7 (1997) 187–195. https://doi.org/10.1089/oli.1.1997.7.187.
[269] T. Liao, X. Li, Q. Tong, K. Zou, H. Zhang, L. Tang, Z. Sun, G.-J. Zhang, Ultrasensitive detection of MicroRNAs with morpholino-functionalized nanochannel biosensor, Anal. Chem. 89 (2017) 5511–5518. https://doi.org/10.1021/acs.analchem.7b00487.
[270] S. Zhang, J. Cheng, W. Shi, K.-B. Li, D.-M. Han, J.-J. Xu, Fabrication of a biomimetic nanochannel logic platform and its applications in the intelligent detection of miRNA related to liver cancer, Anal. Chem. 92 (2020) 5952–5959. https://doi.org/10.1021/acs.analchem.0c00147.
[271] C. Coulouarn, V.M. Factor, J.B. Andersen, M.E. Durkin, S.S. Thorgeirsson, Loss of miR-122 expression in liver cancer correlates with suppression of the hepatic phenotype and gain of metastatic properties, Oncogene 28 (2009) 3526–3536. https://doi.org/10.1038/onc.2009.211.
[272] M. Ali, B. Yameen, R. Neumann, W. Ensinger, W. Knoll, O. Azzaroni, Biosensing and supramolecular bioconjugation in single conical polymer nanochannels. Facile incorporation of biorecognition elements into nanoconfined geometries, J. Am. Chem. Soc. 130 (2008) 16351–16357. https://doi.org/10.1021/ja8071258.
[273] I. Vlassiouk, T.R. Kozel, Z.S. Siwy, Biosensing with nanofluidic diodes, J. Am. Chem. Soc. 131 (2009) 8211–8220. https://doi.org/10.1021/ja901120f.
[274] S.L. Cai, S.H. Cao, Y. Bin Zheng, S. Zhao, J.L. Yang, Y.Q. Li, Surface charge modulated aptasensor in a single glass conical nanopore, Biosens. Bioelectron. 71 (2015) 37–43. https://doi.org/10.1016/j.bios.2015.04.002.
[275] M. Lepoitevin, M. Bechelany, E. Balanzat, J.M. Janot, S. Balme, Non-Fluorescence label protein sensing with track-etched nanopore decorated by avidin/biotin system, Electrochim. Acta 211 (2016) 611–618. https://doi.org/10.1016/j.electacta.2016.06.079.
[276] M. Lepoitevin, G. Nguyen, M. Bechelany, E. Balanzat, J.M. Janot, S. Balme, Combining a sensor and a pH-gated nanopore based on an avidin-biotin system, Chem. Commun. 51 (2015) 5994–5997. https://doi.org/10.1039/c4cc10087e.
[277] L.N. Johnson, R.J. Lewis, Structural basis for control by phosphorylation, Chem. Rev. 101 (2001) 2209–2242. https://doi.org/10.1021/cr000225s.
[278] S. Nasir, M. Ali, I. Ahmed, C.M. Niemeyer, W. Ensinger, Phosphoprotein detection with a single nanofluidic diode decorated with zinc chelates, ChemPlusChem 85 (2020) 587–594. https://doi.org/10.1002/cplu.202000045.
[279] J. Feher, Digestion and absorption of the macronutrients, in: Quant. Hum. Physiol, Elsevier, 2017, pp. 821–833. https://doi.org/10.1016/b978-0-12-800883-6.00081-1.
[280] L. Deng, L. Wang, F. Yong, J. Xiong, T. Jin, D. De La Iglesia-Garcia, S. Bharucha, K. Altaf, W. Huang, Q. Xia, Prediction of the severity of acute pancreatitis on admission by carboxypeptidase-B activation peptide: a systematic review and meta-analysis, Clin. Biochem. 48 (2015) 740–746. https://doi.org/10.1016/j.clinbiochem.2015.04.018.
[281] X. Zhang, L. Zhang, J. Li, Peptide-modified nanochannel system for carboxypeptidase B activity detection, Anal. Chim. Acta 1057 (2019) 36–43. https://doi.org/10.1016/j.aca.2019.01.018.
[282] International Agency for Research in Cancer (IARC), World Cancer Report 2014, 2014.
[283] P.F. Hockl, A. Wolosiuk, J.M. Pérez-Sáez, A.V. Bordoni, D.O. Croci, Y. Toum-Terrones, G.J.A.A. Soler-Illia, G.A. Rabinovich, Glyco-nano-oncology: novel therapeutic opportunities by combining small and sweet, Pharmacol. Res. 109 (2016) 45–54. https://doi.org/10.1016/j.phrs.2016.02.005.
[284] A.F. Chambers, A.C. Groom, I.C. MacDonald, Dissemination and growth of cancer cells in metastatic sites, Nat. Rev. Canc. 2 (2002) 563–572. https://doi.org/10.1038/nrc865.
[285] D. Shangguan, Z. Cao, L. Meng, P. Mallikaratchy, K. Sefah, H. Wang, Y. Li, W. Tan, Cell-specific aptamer probes for membrane protein elucidation in cancer cells, J. Proteome Res. 7 (2008) 2133–2139. https://doi.org/10.1021/pr700894d.
[286] K. Ohtsubo, J.D. Marth, Glycosylation in cellular mechanisms of health and disease, Cell 126 (2006) 855–867. https://doi.org/10.1016/j.cell.2006.08.019.
[287] S. Hakomori, Glycosylation defining cancer malignancy: new wine in an old bottle, Proc. Natl. Acad. Sci. U.S.A. 99 (2002) 10231–10233. https://doi.org/10.1073/pnas.172380699.
[288] F.F. Liu, X.P. Zhao, X.W. Liao, W.Y. Liu, Y.M. Chen, C. Wang, Ultrasensitive and label-free detection of cell surface glycan using nanochannel-ionchannel hybrid coupled with electrochemical detector, Anal. Chem. 92 (2020) 5509–5516. https://doi.org/10.1021/acs.analchem.0c00330.
[289] L. Chen, Y. Fu, N. Wang, A. Yang, Y. Li, J. Wu, H. Ju, F. Yan, Organic electrochemical transistors for the detection of cell surface glycans, ACS Appl. Mater. Interfaces 10 (2018) 18470–18477. https://doi.org/10.1021/acsami.8b01987.
[290] Y.L. Ying, Y.X. Hu, R. Gao, R.J. Yu, Z. Gu, L.P. Lee, Y.T. Long, Asymmetric nanopore electrode-based amplification for electron transfer imaging in live cells, J. Am. Chem. Soc. 140 (2018) 5385–5392. https://doi.org/10.1021/jacs.7b12106.
[291] J. Song, C.H. Xu, S.Z. Huang, W. Lei, Y.F. Ruan, H.J. Lu, W. Zhao, J.J. Xu, H.Y. Chen, Ultrasmall nanopipette: toward continuous monitoring of redox metabolism at subcellular level, Angew. Chem. Int. Ed. 57 (2018) 13226–13230. https://doi.org/10.1002/anie.201808537.
[292] X. Lou, Y. Song, R. Liu, Y. Cheng, J. Dai, Q. Chen, P. Gao, Z. Zhao, F. Xia, Enzyme and AIEgens modulated solid-state nanochannels: in situ and noninvasive monitoring of H2O2 released from living cells, Small Methods 4 (2020) 1900432. https://doi.org/10.1002/smtd.201900432.
[293] M. Ali, S. Nasir, W. Ensinger, Stereoselective detection of amino acids with protein-modified single asymmetric nanopores, Electrochim. Acta 215 (2016) 231–237. https://doi.org/10.1016/j.electacta.2016.08.067.
[294] B.D. Mather, K. Viswanathan, K.M. Miller, T.E. Long, Michael addition reactions in macromolecular design for emerging technologies, Prog. Polym. Sci. 31 (2006) 487–531. https://doi.org/10.1016/j.progpolymsci.2006.03.001.
[295] Y. Sun, S.-Q. Cheng, J. Ma, F. Zhu, W. Hong, H. Li, Biomimetic nanochannels platform for detecting N-acetylglucosamine analogues, Sensor. Actuator. B Chem. 323 (2020) 128705. https://doi.org/10.1016/j.snb.2020.128705.
[296] Y. Sun, F. Zhang, J. Quan, F. Zhu, W. Hong, J. Ma, H. Pang, Y. Sun, D. Tian, H. Li, A biomimetic chiral-driven ionic gate constructed by pillar[6]arene-based host–guest systems, Nat. Commun. 9 (2018) 2617. https://doi.org/10.1038/s41467-018-05103-w.
[297] T.M.S.J.H. Kandel, Principles of Neural Science, fifth ed., McGraw-Hill Professional, New York, 2012.
[298] E.W. Gelfand, Role of histamine in the pathophysiology of asthma: immunomodulatory and anti-inflammatory activities of H1-receptor antagonists, Am. J. Med. 113 (2002) 2–7. https://doi.org/10.1016/S0002-9343(02)01431-6.
[299] J.C. Schwartz, Histamine as a transmitter in mammalian brain, in: Neurotransmission, Elsevier, 1976, pp. 71–79. https://doi.org/10.1016/B978-0-08-020540-3.50013-5.
[300] M. White, The role of histamine in allergic diseases, J. Allergy Clin. Immunol. 86 (1990) 599–605. https://doi.org/10.1016/S0091-6749(05)80223-4.
[301] S. Zhou, L. Zhang, L. Xie, J. Zeng, B. Qiu, M. Yan, Q. Liang, T. Liu, K. Liang, P. Chen, B. Kong, Interfacial super-assembly of nanofluidic heterochannels from layered graphene and alumina oxide arrays for label-free histamine-specific detection, Anal. Chem. 93 (2021) 2982–2987. https://doi.org/10.1021/acs.analchem.0c04976.
[302] D.-S. Kim, E.-S. Kang, S. Baek, S.-S. Choo, Y.-H. Chung, D. Lee, J. Min, T.-H. Kim, Electrochemical detection of dopamine using periodic cylindrical gold nanoelectrode arrays, Sci. Rep. 8 (2018) 14049. https://doi.org/10.1038/s41598-018-32477-0.
[303] P. Li, G. Xie, P. Liu, X.Y. Kong, Y. Song, L. Wen, L. Jiang, Light-driven ATP transmembrane transport controlled by DNA nanomachines, J. Am. Chem. Soc. 140 (2018) 16048–16052. https://doi.org/10.1021/jacs.8b10527.
[304] E. Lescop, L. Briand, J.-C. Pernollet, E. Guittet, Structural basis of the broad specificity of a general odorant-binding protein from honeybee, Biochemistry 48 (2009) 2431–2441. https://doi.org/10.1021/bi802300k.
[305] A. Schiefner, R. Freier, A. Eichinger, A. Skerra, Crystal structure of the human odorant binding protein, OBP IIa, Proteins Struct. Funct. Bioinforma. 83 (2015) 1180–1184. https://doi.org/10.1002/prot.24797.
[306] B.S. Williams, A. Buvanendran, Nonopioid analgesics: nsaids, COX-2 inhibitors, and acetaminophen, in: Essentials Pain Med., Elsevier, 2011, pp. 130–139. https://doi.org/10.1016/B978-1-4377-2242-0.00026-2.
[307] I. Boussouar, Q. Chen, X. Chen, Y. Zhang, F. Zhang, D. Tian, H.S. White, H. Li, Single nanochannel platform for detecting chiral drugs, Anal. Chem. 89 (2017) 1110–1116. https://doi.org/10.1021/acs.analchem.6b02682.

[308] Q. Zhou, A. Yen, G. Rymarczyk, H. Asai, C. Trengrove, N. Aziz, M.T. Kirber, G. Mostoslavsky, T. Ikezu, B. Wolozin, V.M. Bolotina, Impairment of PARK14-dependent Ca2+ signalling is a novel determinant of Parkinson's disease, Nat. Commun. 7 (2016) 10332. https://doi.org/10.1038/ncomms10332.
[309] Q. Lu, Q. Tang, Z. Chen, S. Zhao, G. Qing, T. Sun, Developing an inositol-phosphate-actuated nanochannel system by mimicking biological calcium ion channels, ACS Appl. Mater. Interfaces 9 (2017) 32554–32564. https://doi.org/10.1021/acsami.7b09992.
[310] S. Peng, B. Bhushan, Smart polymer brushes and their emerging applications, RSC Adv. 2 (2012) 8557–8578. https://doi.org/10.1039/c2ra20451g.
[311] J. Wang, J. Hou, H. Zhang, Y. Tian, L. Jiang, Single nanochannel-aptamer-based biosensor for ultrasensitive and selective cocaine detection, ACS Appl. Mater. Interfaces 10 (2018) 2033–2039. https://doi.org/10.1021/acsami.7b16539.
[312] M. Guerrini, Z. Zhang, Z. Shriver, A. Naggi, S. Masuko, R. Langer, B. Casu, R.J. Linhardt, G. Torri, R. Sasisekharan, Orthogonal analytical approaches to detect potential contaminants in heparin, Proc. Natl. Acad. Sci. Unit. States Am. 106 (2009) 16956–16961. https://doi.org/10.1073/pnas.0906861106.
[313] R. Sasisekharan, Z. Shriver, From crisis to opportunity: a perspective on the heparin crisis, Thromb. Haemostasis 102 (2009) 854–858. https://doi.org/10.1160/TH09-02-0083.
[314] T. Ma, E. Balanzat, J.-M. Janot, S. Balme, Single conical track-etched nanopore for a free-label detection of OSCS contaminants in heparin, Biosens. Bioelectron. 137 (2019) 207–212. https://doi.org/10.1016/j.bios.2019.05.005.
[315] Z. Xie, M. Yang, L. Luo, Y. Lv, K. Song, S. Liu, D. Chen, J. Wang, Nanochannel sensor for sensitive and selective adamantanamine detection based on host-guest competition, Talanta 219 (2020) 121213. https://doi.org/10.1016/j.talanta.2020.121213.
[316] P. Li, X.-Y. Kong, G. Xie, K. Xiao, Z. Zhang, L. Wen, L. Jiang, Adenosine-activated nanochannels inspired by G-protein-coupled receptors, Small 12 (2016) 1854–1858. https://doi.org/10.1002/smll.201503863.
[317] R. Pinalli, A. Pedrini, E. Dalcanale, Biochemical sensing with macrocyclic receptors, Chem. Soc. Rev. 47 (2018) 7006–7026. https://doi.org/10.1039/C8CS00271A.
[318] J.N. Martins, J.C. Lima, N. Basílio, Selective recognition of amino acids and peptides by small supramolecular receptors, Molecules 26 (2020) 106. https://doi.org/10.3390/molecules26010106.
[319] O.S. Wolfbeis, Editorial: probes, sensors, and labels: why is real progress slow? Angew. Chem. Int. Ed. 52 (2013) 9864–9865. https://doi.org/10.1002/anie.201305915.
[320] I. Bazin, S.A. Tria, A. Hayat, J.-L. Marty, New biorecognition molecules in biosensors for the detection of toxins, Biosens. Bioelectron. 87 (2017) 285–298. https://doi.org/10.1016/j.bios.2016.06.083.
[321] P.V.V. Romanholo, C.A. Razzino, P.A. Raymundo-Pereira, T.M. Prado, S.A.S. Machado, L.F. Sgobbi, Biomimetic electrochemical sensors: new horizons and challenges in biosensing applications, Biosens. Bioelectron. 185 (2021) 113242. https://doi.org/10.1016/j.bios.2021.113242.
[322] Z. Li, C. Pei, F. Yang, Method to Form Nanopore Array, 2012. US20120040512A1.
[323] S. Polonsky, S.M. Rossnagel, G.A. Stolovitzky, Systems and Methods for Controlling Position of Charged Polymer inside Nanopore, 2011. US8003319B2.
[324] X. Su, A.A. Berlin, Methods and Device for Biomolecule Characterization, 2010. US7744816B2.
[325] P.W. Barth, Apparatus and Method for Making a Low Capacitance Artificial Nanopore, 2006. US7075161B2.
[326] C.A. Flory, Apparatus and Method for Biopolymer Identification during Translocation through a Nanopore, 2008. US7410564B2.
[327] J. Feng, K. Liu, A. Radenovic, Y. Astier, Nanopore Forming Method and Uses Thereof, US20180073161A1, 29AD.
[328] J. Shim, D.-H. Lee, K. Eom, T. Jeon, H. Jeong, Method for Analyzing Biomolecules Using Asymmetric Electrolyte Concentration, 2014. US20140021047A1.